Consolidated composite adsorbent containing graphite flake for sorption cooling systems

by

Khorshid Fayazmanesh

M.Sc., University of Birmingham, 2012
M.Eng, University of Birmingham, 2011

Thesis Submitted in Partial Fulfillment of the

Requirements for the Degree of

Doctor of Philosophy

in the

School of Mechatronic Systems Engineering

Faculty of Applied Sciences

© Khorshid Fayazmanesh 2017

SIMON FRASER UNIVERSITY

Summer 2017

Approval

Name:	**Khorshid Fayazmanesh**
Degree:	**Doctor of Philosophy**
Title:	***Consolidated composite adsorbent containing graphite flake for sorption cooling systems***
Examining Committee:	**Chair:** Dr. Kevin Oldknow Senior Lecturer

Dr. Majid Bahrami
Senior Supervisor
Professor

Dr. Gary Leach
Supervisor
Professor

Dr. Woo Soo Kim
Supervisor
Associate Professor

Dr. Byron Gates
Internal Examiner
Associate Professor
Department of Chemistry

Dr. Angelo Freni
External Examiner
Researcher
Italian National Research Council
institute for Advanced Energy
Technologies

Date Defended/Approved: 07-06-2017

Abstract

Heat-driven sorption technology, as a sustainable and clean solution for thermal management and heat storage, has drawn a significant interest in academic and industrial research community. This interest has been intensified in the last decade as environmental and climate changes issues are becoming major global challenges. Numerous studies aim to improve materials sorption performances, as it is at the core of sorption cooling or storage systems. Due to the nature of the sorption process, heat and transport properties, e.g., thermal diffusivity and thermal conductivity of the adsorbent material play an important role in their performance. Higher thermal diffusivity can enhance the heat transfer rate and lead to faster sorption/desorption cycles and more efficient (more compact) heat-driven sorption chillers. A key part of the sorption chillers design is developing adsorbent materials (or composites) with superior hydrophilicity, high water uptake capacity, low regeneration temperature (60-150°C), and high thermal diffusivity.

The focus of this research is to design tailored consolidated composite adsorbent containing graphite flakes with improved heat and mass transfer properties for sorption cooling systems. The presented Ph.D. dissertation is divided into three main parts: (i) composite adsorbent fabrication and characterization; (ii) consolidated composite characterization; and (iii) thermal properties modeling of consolidated composite adsorbent. Fabricated loose grain and consolidated composite were characterized in Dr. Bahrami's Laboratory for Alternative Energy Conversion (LAEC) and SFU 4D LABS.

Keywords: Sorption chiller, consolidated adsorbent, water sorption, thermal conductivity, silica gel, graphite flakes

To my beloved parents and my brother

Acknowledgements

Contents

List of Figures

List of Tables

Nomenclature

W	Weight of adsorbed gas
P_0/P	Relative pressure
W_m	Weight of adsorbate as monolayer
C	BET constant
s	Slope
i	Intercept
N	Avogadro's number (6.0233×10^{23})
M	Molecular weight of adsorbate
A_{CS}	Adsorbate cross sectional area (16.2 Å^2 for nitrogen)
S_t	Total surface area (m^2)
S_{BET}	Specific surface area ($m^2 \cdot g^{-1}$)
c_p	Specific heat capacity ($MJ \cdot m^{-3} \cdot K^{-1}$)
T	Temperature (°C)
P_a	Adsorption pressure (Pa)
P_d	Desorption pressure (Pa)
Q	Heat flow rate (W)
ρ	Density ($Kg \cdot m^{-3}$)
L	Latent heat of vaporization ($KJ \cdot Kg^{-1}$)
D	Diameter (nm)
V	Volume($cm^3 \cdot g^{-1}$)
$\dot{Q}$	Power from the heat source (W)
T	Temperature $\left({}^{\circ}C \right)$
A	Area (m^2)
t_{sample}	Sample thickness (m)
P_{H_2O}	Water vapor pressure (mbar)
K	Thermal conductivity ($W \cdot m^{-1} \cdot K^{-1}$)
r_p	Particle radius (m)
a	Basic unit cell (m)
n	Shape factor
R	Resistance

t	Thickness (μm)
w	Width of unit cell
r	Radius (μm)
h_{fg}	Water enthalpy of evaporation ($KJ \cdot kg^{-1}$)
k	Time constant
u(t)	Sorption at time t

Subscripts

e	effective
m	medium
L	Lower bound
U	Upper bound
eff	effective
p	particle
c	cold
h	hot
eva	evaporator
con	condenser
s	Solid, silica gel-$CaCl_2$-PVP
g	Graphite flake
1	Continuous medium (solid)
2	Solid particle (dispersed)
ads	adsorbent

Greek symbols

α	Thermal diffusivity ($m^2/2$)
λ	Solid to fluid thermal conductivity ratio
φ	Volume fraction
n	Shape factor
ψ	Sphericity
ρ	Density ($g \cdot cm^{-3}$)
θ	Angle, degree
n	Shape factor
τ	Characterization time (s)

Acronyms

A/C	Air conditioning
AHP	Adsorption Heat Pump
BET	Brunauer, Emmett, and Teller
BJH	Barrett, Joyner, and Halenda
COP	Coefficient of Performance
HVAC	Heating, Ventilation, and Air Conditioning
IUPAC	International Union of Pure and Applied Chemistry
LDF	Linear Driving Force
RC	Resistance-Capacitance
RH	Relative Humidity
SCP	Specific Cooling Power
SCS	Sorption Cooling System
SEM	Scanning Electron Microscope
TGA	Thermo-Gravimetric Analyzer
TMA	Thermo-Mechanical Analyzer
TPS	Transient Plane Source
VS	Vapor Sorption
XRD	X-Ray Diffraction

Executive Summary

Heat-driven sorption cooling is an emerging green technology in which an environmentally friendly refrigerant, such as water, is adsorbed by a porous adsorbent material. Sorption cooling systems (SCS) can be designed to operate through using waste heat, i.e., temperatures less than 100°C, from a variety of sources including: internal combustion engines, geothermal sites, power plants, solar thermal, and biofuel facilities, to name a few, for residential, industrial and automotive air conditioning applications. International pilot projects have proven the potential of SCS to providing air conditioning for buildings and vehicles. However, more compact and energy efficient technology needs to be developed for widespread adoption of SCS.

One of the critical challenges facing the widespread of SCS includes development of new sorbent materials featuring: i) low regeneration temperatures; ii) efficient mass and thermal transport properties; iii) high sorption-desorption capacity; and, iv) long-life under cyclic operating temperatures and pressures. This project focuses on the fabrication and characterization of such new consolidated composite adsorbent materials.

Objective

The research objectives are as follows:

- Preparation and textural characterization of novel composite materials with high sorption capacity which can be regenerated at temperatures less than 60°C;
- Improving the heat transfer properties of adsorbent materials, as well as their durability under cyclic pressure and temperature operating conditions, by adding thermally conductive additive, such as graphite flakes;
- Providing an in-depth understanding of the heat transfer mechanisms involved, to accurately predict the effective thermal conductivity and thermal diffusivity of consolidated composite containing graphite flakes; and
- Providing a complete set of mechanical and thermal properties of the prepared consolidated composite adsorbent materials.

Methodology

The following steps describe a brief overview of the methodology used for achieving the objective of this research project, Figure 1 shows the roadmap and the components of this thesis:

1. Mass transfer enhancement:

   - Selected the based adsorbent composite, i.e., mesoporous matrix (silica gel) pore and particle size based on the available adsorbent performances in the literature;

   - Synthesized hygroscopic salt supported by mesoporous matrix (composite)

   - Characterized the synthesized composites for sorption and microstructure properties, e.g., water uptake capacity, crystal structure, surface characteristics;

   - Synthesized and characterized the composite pellets (binder selection, water uptake capacity, and pore size distribution); and

   - Designed and custom-built a new small-scale water uptake testbed to measure the uptake performance of the synthesized composites at larger.

2. Heat transfer improvement:

   - Prepared a number of new composites with increased thermal conductivity by adding graphite flakes;

   - Characterized textural and thermophysical properties of the composites, including: pore size distribution, thermal conductivity, specific heat and thermal diffusivity;

   - Studied potential hysteresis effects and uptake durability using thermogravimetric analyzer; and

   - Modelled effective thermal conductivity and thermal diffusivity of the prepared coated composite materials.

3. Mechanical properties:

   - Studied the mechanical properties of the prepared composite adsorbents, including compression test and thermal expansion; reported effective Young modulus and coefficient of thermal expansion (CTE).

```
┌─────────────────────────────────────────────────────────────────────────┐
│              Material preparation, characterisation and modeling          │
└─────────────────────────────────────────────────────────────────────────┘
        │                          │                          │
        ▼                          ▼                          ▼
┌──────────────────┐    ┌──────────────────┐    ┌──────────────────────────┐
│ Structural       │    │ Water Uptake     │    │ Thermal properties       │
│ properties       │    │                  │    │                          │
│                  │    │ • Water uptake at│    │ • Thermal conductivity   │
│ • Pore volume    │    │   different      │    │                          │
│   distribution   │    │   pressure       │    │ • Specific heat          │
│                  │    │   and temperature│    │                          │
│ • Average pore   │    │                  │    │ • Coefficient of thermal │
│   diameter       │    │ • Durability     │    │   expansion              │
│                  │    │                  │    │                          │
│ • BET surface    │    │                  │    │ • Effective thermal      │
│   area           │    │                  │    │   conductivity modeling  │
│                  │    │                  │    │                          │
│ • Effective Young│    │                  │    │ • Thermal diffusivity    │
│   Modulus        │    │                  │    │   modeling               │
└──────────────────┘    └──────────────────┘    └──────────────────────────┘
        │                          │                          │
        └──────────────────────────┼──────────────────────────┘
                                   ▼
┌─────────────────────────────────────────────────────────────────────────┐
│        Developing high performance composite for sorption cooling systems │
└─────────────────────────────────────────────────────────────────────────┘
```

Figure 1. Research Roadmap and components of thesis

Contributions

Main contributions of this research project are highlighted below:

- A new tailored composite adsorbent material was prepared and characterized with high water uptake capacity [Accepted, *International Journal of Applied Thermal Energy*];

- A new tailored consolidated composite adsorbent material with significantly improved water uptake property was fabricated by selecting proper binder. Surface properties and water uptake capacity of prepared samples were studied using an Autosorb Instrument and thermogravimetric analyzer at different temperature and pressures [Accepted, *International Journal of Applied Thermal Energy*];

xviii

- Thermal conductivity of composite coating material was significantly improved, up to 107% increase was observed, by adding graphite flakes [Accepted, *International Journal of Applied Thermal Energy*];

- Mechanical properties of the prepared composite adsorbent were studied. Effective thermal conductivity of consolidated composite containing graphite flakes was analytically modeled when graphite flakes shape, size and orientation considered [Accepted, *International Journal of Heat and Mass Transfer*];

- Thermal properties, namely thermal conductivity, specific heat, and thermal diffusivity of the prepared consolidated composite containing graphite flakes were modeled at various relative humidity (uptake levels) [Under review, *International Journal of Applied Thermal Energy];*

Publications

1. **K. Fayazmanesh**, M. Rohani, M. Bahrami, "Thermal diffusivity of consolidated composite adsorbent containing graphite flakes: Applications for sorption chillers", (Under review, *International Journal of Applied Thermal Engineering)*

2. **K. Fayazmanesh**, S. Salari, M. Bahrami, **"**Effective thermal conductivity modeling of composite adsorbent containing graphite flakes", *International Journal ofHeat Mass Transf.*, vol. 115, pp. 73–79, 2017

3. **K. Fayazmanesh**, C. McCague, and M. Bahrami, "Consolidated adsorbent containing graphite flakes for heat-driven water sorption cooling systems," *Applied Thermal Engineering*, vol. 123, pp. 753–760, 2017

4. Sharafian, **K. Fayazmanesh**, C. M. McCague, M. Bahrami, " Thermal conductivity and contact resistance of mesoporous silica gel adsorbents bound with polyvinylpyrrolidone in contact with a metallic substrate for adsorption cooling system applications", *International Journal of Heat and Mass Transfer*, Volume 79, Pages 64-71, 2014.

Conferences and symposiums

1. S. Bahrehmand, **K. Fayazmanesh**, W. Huttema, M. Ahmadi, C. M. McCague, M. Bahrami, "Modeling of oscillatory heat transfer in coated sorption bed," International Sorption Heat Pump Conference, Toyko, Japan, 2017 (Presentation).

2. **K. Fayazmanesh**, C. M. McCague, M. Bahrami, "Consolidated composite with increased thermal conductivity and sorption capacity for heat-driven sorption cooling systems," SFU Climate and Energy Research Day, Simon Fraser University, Burnaby, Canada, 2017 (Poster).

3. Ronil Tabari, C. M. McCague, **K. Fayazmanesh**, M. Bahrami, "Sustainable closed greenhouse: From waste to clean food and water," SFU Climate and Energy Research Day, Simon Fraser University, Burnaby, Canada, 2017 (Poster).

4. **K. Fayazmanesh**, C. M. McCague, M. Baharmi, "Water adsorbent composites consolidated with graphite flakes for heat driven sorption cooling systems," IV International Symposium on Innovative Materials for Processes in Energy Systems, Taormina, Italy, 2016 (Presentation).

5. M. Nemati Mehr, A. Sharafian, **K. Fayazmanesh**, W. Huttema and M. Bahrami, "Modeling the effects of adding graphite flakes to FAM-Z02 in an adsorber bed,"

IV International Symposium on Innovative Materials for Processes in Energy Systems, Taormina, Italy, 2016(Presentation).

6. C. McCague, M. Ka-Wah Cheung, R. Chatterjee, **K. Fayazmanesh**, Majid Bahrami" CaCl2-silica gel consolidated with polyvinylpyrrolidone and graphite flakes for water-based adsorption cooling systems", IV International Symposium on Innovative Materials for Processes in Energy Systems, Taormina, Italy, 2016 (Poster).

7. **K. Fayazmanesh**, C. M. McCague, M. Bahrami, "Graphite-doped adsorbent coatings for heat-driven water sorption cooling systems," IX Minsk International Seminar on Heat Pipes, Heat Pumps, Refrigeration, Power Sources, Minsk, Belarus, 2015 (Presentation).

8. M. McCague, **K. Fayazmanesh**, Cecilia Berlanga, M. Bahrami, "Evaluation of CaCl2-silica gel adsorbent for water sorption cooling systems" IX Minsk International Seminar on Heat Pipes, Heat Pumps, Refrigeration, Power Sources, Minsk, Belarus, 2015 (Presentation).

9. **K. Fayazmanesh**, C. M. McCague, M. Bahrami, "Composite adsorbent coating materials with increased thermal conductivity and sorption capacity for adsorption cooling systems," SFU Climate and Energy Research Day, Simon Fraser University, Burnaby, Canada, 2015 (Poster).

10. **K. Fayazmanesh**, C. M. McCague, M. Bahrami, "Development of new composite adsorbent coating materials for sustainable cooling systems," Nanolytica Symposium, Simon Fraser University, Burnaby, Canada, 2015 (Poster).

11. M. McCague, **K. Fayazmanesh**, M. Kalra, M. Bahrami, "Water adsorption of $CaCl_2$ confined in mesoporous silica gel with various pore sizes," Proceedings of the International Sorption Heat Pump Conference, Washington, United states, 2014 (Presentation).

12. **K. Fayazmanesh**, C. M. McCague, M. Kalra, M. Bahrami, "Development of new composite adsorbent materials with increased thermal conductivity for adsorption cooling systems," Pacific Center for Advanced Materials and Microstructures, University of Victoria, Victoria, Canada, 2014 (Poster).

13. **K. Fayazmanesh**, C. M. McCague, M. Kalra, M. Bahrami, "Thermogravimetric water sorption analysis of $CaCl_2$ confined is silica gel mesopores," *97th Canadian Chemistry Conference and Exhibition*, Vancouver, Canada, 2014 (Presentation).

14. **K. Fayazmanesh,** C. M. McCague, M. Kalra, M. Bahrami, "Thermogravimetric water sorption analysis of $CaCl_2$ confined is silica gel mesopores for sustainable refrigeration," Nanolytica Symposium, Simon Fraser University, Burnaby, Canada, 2014 (Poster).

Chapter 1.   Introduction

1.1.   Research motivation

Sorption cooling systems utilize low-grade heat (temperature sources less than 100°C), for example waste heat from an engine or solar thermal energy. ACS uses environmental friendly refrigerants such as water as a refrigerant to produce cooling power without environmental impacts on carbon foot. The major challenges facing these systems are their low energy efficiency [low coefficient of performance (COP) and low specific cooling power (SCP)] [1].

The focus of this thesis is on development of novel cost-effective and durable composite sorption materials which have tailored properties, such as high sorption capacity, and can be regenerated at low temperature. The adsorbent material must have high mass and heat transfer properties, as well as high durability under repeated pressure and temperature cycling.

1.2.   Research objectives

The objective of this research project is to fabricate new adsorbent materials with low regeneration temperature, high sorption-desorption capacity, adequate heat and mass transfer properties and durable under operational temperatures and pressures.

1.3.   Thesis structure

Careful investigation of the pertinent literature shows that selecting a proper adsorbent material for desirable conditions has a great effect on the system performance along with system components.

Chapter 3 covers the preparation and detailed study of loose grain silica gel-$CaCl_2$. The main goal of this study was to demonstrate the presence of hygroscopic salt in pores of porous matrix.

Chapter 4 covers preparation and characterization of consolidated composite adsorbent containing thermally conductive additive, graphite flakes. Heat and mass transfer of the adsorbent have a great impact on the system performance. Specific emphasis in this chapter is on the thermal properties of consolidated composite.

Chapter 5 covers thermal conductivity modeling of consolidated composite containing graphite flakes. In this chapter, size, shape, angle and distribution of graphite flakes in the consolidated composite are considered.

Chapter 6 covers Thermal diffusivity of consolidated composite adsorbent containing graphite flakes. In this chapter, a new model is developed to predict the thermal diffusivity of consolidated adsorbent containing graphite flakes at different relative humidities (RHs).

Chapter 7 reports the major contributions of this thesis. Suggestions for future studies are also given in this Chapter.

Chapter 2.   Literature review

The vapor compression system, commonly used for air conditioning and refrigeration, employs environmentally harmful refrigerants and consume significant amounts of electrical power. The power used by the Heating, Ventilation, and Air Conditioning (HVAC) systems to provide thermal comfort in residential and commercial buildings amounts up to 10-20% of the total energy consumption in the developed world [2][3][4]. Efficient, sustainable cooling technologies are presently the focus of significant research and development efforts.

An alternative clean technology for vapor compression systems is heat-driven cooling systems, in which the environmental friendly refrigerant (adsorbate), such as water, is adsorbed by a porous adsorbent. Sorption cooling systems that utilize materials with low regeneration temperatures can be powered by low-grade heat sources, including solar thermal energy and industrial waste heat [5]. Data on sorption (desorption) equilibrium in the same working condition of sorption cooling system, the isosteric heat of sorption and the specific heat capacity of adsorbent (c_p) at various temperatures and water contents are crucially needed to enable an in-depth understanding of the sorption cycle and predict and optimize the thermodynamic performance of the system [6]. All the relevant and salient topics is extensively reviewed in this section.

2.1.   History of sorption

Heat-driven sorption refrigeration systems were patented in 1900s, and household refrigerators became available at 1920s [7]. In 1928, a sorption cooling system for refrigerated railcars was developed utilizing silica gel adsorbent and sulphur dioxide refrigerant [8]. A fleet of sorption cooled railcars were used to transport frozen fish across North America for several years. Shortly thereafter, the quality and affordability of gas compressors improved, allowing vapor-compression refrigeration systems to dominate the marketplace. To date, commercial sorption cooling systems remain rare, despite environmentally favourable attributes relative to vapor compression systems. Sorption cooling systems do not require ozone depleting, or otherwise environmentally harmful refrigerants, their energy consumption is low, and they can be driven by solar thermal energy or industrial waste heat. However, critical challenges remain with respect to

increasing system efficiency and reducing the bulk of the sorbent beds needed to provide sufficient cooling power for refrigeration and air conditioning applications [9][5][10] .

2.2.   The sorption cooling systems

Sorption refrigeration systems are thermally driven systems in which the mechanical compressor in vapor compression systems is replaced by an adsorbent. An sorption cooling system consists of four main parts: absorber bed, evaporator, condenser and the expansion valve. Adsorber bed is filled with an adsorbent material that has the ability to adsorb and desorb the adsorbent (refrigerant). In Figure 2, the flow diagram of a sorption cooling system with two adsorber beds is shown. For better understanding, sorption system operation is presented by Clapeyron diagram, Figure 3. A complete cycle consists of heating the adsorber bed, desorption, cooling, and sorption, see [11] for more details. The following summarizes a thermodynamic sorption cooling cycle:

1-2) Adsorbent materials in adsorber bed are saturated by adsorbate (refrigerant). This step is exothermic, i.e. significant amount of heat is generated and leads to an increase in temperature and vapor pressure in the adsorber bed.

2-3) When adsorber bed reaches to the condensation pressure, the endothermic process of desorption (regeneration) takes place. Adsorbate is released from the adsorbent and flows into the condenser.

3-4) The adsorbate passes through the expansion valve to enter the evaporator with low pressure.

4-1) The necessary heat for adsorbate evaporation is taken from the environment (in this case waste heat or solar energy). The cooling effect is produced while the boiled adsorbate enters the adsorber bed.
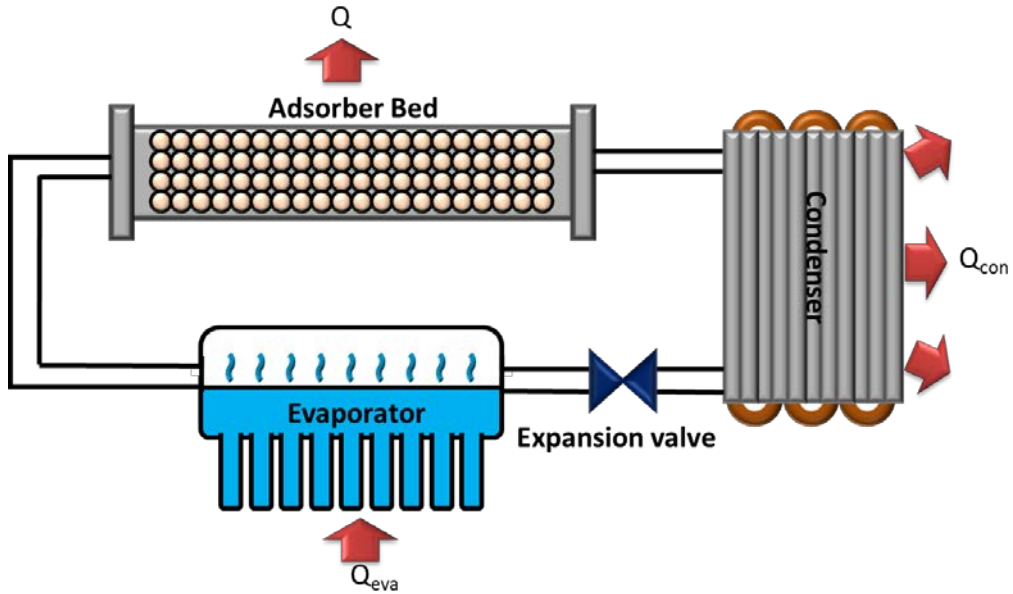
Figure 2. Schematic of sorption cooling system
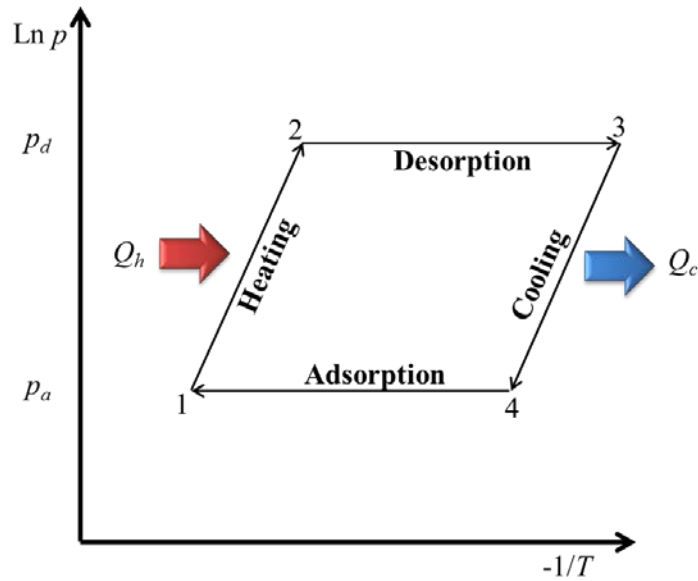
Figure 3. Clapeyron diagram for sorption cooling cycle

2.2.1.   Advantages and disadvantages of sorption cooling systems

Advantages of sorption cooling systems include:

- Low electrical power consumption, since the main input energy is in the form of waste heat [12] or solar thermal energy [13];
- Environmentally friendly adsorbent and adsorbate materials (silica gel, zeolite-water) [14]; and
- No major moving parts, vibration, and noise, so no need for special maintenance [15].

However, sorption cooling systems have several issues limiting their commercialization, including:

- In systems that work with salt confined in a porous matrix as adsorbent and water as adsorbate, there is a possibility of corrosion that effect the overall life of the systems [16] [15];
- The coefficient of performance (COP) and the specific cooling power (SCP) of sorption cooling systems are low in comparison with vapor compression systems [17]; as a result of adsorbent materials low heat and mass transfer [18][10].

2.3. Sorption working pairs

Sorption working pairs consist of an adsorbent and an adsorbate (refrigerant). The selection of pairs for refrigeration applications is highly dependent on the material properties and operating conditions. In Table 1, ideal adsorbent-adsorbate properties are listed [15].

Table 1. Properties of ideal adsorbents and adsorbates [15]

Adsorbent	Adsorbate (refrigerant)
- Large adsorbate uptake capacity at ambient temperatures - Can be regenerated (desorb) with low-grade waste heat (*e.g.*, 70-90°C) - No deterioration with age or use - Non-toxic and non-corrosive - Low cost and widely available	- Evaporation temperature below 0°C - Small molecular size, so it can be adsorbed by the adsorbent - High latent heat of vaporization and low specific volume - Thermally stable with adsorbent at the operating temperature conditions - Non-toxic, non-corrosive and non-flammable - Low saturation pressures (above atmosphere) at normal operating temperatures

Different types of working pairs' uptake capacities and textural, mechanical, and thermal properties have been studied in-depth, and the important ones are listed in Table 2. As mentioned in Table 1, non-toxic and non-flammable refrigerants with low regeneration temperature attracted scientists attention to use waste-heat which significantly reduce environmental impacts associated with conventional vapor compression refrigeration air-conditioning systems that run on electricity often produced burning fossil fuel. Although sorption cooling systems working with ammonia show great performances in comparison with water, methanol, and ethanol systems, water-based sorption cooling systems are receiving an immense attention.

Table 2. Different types of working pairs for sorption cooling systems

	Working pair	Ref.
Physical adsorbent	Activated carbon/ammonia	[19], [20]
	Activated carbon/methanol	[5], [7], [21]–[23]
	Activated carbon/ethanol	[15], [24]
	Silica gel/water	[25]–[27]
	Zeolite/water	[5], [28]–[35]
Chemical adsorbent	Metal chloride/ammonia	[36]–[40]
	Metal Chloride/water	[41]
Composite adsorbents	Silica gel and hydroscopic salts/water	[14], [23], [42]–[50]
	Silica gel and chlorides/methanol	[23], [46], [51], [52]
	Chlorides and porous media/ammonia	[23]
	Zeolite and foam aluminum/water	[53]

2.3.1. Porous adsorbent materials

High surface area adsorbents are porous. There are different kinds of rigid and non-rigid pore structures with different pore sizes and shapes. Pore widths are classified by International Union of Pure and Applied Chemistry (IUPAC) as follows [54]:

- Macro-porous materials: 50-1000 nm
- Meso-porous materials: 2-50 nm
- Micro-porous materials: 0.2-2 nm

Adsorbent materials have the capacity to physically or chemically adsorb vapor (adsorbate). The adsorbed vapor can be removed by heating (regeneration). Different types of adsorbents are described in this section.

Physical adsorbents

Activated carbon, silica gel, zeolite, and aluminophosphates are the common physical adsorbent for sorption cooling systems.

Activated carbon: Materials such as wood, peat, coal, fossil oil, bone coconut shell, and nut stone can be utilized to produce high surface area (500-1500 $m^2 \cdot g^{-1}$) activated carbon. The structure of activated carbon is shown in Figure 4. The sorption performance of activated carbon depends on functional groups connected to the carboatomic ring [41][55]. The microstructure of the activated carbon depends on the method of production and origin of the carbonaceous material. Activated carbons manufactured from petroleum residue or charred coal have small micro pores, large surface area, and high density, while activated carbons made of brown coal have large micro pores, small surface area, and low density [41]. Activated carbon surface can be covered by an oxide matrix and inorganic materials that make it non-polar or weakly polar. This reduces the desorption heat in comparison to other adsorbents [41].
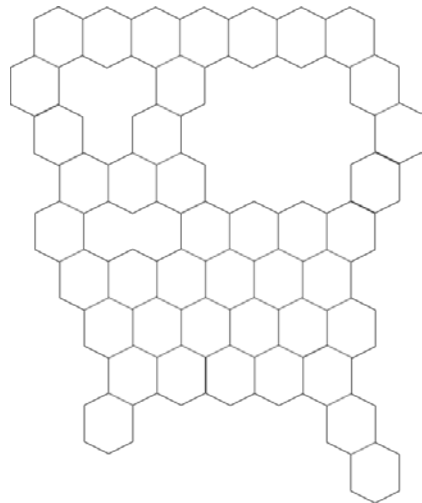
Figure 4. Example of activated carbon microstructure [41]

Silica gel: One type of amorphous synthetic silica is silica gel, which is a rigid, continuous net of colloidal silica. Silica gel is made of grains of SiO_2, as shown in Figure 5. The main reason for sorption is the presence of hydroxyl in the structure, which is polar and can form hydrogen bonds with polar oxides[41].
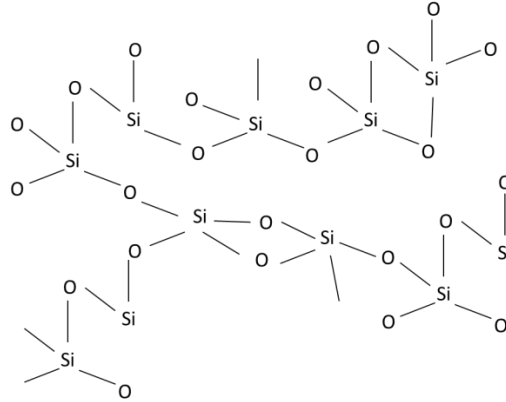
Figure 5. SiO₄ array in silica gel [41]

Silica gel becomes one of the leading materials in sorption cooling systems, because of its pair, water. This working pair is suitable for low grade heat source. The major challenge with silica gel-water sorption cooling system is the system performance in comparison to commercialized systems [27]. To improve silica gel-water uptake capacity, chemical adsorbents such as hygroscopic salts are added. Aritov et al. [48] and Freni et al. [46][56] have studied this area extensively.

Zeolite: Zeolites are microporous aluminosilicate crystals with regular cage-like frameworks, as shown in Figure 6. There are natural and synthesized zeolites available commercially. The main natural zeolites used in sorption refrigeration systems are chabazite, sodium chabazite, and faujasite. Synthesized zeolites are named by one letter or a group of letters, such as type A, type X, type Y, and type ZSM [41].
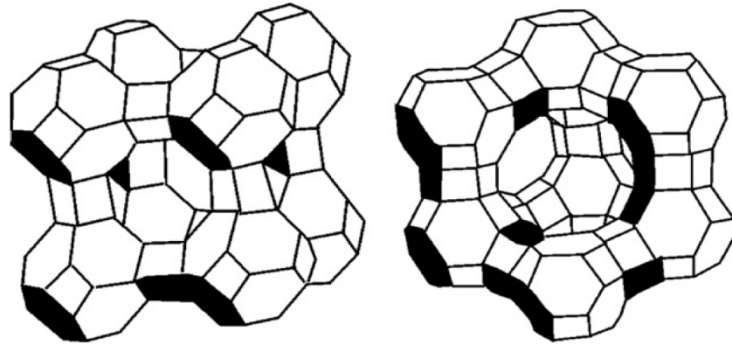
Figure 6. Crystal cell unit of zeolite : (a) type A zeolite crystal cell unit; (b) type X, Y zeolite or faujasite crystal cell unit [41]

The sorption capacity of zeolite depends on the ratio of Si to Al. The main zeolite molecular sieves for sorption refrigeration applications are 4A, 5A, 10X, and 13X. The heats of sorption for zeolites are high in comparison to silica gel and the regeneration temperature of zeolites are about 250-300°C. Zeolites decompose at the temperatures greater than 600-700°C. Zeolites can be used in sorption air conditioning systems with heat sources between 200°C and 300°C.

Aluminophosphates: Aluminophosphates are one of the new generations of adsorbent materials with a relatively low desorption temperature (60-90°C) and pore volume of 0.05-0.35 cm^3/g, which are suitable for sorption cooling systems. The major disadvantages of this type of adsorbent is its high heat of desorption (53.6 kJ/mol) and its cost [57].

Three different types of silicoaluminophosphate are developed by the Mitsubishi Chemical Ltd., known as, FAM-Z01, Z02, and Z05. Mitsubishi Plastic Ltd. provides coated heat exchangers for their customers and small size sorption chillers are found in the market [58].

Chemical adsorbents

Metal chlorides: The most common metal chlorides for sorption cooling systems are calcium chloride, strontium chloride, magnesium chloride, and barium chloride. Water [59] and ammonia [60] are the usual adsorbates for metal chlorides. Heat and mass transfer performance in sorption process is affected by swelling and agglomeration of salt [41]. An additional challenge arises if there are dissimilar metals in the adsorber bed, heat exchanger, or chamber, the salt solution can enhance the rate of galvanic corrosion [61], reducing the life span of metal

11

components and generating background gases that have negative impact on sorption dynamics reference [62].

Composite adsorbents

Composites "salt (hygroscopic salts) in porous matrix" is one of the promising sorbents for heat-driven sorption cooling systems. Variety of composites adsorbent developed and characterized for water [43], methanol [51], and ammonia sorption systems [63]. In a confined salt in porous matrix, salt is the active component and the porous matrix disperses salt which can be an active material as well, such as silica gel.

2.3.2. Refrigerant (adsorbate)

Sorption technology is not limited to only air conditioning and refrigeration but also can be utilized for heat with thermal transfers. Refrigerant should be selected based on the application and working conditions. The common physical properties of the refrigerants for sorption systems are summarized in Table 3 [64].

Table 3. Physical properties of some refrigerants for sorption systems [64]

Refrigerants	Chemical formula	Normal boiling point (°C)	Latent heat of vaporization L (kJ·kg^{-1})	Density ρ (kg·m^{-3})	$\rho \times L$ (MJ.m^{-3})
Water	H_2O	100	2258	958	2163
Ammonia	NH_3	-34	1368	681	932
Methanol	CH_3OH	65	1102	791	872
Ethanol	C_2H_5OH	79	836	789	665

2.4. Principle of sorption and desorption

Sorption is the separation process of the material from vapor phase to solid phase. The sorption process has a significant role in major industries, including water purification (treatment), recovery of chemicals from exhaust gases, and desiccant dehumidification technology [65].

Sorption is a term for sorption and absorption, where sorption is the attachment of one substance (adsorbate) on the surface of other (adsorbent); and absorption is diffusion of the absorptive into the structure of bulk phase (adsorbent) [66].
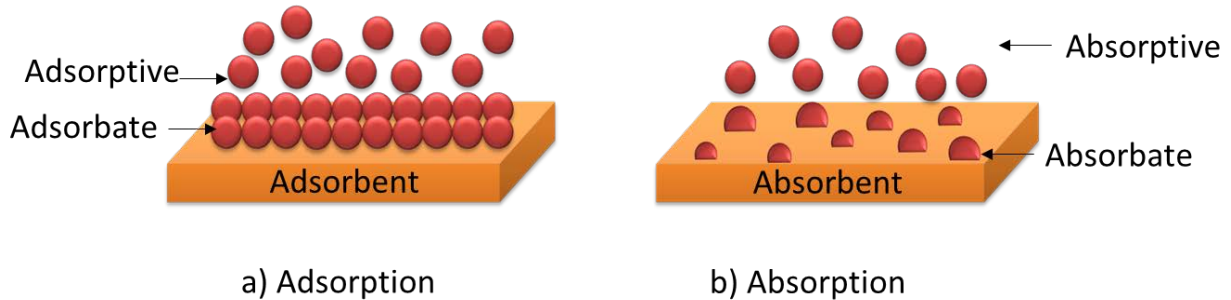
Figure 7. Schematic of a) adsorption and b) absorption [66]

2.4.1. Types of adsorption

The adsorption of gases on solid surfaces depends on the temperature, pressure, nature and surface area of the adsorbent, and the nature and critical temperature of the adsorbate. The amount of gas adsorbed on a given solid surface decreases with increasing temperature. This phenomena can be explained by the equilibrium between the gas in contact with the solid and the adsorbed gas at any given temperature and pressure [67].

Adsorption process at the solid-gas interface is classified into two categories, based on the strength of interaction between adsorbent and adsorptive: chemical adsorption (chemisorption) and physical adsorption (physisorption) [67].

2.4.2. Adsorption isotherms

An adsorption isotherm is the amount of gas adsorbed as a function of relative pressure at a given temperature. The common types of adsorption isotherms observed experimentally in the adsorption of gases by solids are shown in Figure 8 [67]. In the past few years, new subclasses of these isotherms have been introduced but are not mentioned here, see [68]] for further information. Adsorption isotherms are useful for porous solid characterization and industrial adsorption processes design [68].

13
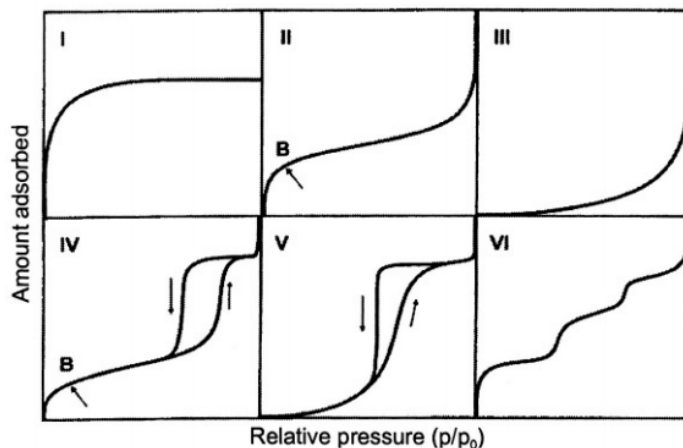
Figure 8. Main types of gas physisorption isotherms (IUPAC) [69]

- Type I isotherms are characterized by a concave shape with respect to relative pressure. The curve has a sharp rise at low relative pressure to reach a plateau [68], which is observed for microporous adsorbents. Due to the small pore size, a single monolayer of adsorbate fills the pores and there is no multilayer adsorption [68][70].

- Type II isotherms are associated with disperse, nonporous, or only macro-porous solids (pore diameter >50 nm) with monolayer adsorption at low pressures, and near saturation multilayer adsorption at higher pressures [70].

- Type III isotherms are observed in systems where adsorbent-adsorbate interaction is small [70].

- Type IV isotherms are described as the creation of single monolayer of adsorbent in microspores at lower pressures and capillary condensation of adsorbent in mesopores with hysteresis between adsorption-desorption [70]. Adsorption of water on silica gel or $CaCl_2$-silica gel is an example for this type of isotherm.

- Type V isotherms have similar behavior as type IV isotherms with a small difference in hysteresis in adsorption-desorption [68].

- Type VI isotherms are associated with layer by layer adsorption on highly uniform surfaces [68].

2.4.3. Measuring the surface area from the isotherms

One of the main parameters that should be determined is the specific surface area of the adsorbents. The surface area of an adsorbent can be interpreted from the equilibrium data based on theories which predict the number of adsorbate molecules that cover the solid surface with a single molecular layer. The common methods to calculate surface area are Langmuir and BET (Brunauer, Emmett, and Teller) [71].

The Langmuir adsorption model describes type I isotherms and assumes that adsorption is limited to a monolayer. Chemisorption always exhibits a Type I isotherm. This model is not valid for Type II to V isotherms. Brunauer, Emmett, and Teller, in 1930, extended Langmuir's kinetic theory to multilayer adsorption. The BET theory assumes that the uppermost molecules in adsorbed stacks are in dynamic equilibrium with the vapor. This means, where the surface is covered with adsorbate molecules, it is in equilibrium with vapor, and when the second layers are adsorbed, the upper layer is in equilibrium with vapor, and so forth [71].

The BET equation in its final form is [71],

$$\frac{1}{W[(\frac{P_0}{P}-1)]} = \frac{1}{W_m C} + \frac{C-1}{W_m C}(\frac{P_0}{P}) \qquad\qquad \text{Eq.1}$$

Where W is the weight of the adsorbed gas, P/P_o is the relative pressure of adsorbate at the temperature of adsorption, W_m is the weight of adsorbate as monolayer, and C is the BET constant.

To determine BET surface area, a plot of $1/[W(P_o/P)\text{-}1]$ versus P/P_o will yield a straight line usually in the range of $0.05 \leq P/P_o \leq 0.35$, as shown in Figure 9a. The adsorption isotherms of three different silica gel particles with different pore size are presented in Figure 9b. Surface characteristics of silica gel particles provided from Silicycle Inc. are shown in Table 4.

Table 4. Surface characteristics of silica gels determined from N$_2$ adsorption-desorption isotherms and material specifications for silica gel lots R10070B-011112, R10070D-080613 and R10072H-111009 provided by Silicycle, Inc.

Sample	S$_{BET}$ (m^2/g)	V (cm^3/g)	D (nm)	Product Specifications S$_{BET}$, V, particle size, D
SilicaFlash B60	490.27	0.77	4.8	514 m^2/g, 0.75 cm^3/g, 0.2-0.5 mm, n/a
SilicaFlash B90	395.35	0.84	6.3	392 m^2/g, 0.83 cm^3/g, 0.2-0.5 mm, 8.4 nm
SilicaFlash B150	256.77	1.10	12.8	271 m^2/g, 1.10 cm^3/g, 0.25-0.5 mm, 16.2 nm
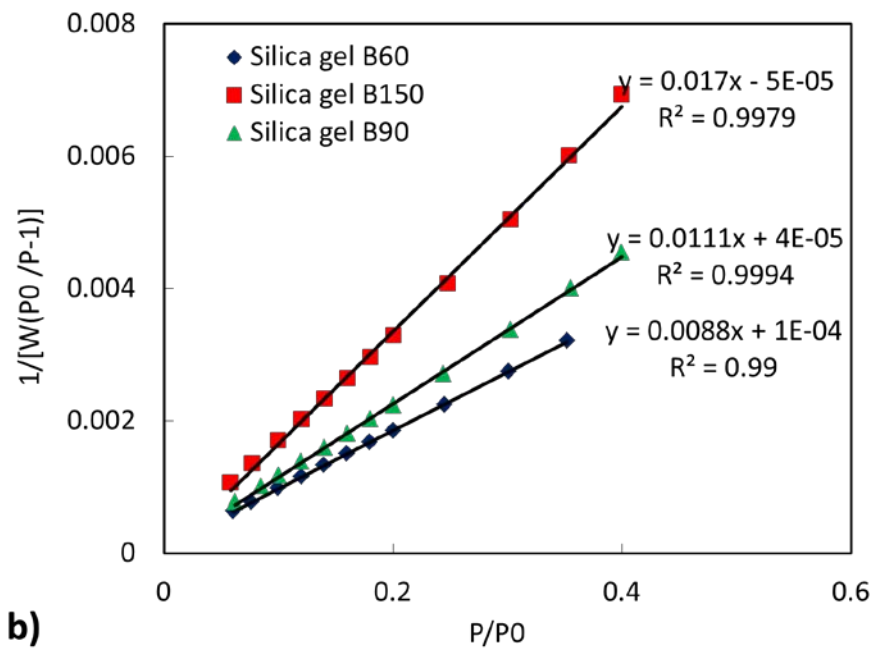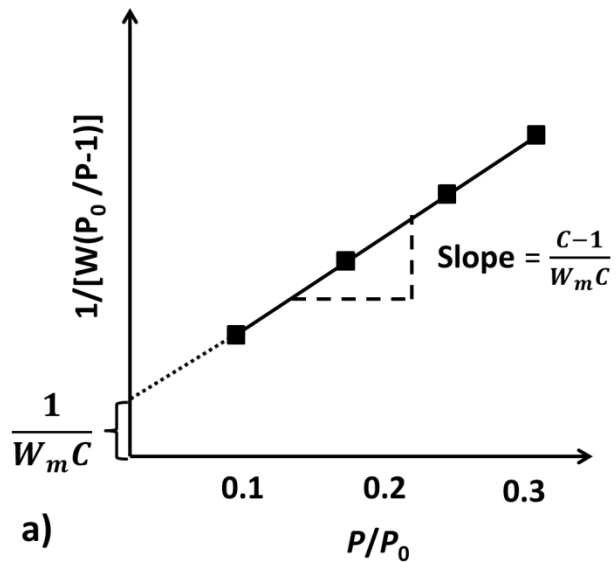
Figure 9. a) A typical BET plot [71], b) Adsorption isotherms of silica gel with different pore sizes including SiliaFlash B60, B90 and B150

The slope, *s*, and the intercept, *i*, of a BET plot are [71];

$$s = \frac{C-1}{W_m C}$$ Eq. 2

Eq. 3

$$i = \frac{1}{W_m C}$$

From the above equations, the weight adsorbed in a monolayer, W_m, and the BET constant, *C*, can be calculated [71].

Eq. 4

$$W_m = \frac{1}{s+i}$$

Eq. 5

$$C = \frac{s}{i} + 1$$

The total surface area can be calculated as follows [71]

Eq. 6

$$S_t = \frac{W_m N A_{cs}}{M}$$

Where *N* is Avogadro's number (6.0233×10^{23}), *M* is the molecular weight of the adsorbate, and A_{cs} is the adsorbate cross sectional area (16.2 Å^2 for nitrogen).

The specific surface area, S_{BET}, is determined by dividing the total surface area by the sample weight [71].

Eq. 7

$$S_{BET} = \frac{S_t}{w}$$

2.5. Adsorbent bed design and performance enhancement techniques

2.5.1. Adsorber bed configuration

Sorption cooling systems consist of the evaporator, the condenser, and the adsorber bed. Among these three components, adsorber bed is particular, and the rest are similar to the conventional systems. The major challenge in solid/vapor adsorber bed is the poor heat transfer. Heat and mass transfer have major roles in systems performance. There are three types of adsorber bed configuration designs in literature which will be explained in this section.

2.5.2. Unconsolidated adsorber bed (fixed bed)

In an adsorber bed, adsorbents are packed between the lamella of a heat exchanger, and a metal mesh is used to hold the adsorbent in place, as shown in Figure 10. The major disadvantage is the poor thermal contact between the adsorbent and the heat exchanger surface, which leads to a low heat transfer coefficient and heat transfer limited sorption kinetics [72].
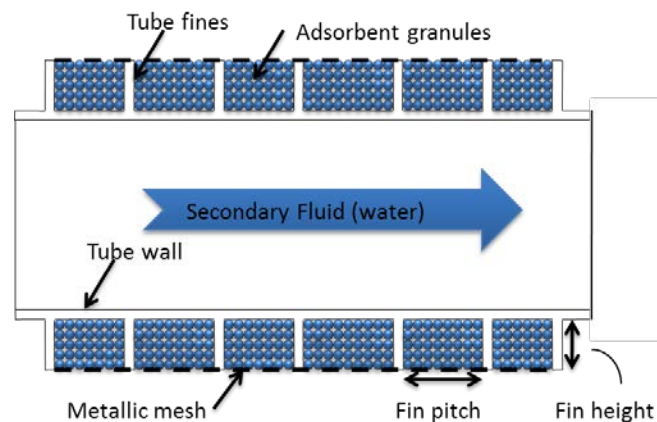
Figure 10. Fixed bed example [72]

To improve the heat transfer, different approaches have been utilized, including [72]:

- Mixing various grain size adsorbents in a multimodal distribution;
- Using metal inserts; and
- Using composite adsorbents with high thermally conductive additives.

2.5.3. Consolidated adsorber bed

The main difference between a consolidated and unconsolidated adsorber bed is the presence of a binder, and the preparation procedure of the adsorbent (compression, moulding or metal foam confinement). Dramatic increase in the thermal conductivity of the adsorbent can be seen while pores are blocked by the binder and sorption performance is reduced. Furthermore, permeability, pressure drop, and the mechanical stability of the adsorbent may occur and should be considered. The solutions for better sorption performances are using small segments of the adsorbents and optimizing the adsorbents thicknesses [72].
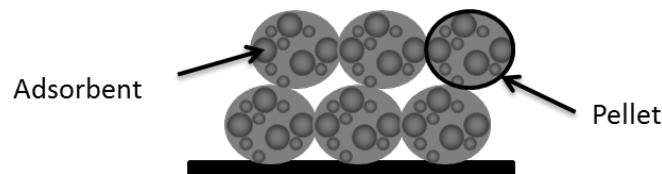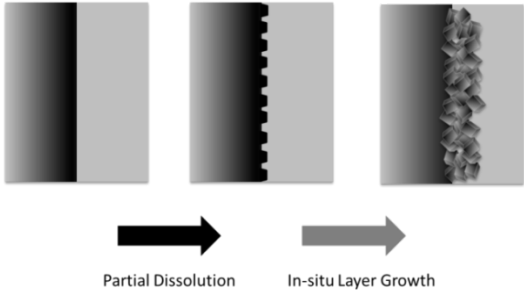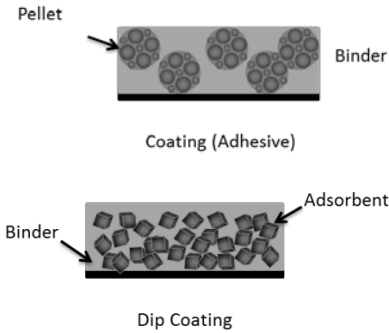
Figure 11. Schematic of a consolidated adsorbent in contact with a heat exchanger surface [72]

2.5.4. Coated adsorber bed

Coating adsorbent on to the surface of the adsorber bed is another configuration. Heat transfer performance is improved in this system, but there will be a noticeable decrease in water uptake rates [73]. For coatings with composite adsorbents, the main issue is choosing a proper binder composition; concentration and thickness should be controlled.

Table 5. Classification of the sorption heat exchanger coating methods [72]

Name	Definition	Schematic
In-situ	Growing an adsorbent layer on supports from gels or solutions containing the reactants for adsorbent formation	Partial Dissolution In-situ Layer Growth
Ex-situ	Gluing adsorbent on a surface or dip coating a surface in a suspension containing adsorbent and binder	Pellet — Binder — Coating (Adhesive) — Binder — Adsorbent — Dip Coating

Recent studies of sorption coatings are summarized in Table 6 which shows the effect of binder on adsorbent performance. Freni et. al performed durability study on coated heat exchanger for 35000 cycles with consistent sorption capacity [74].

Table 6. Composite coating adsorbents reported in the literature

Composite	Coating technique	Water sorption tests	Results	Ref.
SAPO34 (zeolite) and 10% N-propyl-trimethoxy-silane binder	Dip coating	30-150°C 11 mbar	• S-shape isotherm • SAPO34: ~27 wt% water uptake at 30 °C, ~25 wt% uptake for 10 wt% binder sample	[75]
Mitsubishi ASQOA FAM-Z02 and 15 wt% clay based binder	1. MPI coating by Mitsubishi Plastics 2. ITAE coating by CNR-ITAE	20-160°C 10, 25 mbar	• S-shape isotherm • Uptake at 20°C, 10 mbar: FAM-Z02 ~26 wt%, MPI coating ~24 wt%, ITAE coating ~24 wt%	[74]
Silica gel and 0.5-1 vol.% tetraethyl-orthosilicate binder	Electrophoretic deposition (EPD)	25°C P/P_0=0-1 (31 mbar)	Uptake at P/P_0 ~1: • Silica gel: ~ 0.5 g/g • TEOS free silica gel: ~0.48 g/g • 0.5 v% TEOS silica: ~0.48 g/g • 0.1 v% TEOS silica:~ 0.4 g/g	[76]
Aluminium phosphate (AIPO-18) and 6 wt% polyvinyl alcohol binder	Coating suspensions deposited by pipette on substrate	9-15°C 11.5,17mbar	• Mass flow decreases with increasing adsorbent thickness	[77]

2.6. The parameters that affect the adsorbent bed performance

The majority of the commercial sorption cooling systems use a granular adsorbent packed in a finned-tube heat exchanger. However, the high contact thermal resistance between granules and the heat exchanger surface remains a major challenge [78]. Several methods to improve heat transfer have been investigated, such as synthesizing adsorbent on the heat exchanger surface, consolidating sorbents by compacting them with thermally conductive materials into a solid matrix [79], and coating the heat exchanger surface with a composite adsorbent. The first two methods improve the heat transfer performance, but can decrease the water uptake rate [80]. For coatings with composite adsorbents, the main issue is choosing a binder composition and concentration without blocking pores.

2.6.1. Pore size and geometry

Significant progress in material science allows the formulation of tailored adsorbents with specific properties for better performance. Composite "salt confined in a porous matrix" adsorbents have been studied for sorption cooling systems. The properties of these types of adsorbents depend on the chemical nature and amount of the confined salt, the matrix composition, and the pore size distribution.

Aristov et al. performed a detailed analysis of the pore size and geometry effect on $CaCl_2$/silica gel water sorption properties [81] and compared their data with other composite adsorbents, Figure 12. $CaCl_2$/SBA-15 (11.8 nm) has faster water uptake rate in comparison with Fuji silica gel type of RD and SWS-1L ($CaCl_2$ confined KSK silica gel with twisted channel pores), due to the straight mono-size channels pores. Thermophysical properties of the mentioned adsorbents are presented in Table 6 [81][16].
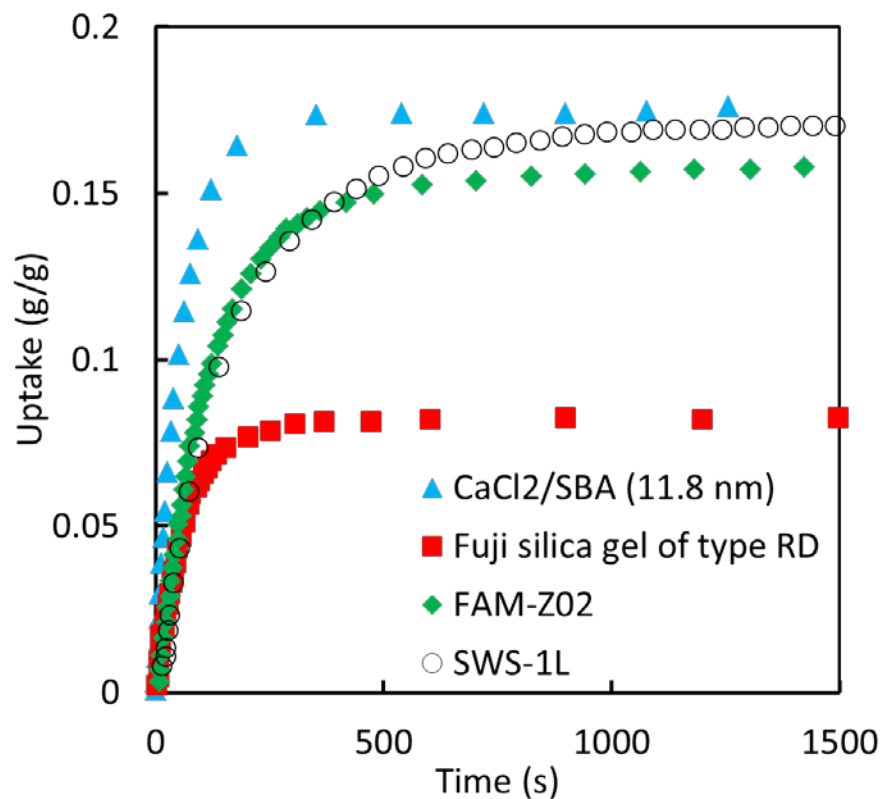
Figure 12. Water uptake kinetics of the adsorbents for 60°C to 35°C temperature jump with 1.23 kPa water vapor pressure [81]

Table 7. Textural properties of the adsorbents calculated by the BJH and BET methods [16][81]

Adsorbent	Specific surface area (S_{BET}) ($m^2 \cdot g^{-1}$)	Pore volume ($cm^3 \cdot g^{-1}$)	Average pore diameter (nm)
CaCl$_2$/SBA (11.8 nm)	483	0.66	11.8
Fuji RD	820	0.4	2.2
SWS-1L	230	0.6	15
FAM-Z02	N/A	N/A	0.38

2.6.2. Effect of the hygroscope salts on the water uptake capacity of adsorbent materials

Detail studies on hygroscopic salts confined in porous host matrixes for sorption systems have been performed at the Boreskov Institute of Catalysis and ITAE/SNR in Messina, Italy [82].

The properties of this family of materials depends on the structure of host matrix, the chemical nature of salt and the amount of salt content [48][83]. Cortes et. al [43] and Aristov et. al [48] compared different salt and silica gel compositions for water based sorption cooling systems and concluded that 33 wt% of $CaCl_2$ in mesoporous silica gel is an effective sorbent. Ponomarenko et al. prepared $CaCl_2$ confined in SBA-15 silica gel with water sorption capacity of 0.47 g/g at 50°C and water vapor $P/P_0 < 0.3$ [84]. Temperature swing water sorption tests (60°C to 30°C) with vapor pressure of 1.23 kPa have been performed to compare $CaCl_2$/SBA (mesoporous silica gel, average pore diameter 11.8 nm) with microporous silica gel (Fuji RD) under sorption system operating conditions. The $CaCl_2$/SBA has over twice the specific cooling power calculated from the measured sorption rate [85]. SWS-1L (30 wt% $CaCl_2$ in mesoporous silica gel) demonstrated the coefficient of performance (COP) 0.6 at desorption as low as 85-95°C in compare to silica gel-water and zeolite-water systems at low temperature heat generation [48]. Freni et al. provided a detailed comparative study on the most promising working pairs for thermal driven adsorptive heat pump, air conditioning and refrigeration applications [86]. For air conditioning and pumping purposes working with water as adsorbate, the highest heating/cooling COP up to 1.62/0.71 is reported for AQSOA-FAM Z02, silica gel-LiBr and silica gel- $CaCl_2$ [86].

Ponomarenko et al. prepared $CaCl_2$ confined in SBA-15 silica gel with water sorption capacity of 0.47 g/g at 50°C and water vapor $P/P_0 < 0.3$ [84]. Temperature swing water sorption tests (60°C to 30°C) with vapor pressure of 1.23 kPa have been performed to compare $CaCl_2$/SBA (mesoporous silica gel, average pore diameter 11.8 nm) with microporous silica gel (Fuji RD) under sorption system operating conditions. The $CaCl_2$/SBA has over twice the specific cooling power calculated from the measured sorption rate [85]. SWS-1L ($CaCl_2$ in mesoporous silica gel) demonstrated the coefficient of performance (COP) of 0.6 at desorption as low as 85-95°C in compare to silica gel-water and zeolite-water systems at low temperature heat generation [48].

The mass and heat transfer performance of the adsorbent-adsorbate system highly depends on the inter-particle and intra-particle porosity of the host matrix, as well as the thickness of the layers of free or consolidated sorbent coating in the adsorber bed. For loose grain adsorbent-heat exchanger designs, sorption kinetic studies have revealed that for grain sizes below 0.5-0.8 mm, the kinetic curves do not change appreciably, for example, one layer of 0.8 mm silica gel grains can deliver the same specific cooling power as four layers of 0.2 mm grains [87][88][89]. The sorption rate depends on the transport of water vapor in the porous matrix and the dissipation of the heat of adsorption. In the case of salt in silica gel composites, absorption of

water vapor by the salt dispersed in the porous matrix creates a solid hydrate, and then an aqueous solution [44]. The solution formation complicates sorption kinetics compared to water sorbed by silica gel or zeolite surfaces. Ilis et al. numerically modelled adsorbate concentration, pressure, and temperature in silica gel adsorber beds to determine the optimum particle size and the bed thicknesses [90]. Sharafian et al. presented a new compact relationship, with a good agreement with available analytical solutions, to predict the adsorbate uptake rate and the mass diffusivity, utilizing a resistance-capacitance (RC) model [91]. The impact of the silica gel particle size and the layer thickness on the heat and mass transfer for sorption cooling applications has been studied experimentally by Chang et al. [92].

2.6.3. Thermal properties of loose grain and consolidated composite

The majority of sorption cooling systems use a granular adsorbent in a packed bed design. These systems have high mass transfer rates, however high thermal resistance between granules and the heat exchanger surface and low thermal conductivity of adsorbent grains remain major challenges [78]. The thermal conductivity of sorbents has a great impact on the dynamic performance of the sorption systems. Different methods to improve the heat transfer have been investigated, such as binding [78][93][94] or synthesizing adsorbent [40] onto the heat exchanger surface [95], confining adsorbent into the thermally conductive porous matrix [96][97], and adding thermally conductive materials, such as metal additives [73][98]. These methods improve the heat transfer performance, but can decrease the water uptake rate [80].

Aristov et al. observed that the thermal conductivity of zeolite with 40 wt% aluminum hydroxide is 0.43 $W \cdot m^{-1} \cdot K^{-1}$ which is greater than the thermal conductivity of the zeolite with 40 wt% graphite or 40 wt% PTFE (polythetrafluoroethylene) 0.36 and 0.25 $W \cdot m^{-1} \cdot K^{-1}$, respectively [93]. The thermal conductivity of the composite adsorbents made using a sol-gel process with copper nano-powder were measured by the transient plane source (TPS) method and showed 20% enhancement in the thermal conductivity compared to the composites without additives [99]. Effective thermal conductivity of the unconsolidated adsorbent improved from 0.106 to 0.363 $W \cdot m^{-1} \cdot K^{-1}$, by adding 15 wt% shaved aluminum [100]. The effective thermal conductivity of calcined silica gel (KSK) and $CaCl_2$ composite was measured by Aristov et al. [101], using the transient hot wire method at 290-300 K with 0.1 to 0.8 g/g water content. The thermal conductivity of sample increased from 0.1 to 0.5 $W \cdot m^{-1} \cdot K^{-1}$ with increasing water content. Tanashev et al. showed that the thermal conductivity of $CaCl_2$/silica gel KSK increased from 0.13 $W \cdot m^{-1} \cdot K^{-1}$ to 0.5 $W \cdot m^{-1} \cdot K^{-1}$ as

absorbed water content increased from 0.1 g/g to 0.8 g/g [42]. Freni and Aristov et al. [102] measured the thermal conductivity of consolidated sorbents, silica gel (KSK) with 36.6 wt% $CaCl_2$ and silica gel (KSK) with 42.7 wt% LiBr and observed that the thermal conductivity increased significantly as the water uptake of the sorbent increased, while the effect of temperature and pressure on thermal conductivity was almost negligible. Thermal conductivity of a wide range of adsorbents, reported in literature, are shown in Table 8.

It can be seen in Table 8 that the composite adsorbent with expanded graphite has higher thermal conductivity in comparison with silica or zeolite based composites while by adding activated carbon, the thermal conductivity increases considerably [103][104][105] .

Table 8. Thermal conductivity of the adsorbent materials

Adsorbent material	Thermal conductivity $W \cdot m^{-1} \cdot K^{-1}$	Measurement method and experiment condition	Ref.
Calcined silica gel (KSK)/CaCl$_2$	0.1-0.5	- Transient hot wire method - Water content (0-0.8 g/g) - Temperature 16-27°C	[101]
Consolidated silica gel (KSK)/CaCl$_2$ (36.6 wt%)	0.12-0.16	- Transient hot wire method - Air pressure: 10-1000 mbar - Binder: 20%wt aluminium hydroxide	[102]
Consolidated silica gel (KSK)/LiBr (42.7 wt%)	0.1-0.13		
Consolidated silica gel (15% binder)	0.24-0.26	- Guarded-hot plate apparatus - Silica gel coated between copper plates - Temperature: 35-50°C - Contact pressure: 0-90 bar - Polyvinylpyrrolidone used as a binder	[78]
Compressed silica gel (KSK)/CaCl$_2$ Compressed silica gel (KSK)/LiBr Compressed silica gel (KSK)/MgCl$_2$ Alumina/CaCl$_2$	0.12-0.5 0.16-0.4 0.14-0.42 0.12-0.41	- Transient hot wire method - Measurements took place at 16-27°C - Water content (0-0.9 g/g) - No binder used	[42]
Wetted Zeolite 4A	0.17-0.25	- Transient hot wire method - Filling gas :air at 1 bar - Measurement temperatures (50-200°C) - Water content (0.02-0.2 g/g)	[106]
Consolidated composite activated carbon	1-4	- ASTM E1530 guarded thermal flow meter method - Samples with different ratio of activated carbon were made (33-50%)	[103]
Consolidated composite activated carbon	0.9-2.5	- The guarded hot plate method - Samples with different ratio of activated carbon and expanded graphite were made	[104]
Pure CaCl$_2$ (powder) Pure CaCl$_2$ (pellet) Composite-KP50 expanded graphite (20%) and CaCl$_2$ Consolidated composite-KP50 expanded graphite (20) and CaCl$_2$	0.31-0.39 0.11-0.14 0.4-0.47 0.31-0.47	- Transient hot wire method - Filling gas :air at 1 bar - Measurement take place at different temperature - Different pressure applied for making consolidated samples (0-0.67-20) - Used dry samples	[105]

Thermal diffusivity is defined as: $\alpha = k/\rho c_p$, where k, ρ, and c_p are thermal conductivity, density and specific heat, respectively. Table 9 shows the specific heat, density and thermal conductivity of adsorbents reported in the literature for a number of sorbents. Thermal properties of silica gel 125 from W. R. Grace Ltd. were measured with transient hot-Strip at 22°C when water content of silica gel increased from 0.008 to 0.329 g/g by Carlsson et. al [107]. Specific heat of silica gel 125 increased from 860 to1650 J·kg^{-1}·K^{-1} by increasing water content [107]. Thermal properties of three different silica gels, namely, Type A, Type 3A and Type RD are measured by Ng et. al. [108]. Although the reported specific heat of the three silica gels types is the same, their performance in a sorption system could be different, as it is highly dependent on the surface physical properties such as: particle size, pore diameter and its distribution, specific surface area and pore volume [108]. Specific heat of hygroscopic salts ($CaCl_2$) confined to silica gel (KSK) was measured at anhydrous and hydrated states by Aristov et. al [109].The measurements are obtained over the temperature range of -257°C to 30°C with a vacuum adiabatic calorimeter. Specific heat of anhydrous composite increased from 20 to 733 J·kg^{-1}·K^{-1} by increasing temperature when in hydrated state specific heat raised from 15 to 1007 J·kg^{-1}·K^{-1} in similar condition [109]. Novel water adsorbent Zeolite-based materials (FAM Z01 and FAM Z02) were developed for Adsorption Heat Pump (AHP) and desiccant air conditioning system by Kakiuchi et. al. [110] [111]. Heat insulation type specific heat measurement apparatus (SH3000 of Shinku Riko Inc.) was utilized to measure specific heat and a hot wire apparatus (ARC-TC-1000 of Agne Gijutu Cneter Inc.) for thermal conductivity measurements. Specific heat of FAM Z01 and Z02 were reported 805 and 822 J·kg^{-1}·K^{-1} at 30°C [110] [111].

Table 9. Thermal properties of adsorbent reported in the literature

Adsorbent	c_p (J·kg^{-1}·K^{-1})	ρ (kg·m^3)	k (W·m^{-1}·K^{-1})	Application	Ref.
Silica gel 125	860-1650	868-1113	0.164-0.265	Absorption heat pump	[107]
Silica gel 127B	960	825	-	Thermally Driven Chillers	[112]
Silica gel Type RD	921	800	0.198		
Silica gel Fuji Type A	921	730	0.174	Adsorption Chillers	[108]
Silica gel Fuji Type 3A	921	770	0.174		
Silica gel Type RD	921	700	-	Adsorption desalination systems	[113]
Silica gel KSK-CaCl$_2$	1000	1300	-	Sorption cooling system	[56]
Silica gel KSK-CaCl$_2$	20-733 (-257-30°C)	-	-	Low temperature heat capacity of the system	[109]
Silica gel KSK-CaCl$_2$·2.04H$_2$O	15-1007 (-258-28°C)	-	-		
Zeolite FAM Z01	805	600-700	0.113 (30°C)	Adsorption Chillers	[111]
Zeolite FAM Z01	805 (30°C)	-	0.113 (30°C)	AHP and	
	896 (70°C)	-	0.123 (70°C)		[110]
Zeolite FAM Z02	822 (30°C)	-	0.117 (30°C)	Desiccant air conditioning system	
	942 (90°C)	-	0.128 (90°C)		

To the best of our knowledge, the open literature lacks the information on thermal properties of consolidated composite adsorbent containing graphite flakes.

2.7. Major parameters to evaluate the performance of sorption cooling systems

Two major parameters to evaluate the overall performance of sorption cooling systems are (SCP) and (COP).

Specific Cooling Power (SCP)

Specific cooling power can be calculated from the ratio of evaporative cooling energy to the dry mass of adsorbent multiplied by cycle time (W /kg dry adsorbent) [1]. Sorption rate and cycle time are the main factors that can affect SCP which depends of application (e.g. automotive application cycle time is 20 min). Sorption rate can be improved by decreasing heat and mass transfer resistance within sorber bed as well as synthesizing tailored sorbent with high sorption rate [1][114].

The SCP of sorption cooling systems should be enhanced since the foot-print and system weight has great importance. Common value reported for the SCP of heat driven sorption cooling systems is 80-500 W/kg dry sorbent [1].

Coefficient of Performance (COP)

The efficiency of sorption cooling cycle can be evaluated from the ratio of evaporative cooling energy to the amount of supplied heat. This parameter is important when the supplied energy is costly and limited while in waste-heat driven sorption cooling systems the supplied energy is provided from waste heat, solar or geothermal energy. The COP of waster-heat driven sorption cooling system is less than vapor compression systems. Reported value in literature for COP is about 0.1-0.6. However, sorption cooling systems with high COP are preferred [1].

Table 10 is the summary performance of existing sorption cooling systems reported in literature. Systems with consolidated [115] and coated [116] [117] sorbent have higher specific cooling power as a result of higher thermal diffusivity and lower thermal contact resistance between bed and sorbent. Aristov et al. tested adsorption and desorption rate of activated carbon consolidated with binder compared with loose grain and concluded that presence of binder improves dynamic

sorption/desorption of material by factor of 1.5-3.5 [118]. When binder and/or other additives are used to increase the heat transfer rate, there is an associated the decrease in equilibrium uptake capacity of the overall composite adsorbent due to the added non-adsorbing material. However, the optimum composition depends on the dynamic sorption performance. Improvement in the heat and mass transfer of a consolidated adsorbent can also enable sorber bed configurations with lower thermal inertia (e.g. wider fin spacing).

Table 10. Summary of existing sorption cooling systems performance

Working pairs	Adsorbent configuration	COP	SCP	Ref.
Silica gel-water	Loose Grain	0.43	48	[119][120]
Silica gel-water	Loose Grain	0.29	35	[121]
Silica gel-water	Loose Grain	0.29	158	[122]
Silica gel-water	Loose Grain	0.42	122	[123][124]
Silica gel-water	Loose Grain	0.31	46	[125]
Silica gel-water	Loose Grain	-	146	[126]
Silica gel-methanol	Loose Grain	-	30	[127]
SWS-1L-water	Loose Grain	0.43	23	[128]
SWS-1L-water	Coated	0.15	137	[116]
Silica gel+CaCl$_2$-water	Loose Grain	0.23	43	[129]
Silica gel+LiCl-water	Loose Grain	0.41	122	[130]
Silica gel+LiCl-methanol	Loose Grain	0.41	76	[123]
Activated Carbon/Ammonia	Consolidated	0.06	33	[131]
Activated Carbon+CaCl$_2$/Ammonia	Consolidated	-	536	[115]
Expanded Graphite+CaCl$_2$/Ammonia	Loose Grain	0.11	7	[132]
Expanded Graphite+CaCl$_2$/Ammonia	Loose Grain	0.16	78	[133]
Expanded Graphite+NaBr/Ammonia	Coated	0.35	296	[117]
AQSOA FAM-Z02/water	Loose Grain	-	2300	[134]
AQSOA FAM-Z02/water	Loose Grain	0.45	330.2	[34]
AQSOA FAM-Z02/water	Loose Grain	-	300-600	[135]
AQSOA FAM-Z02/water	Loose Grain	-	152	[136]

Chapter 3.   Characterization of loose grain CaCl₂-silica gel composite adsorbents

The CaCl$_2$-silica gel composites were prepared utilizing three commercially available silica gels. The surface area, pore size distribution, and CaCl$_2$ crystallinity were examined. Water uptake of the samples was measured with a dynamic vapor sorption analyser and a custom-built gravimetric test apparatus.

3.1.   Sample preparation

Composite silica-supported salt samples were prepared utilizing chromatography-grade commercial silica gels with irregular-shaped grains (0.2-0.5 mm) and average pore diameters of 6, 9 and 15 nm from Silicycle, Inc. (Quebec, Canada). In batches of 100 or 500 g, the dry mesoporous silica was wetted with ethanol, and then soaked with concentrated aqueous CaCl$_2$ solutions. The silica gel salt mixture was placed on open trays in a fume hood and left to dry for 24 hrs. The 500 g batch was warmed with a hotplate to accelerate drying. The concentration and volume of CaCl$_2$ added to the silica was such that complete deposition of the salt into the mesoporous silica would produce a 28% wt CaCl$_2$ product. The damp material was baked at 200˚C until judged to be dry by consistent weight measurements. The mesoporous silica, SiliaFlash types B60, B90 and B150, will be referred to hereafter as S6, S9 and S15; while the silica supported salt composites will be referred to as CaCl$_2$-S6, CaCl$_2$-S9 and CaCl$_2$-S15.

3.2.   Characterization

The specific surface area (S_{BET}), average pore diameter (D), and pore volume (V) of the silica and the silica-supported CaCl$_2$ samples were measured by nitrogen sorption at -196°C in a gas sorption analyzer (Micromeritics ASAP 2020). To degas, all samples were heated under vacuum with 1 hour ramp to 150˚C followed by 2 hours at 200°C. Dry and oil free diaphragm pump (Pfeiffer vacuum MVP015-2) were used for degassing at 0.45 kPa. The BET model was used to calculate S_{BET} [9]. The mesopore volumes were calculated from desorption curves using the Barrett, Joyner and Halenda (BJH) model [137].

X-ray diffraction (XRD) patterns were collected with the Bruker D8 Discover diffractometer with a temperature controlled reactor chamber. The sample holder of thermal vacuum stage is an alumina cup. Diffraction patterns were collected with the silica-supported $CaCl_2$ powder samples with 2θ scans in 0.02˚ steps from 10° to 60° with 2 s signal collection per step. The sample was hydrated by exposure to 43.8% relative humidity (RH) for 4 hours prior to the run. A diffraction pattern was collected at room temperature (23.4°C) and 39.3 %RH. The thermal stage of the XRD then heated the sample to 200˚C and a diffraction pattern was collected after a half an hour drying period. Diffraction patterns were collected from a second sample under vacuum condition, first at 200°C after 1 hour drying period, then after cooling to 30°C without breaking vacuum.

A custom-built gravimetric vapor sorption (VS) test apparatus was designed and used to measure water uptake by 8 to 40 g samples. The custom vapor sorption apparatus consisted of two 500 mL Buchner flasks (sample holder and evaporator), a vacuum pump, valves, temperature controlled bath, pressure gauge, balance, thermocouples (Type T) to monitor the sample and evaporator. The ends of the thermocouples were inserted through a 1/4" X 1/4" heat-resistant rubber strip which adheres to the bottom surface of the flask, in order to ensure that the thermocouples were directly in contact with the adsorbent. The VS apparatus is shown schematically in Figure 13.

Samples were dried in an oven at 180°C, transferred to the VS test apparatus and further dried under vacuum at 200˚C. The samples were cooled to room temperature, and then exposed to water vapor at a controlled pressure. The water in the evaporator flask was maintained at 10°C by a temperature controlled bath to produce a steady supply of 1.1 kPa water vapor. Five thermocouples monitored the temperature of the sample during sorption tests, while the change in the weight of the flask containing the sample was measured with a high capacity analytical balance with 0.01 g resolution. Pressure, temperature, and weight data collection was automated and measurements recorded every second for sorption experiments lasting 3 to 18 hours.
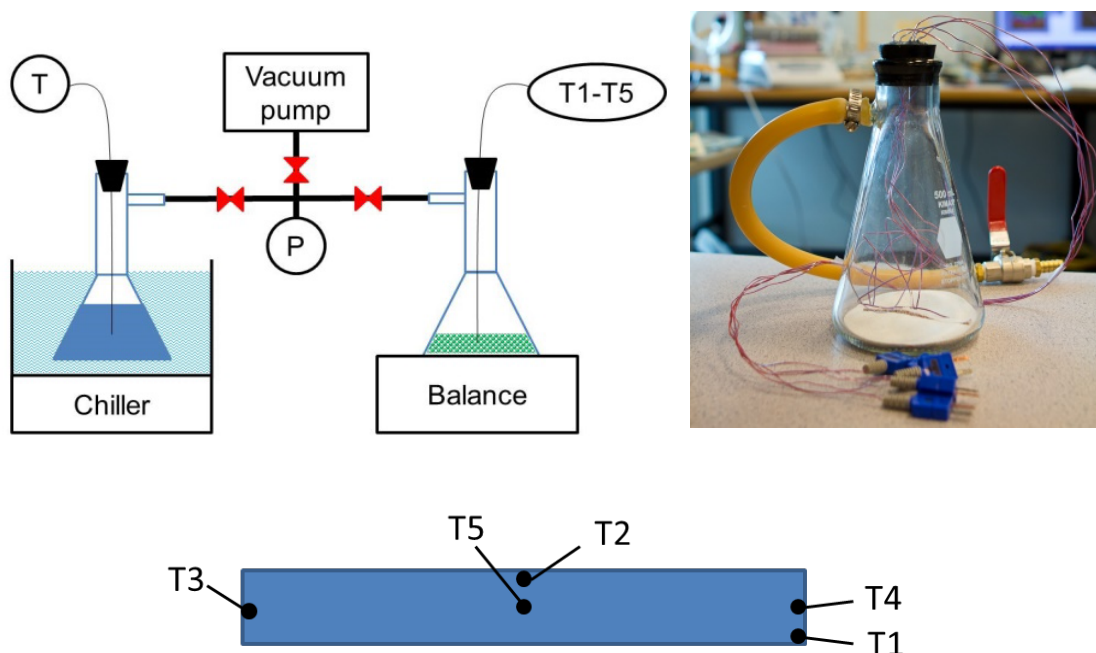
Figure 13. Vapor sorption test apparatus schematic, photo of the flask with adsorbent and thermocouple orientation inside flask.

Table 11. Surface characteristics of silica gels and silica-supported CaCl$_2$ composites. The specific surface area (S$_{BET}$), pore volume (V), and average pore diameter (D) determined from N$_2$ adsorption-desorption isotherms, and material specifications for silica gel lots R10070B-011112, R10070D-080613 and R10072H-111009 provided by Silicycle, Inc.

Sample	S$_{BET}$ (m^2·g^{-1})	V (cm^3·g^{-1})	D (nm)	Product Specifications S$_{BET}$, V, particle size, D
S6	494	0.77	4.8	514 m^2/g, 0.75 cm^3/g, 0.2-0.5 mm, n/a
S9	406	0.84	6.3	392 m^2/g, 0.83 cm^3/g, 0.2-0.5 mm, 8.4 nm
S15	276	1.10	12.8	271 m^2/g, 1.10 cm^3/g, 0.25-0.5 mm, 16.2 nm
CaCl$_2$-S6	134	0.31	7.0	--
CaCl$_2$-S9	148	0.37	7.8	--
CaCl$_2$-S15a	145	0.58	12.8	--
CaCl$_2$-S15b	136	0.59	13.4	--

3.3.   Results and discussion

3.3.1.   Pore size distribution

Differential pore volume distribution curves obtained through analysis of the desorption branch of the N_2 isotherms for the silica and silica-support salt samples are shown in Figure 14 (Appendix A and B). The artifact in each curve at ~ 4.2 nm is characteristic of the nitrogen adsorbate. As summarized in Table 11, in each case, the 28% wt $CaCl_2$ added to the mesoporous silica is distributed within the pores, reducing the specific surface area (S_{BET}) and pore volume. This is consistent with the studies by Ponomarenko et al. [138] and Cortes et al. [43]. Preferential filling of the finest pores increased the average pore diameter of composite samples relative to the supporting silica gels. The addition of $CaCl_2$ increased the average pore diameter from 4.8 to 7.0 nm, and 6.3 to 7.8 nm for S9. $CaCl_2$-S15 was prepared from 100 and 500 g batches of silica gel S15, to produce samples $CaCl_2$-S15a and $CaCl_2$-S15b, respectively. These batches of composite material had consistent pore volume distributions. The average pore diameter specifications for silica gels S9 and S15 provided by the supplier (see Table 11) are greater than those determined by BJH desorption analysis, but agree with the less accurate BET pore sizes calculated from the N_2 desorption isotherms collected from these samples.
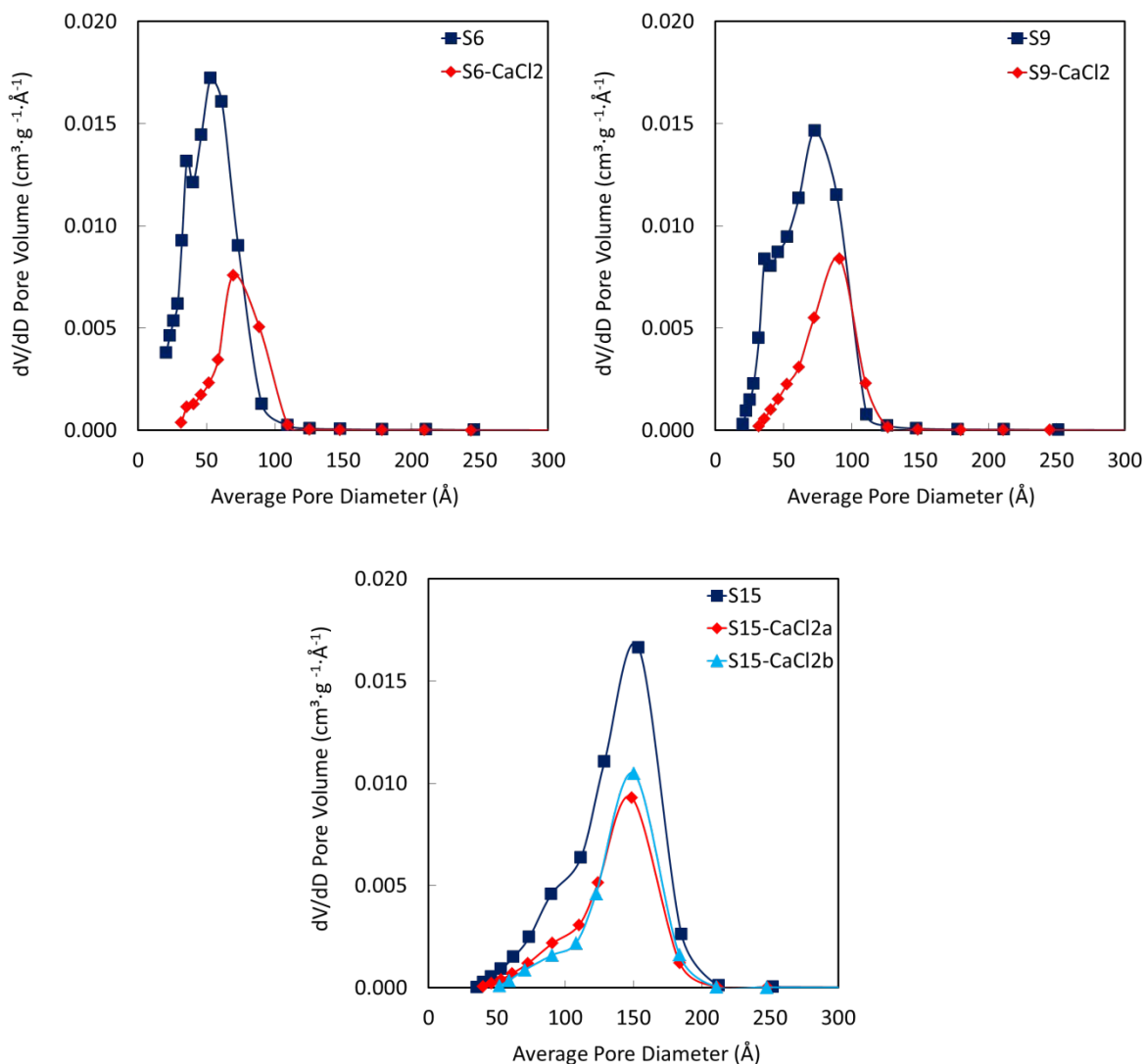
Figure 14. Pore volume dV/dD plots for mesoporous silica gels and silica-supported CaCl₂ (28% wt salt) as determined from N₂ desorption isotherms fit with BJH model s for a) silica S6 and CaCl₂ supported by S6, b) silica S9 and CaCl₂ supported by S9, and c) silica S15 and CaCl₂ supported by S15 prepared in small and large batches.

3.3.2. X-ray diffraction

The XRD patterns of silica-supported $CaCl_2$ sample $CaCl_2$-S15a were collected at room temperature, 23.7°C with 39 %RH, and at 200°C shown in Figure 15a and correspond to $CaCl_2 \cdot 2H_2O$ and $CaCl_2$ diffraction patterns, respectively [139][140]. A broad amorphous silica peak appears at 22°C in all the diffraction patterns. The XRD pattern collected under vacuum at 200°C is consistent with the pattern collected after the sample cooled to 30°C under vacuum (Figure 15b).
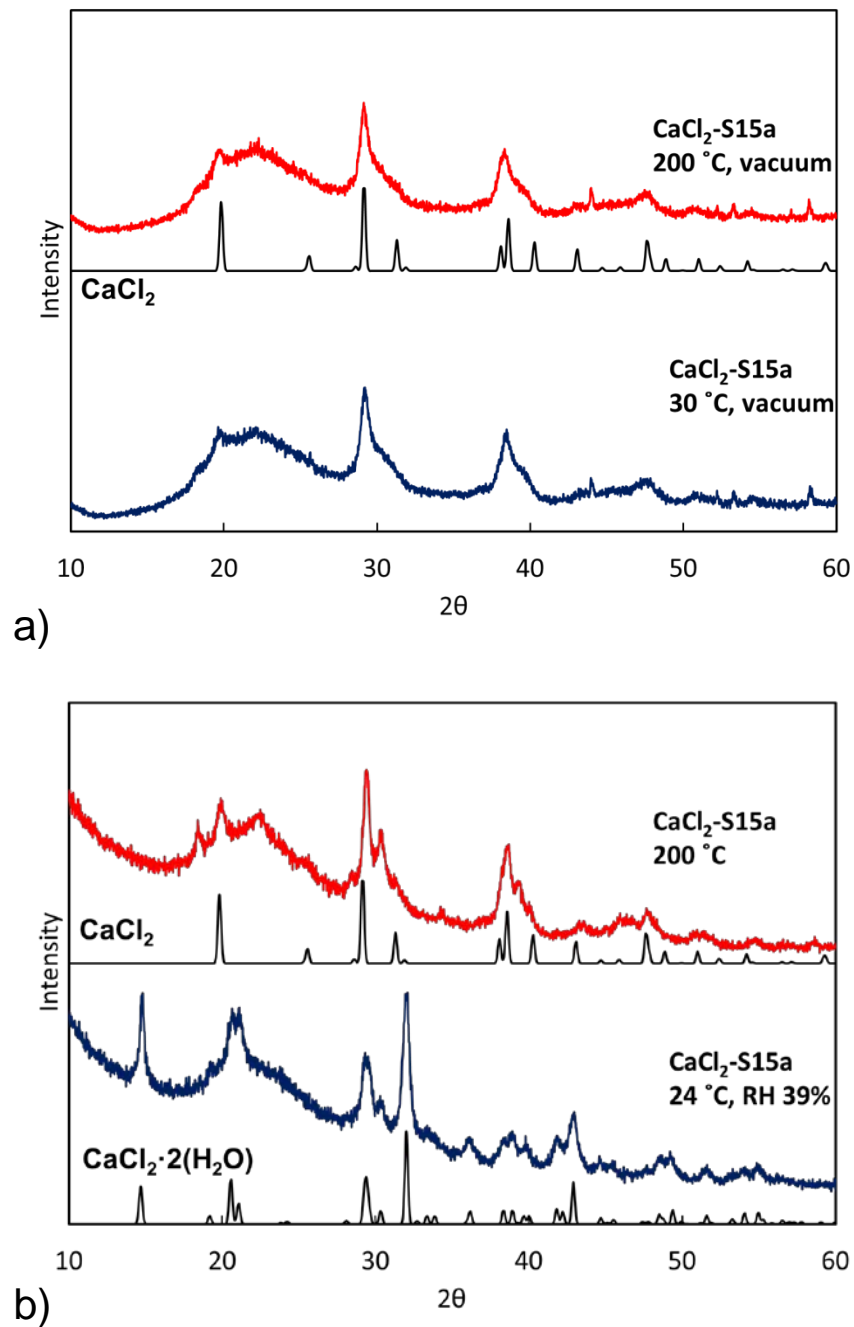
Figure 15. X-ray powder diffraction patterns for CaCl₂-S15a collected at a) 24˚C then heated to 200˚C with ambient 39 %RH and b) 200˚C then cooled to 30˚C under vacuum. Reference diffraction patterns for CaCl₂ [139] and CaCl₂·2(H₂O) [140] are shown for comparison.

3.3.3. Water vapor sorption

The initial vapor sorption rate for 8, 18, and 40 g samples of CaCl₂-S15b are plotted in

Figure **16**. The result for a 20 g sample of the pure silica support is shown for comparison. The powder samples were spread in the 96 mm diameter base of a glass Buchner flask with thicknesses of 1, 2 and 4 mm. The accompanying temperature plots show that the exothermic sorption process elevated the 8, 18 and 40 g samples to maximum temperatures of 46.5, 56.7, and 54.5°C, respectively. After one hour, the 8 g sample absorbed 0.273 g/g of water. The uptake of this sample was 0.406 g/g after 6 hours.
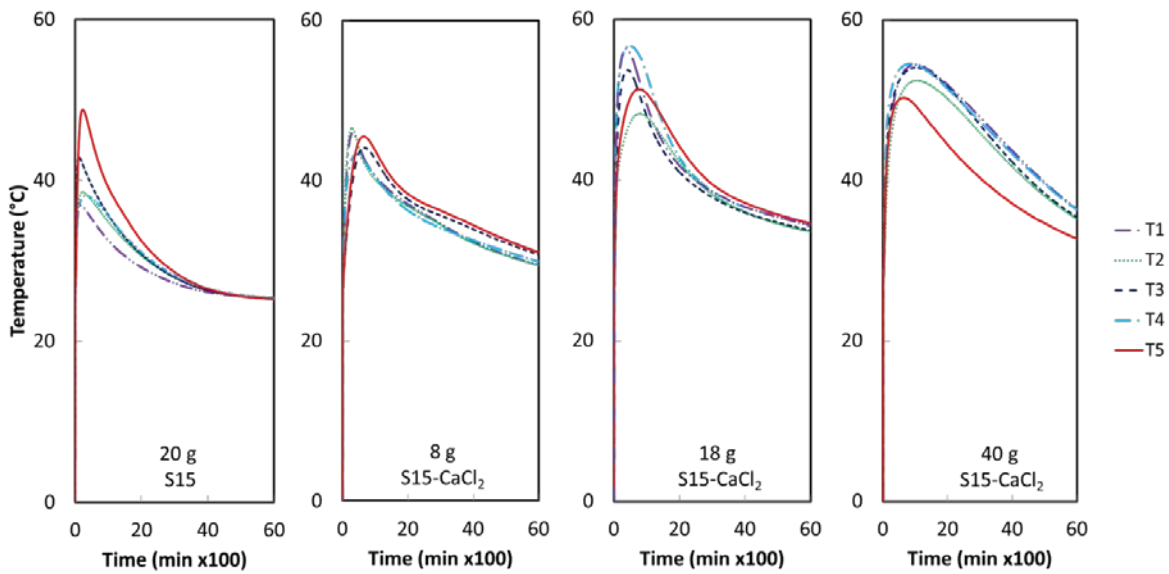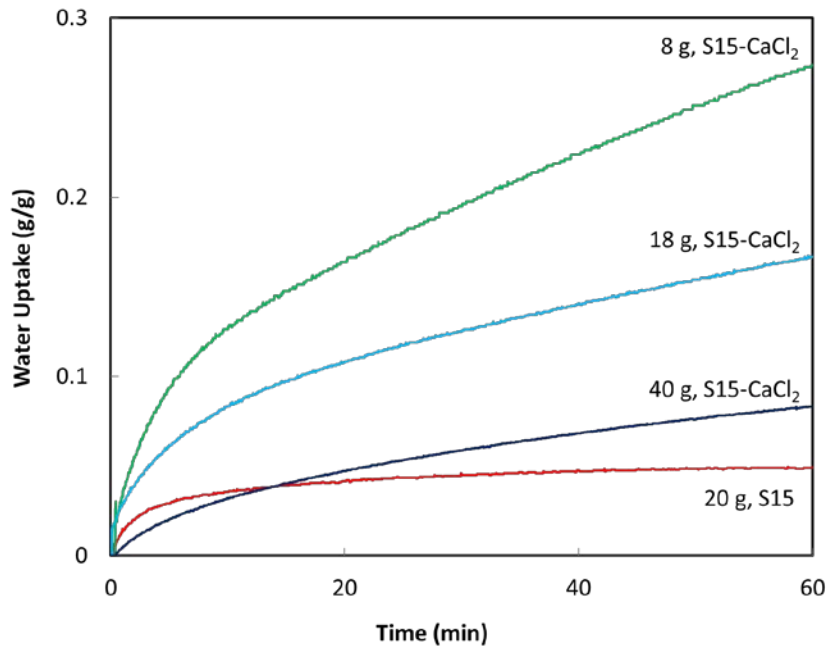
Figure 16. Water uptake (g water/g dry sorbent) and sample temperature plots for CaCl$_2$ supported by silica S15 and pure S15 exposed to 1.1 kPa water vapor illustrate the impact of sample thickness on uptake rate and heat generation and dissipation

3.4. Summary

CaCl$_2$-silica gel composites were prepared from three silica gels and the textural characteristics and water sorption capacity of the composites were evaluated. The CaCl$_2$/silica gel had smaller surface area and greater average pore diameter that the pure silica substrates. The water uptake of the composites was up to 0.40 g/g (1 kPa H$_2$O) at room temperature. A gravimetric vapor sorption apparatus was constructed to study the sorption performance of adsorber bed layers.   In the initial tests, loose grain samples the heat of reaction significantly slowed the water sorption rate of the thicker samples.

Chapter 4.   Consolidated adsorbent containing graphite flakes for heat-driven water sorption cooling systems

Several CaCl$_2$-silica gel composites were prepared with organic binders and thermally conductive additives. The surface area and pore size distribution were examined. Water uptake, multi-cycle performance of the samples, and the thermal conductivity of the composite adsorbents and a mixture of silica gel and graphite flakes (0-20 wt %) were measured at different temperatures.

4.1.   Sample preparation

Composite sorbents were prepared utilizing chromatography-grade commercial silica gel (SiliaFlash® B60, Lot 011112, Silicycle, Inc., Quebec, Canada) with 0.2-0.5 mm irregularly shaped grains and average pore diameter of 6 nm. In batches of 50 g, the dry mesoporous silica gel was wetted with ethanol.   An aqueous solution containing CaCl$_2$ and either 10,000 MW polyvinylpyrrolidone (PVP10) binder (Sigma Aldrich) or 40,000 MW polyvinylpyrrolidone (PVP40) binder (Amresco) was added, and the slurry was dried in a fume hood for 24 hours. The damp materials were oven dried at 180°C for over 2 hours. The composition and volume of solution added to the silica gel were such that the consolidated composite produced was 28 wt% CaCl$_2$ and 15 wt% PVP. Dry silica gel in 4 g batches was combined with PVP (12-15 wt%) and thermally conductive graphite flakes (150 μm, Sigma-Aldrich) or copper powder (<425 μm, Sigma-Aldrich). The graphite flakes added to the composite included both fine particles and thin flakes up to 1.3 mm long, while the copper particles were small (up to 0.41 mm). Consolidated composites with thickness of 3.6 mm were also prepared with and without CaCl$_2$. The slurries were baked for one hour at 50°C until damp or dry, and then heated to 180°C for one hour. The sample names and compositions of the sorbent composites are given in Table 12.

Table 12. Composites prepared with SiliaFlash B60 silica gel matrix

Sample name	Silica gel	$CaCl_2$	PVP	Graphite flakes
S6-0%G	4 g	-	-	-
S6-5%G	4 g	-	-	0.21 g
S6-10%G	4 g	-	-	0.44 g
S6-20%G	4 g	-	-	1 g
S6-$CaCl_2$-PVP10	50 g	25 g	20 g	-
S6-$CaCl_2$-PVP40	50 g	25 g	20 g	-
S6-PVP40-0%G	4 g	-	0.7	-
S6-PVP40-5%G	4 g	-	0.7	0.24
S6-PVP40-10%G	4 g	-	0.7	0.52
S6-PVP40-20%G	4 g	-	0.7	1.175
S6-$CaCl_2$-PVP40-0%G	4 g	1.71 g	1 g	-
S6-$CaCl_2$-PVP40-5%G	4 g	1.71 g	1 g	0.35 g
S6-$CaCl_2$-PVP40-10%G	4 g	1.71 g	1 g	0.74 g
S6-$CaCl_2$-PVP40-20%G	4 g	1.71 g	1 g	1.67 g
				Copper powder
S6-PVP40-0%C	4 g	-	0.7	-
S6-PVP40-5%C	4 g	-	0.7	0.24
S6-PVP40-10%C	4 g	-	0.7	0.52

4.2. Characterization

Nitrogen sorption isotherms of the samples were collected with a volumetric physisorption analyser (ASAP 2020, Micromeritics Instruments) to determine the specific surface area (S_{BET}), average pore diameter (D) and pore volume (V). Prior to testing, the samples were dried under vacuum at 150°C for 1 hour, followed by 2 hours at 200°C. The S_{BET} was calculated with the Brunauer, Emmett and Teller (BET) model while the Barrett, Joyner and Halenda (BJH) model was used to calculate the incremental pore volume from the adsorption curves [137][9]. The composite microstructure was imaged with a scanning electron microscope (FEI/Aspex-Explorer) at room temperature.

A transient plane source 'hot disk' thermal constants analyzer (TPS 2500S, ThermTest Inc., Fredericton, Canada) was used to measure the thermal conductivity, diffusivity and specific heat of the samples (Figure 17 a, b). The 'hot disk', a Kapton encapsulated double spiral nickel wire sensor (design #7577) with a 2 mm radius, is used for both transient heating of the sample and as precise resistance thermometer for simultaneous temperature measurements. The sensor is placed between a pair of identical samples. The roughness of the surfaces should be approximately smaller than the disk diameter by about an order of magnitude. Constant temperature difference develops at the sample-sensor interfaces as a result of contact resistance between the sensor and sample surface. The effect of this constant temperature difference on the measured sample properties is de-convoluted in the calculations [21–23].

Tests were performed in a temperature and humidity controlled chamber. Humidity was monitored in the chamber and controlled by a humidifier (P-10C-1C-2-0-031300-v7, Cellkraft AB, Sweden) with a flow rate of 5 nominal litres per minute. The samples with the thickness of 3.5 mm in average were tested at 5%RH and 20%RH at 35°C. The thermal conductivity of three different areas of each S6-CaCl$_2$-PVP40-G composite sample was tested five times under each condition.

Water sorption isotherms (0-2.7 kPa) for the composite adsorbents were measured using a thermogravimetric vapor sorption analyzer, shown in Figure 18 (IGA-002, Hiden Isochema). Isotherms were collected at 35 and 78°C. Prior to water sorption cycle tests, the samples were dried under vacuum for 6 hours at 90°C and the dry masses were recorded.
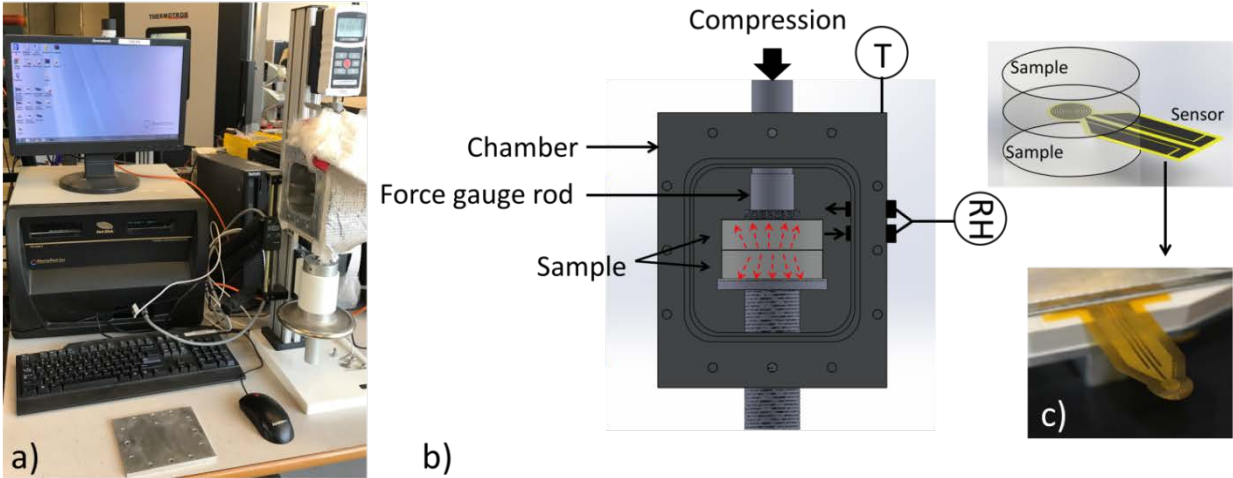
Figure 17. a) Transient plane source (TPS). b) Schematic of TPS. c) Double spiral "hot disk" nickel sensor.
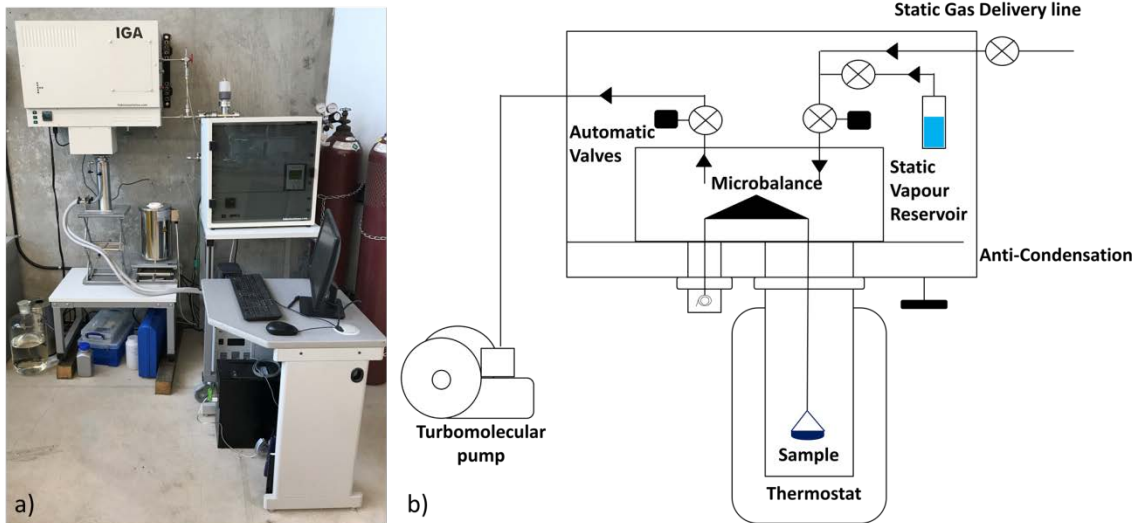
Figure 18. a) Thermogravimetric analyzer. b) Schematic of thermogravimetric analyzer

Compression at different loading conditions temperatures of consolidated composites containing graphite flakes were measured by a thermomechanical analyzer (TMA) (Q400EM, TA instruments) with macro-expansion probe with a 6.07 mm diameter contact area. Consolidated composite samples (4.5 mm × 4.5 mm) containing different amount of graphite flakes was used

for compression test. The recommended setting is obtained from manual and ASTM standard D695 [144]. Two pieces of consolidated composite samples with different amount of graphite flakes were tested with linear ramp force up to 0.05 N in a dry nitrogen environment at different temperatures (40,70 and 90°C). A schematic of the TMA instrument is shown in Figure 19. TMA measures sample displacement at various temperatures, time and applied forces and its resolution for displacement is less than 0.5 nm.

Coefficient of thermal expansion (CTE) of consolidated composite sorbent containing graphite flakes were measured with TMA. The experiment is performed according to ASTM standard E831 and ISO standard 11359-2 [145]. In this experiment, temperature increased from 25 to 150°C with ramp rate of 5°C/min according to the recommended setting of device and the dimension was measured with an appropriate probe from CTE. CTE can be calculated from the slope of change in dimension and the temperature. The other important factor to consider is the small preload force sets of 0.02N.
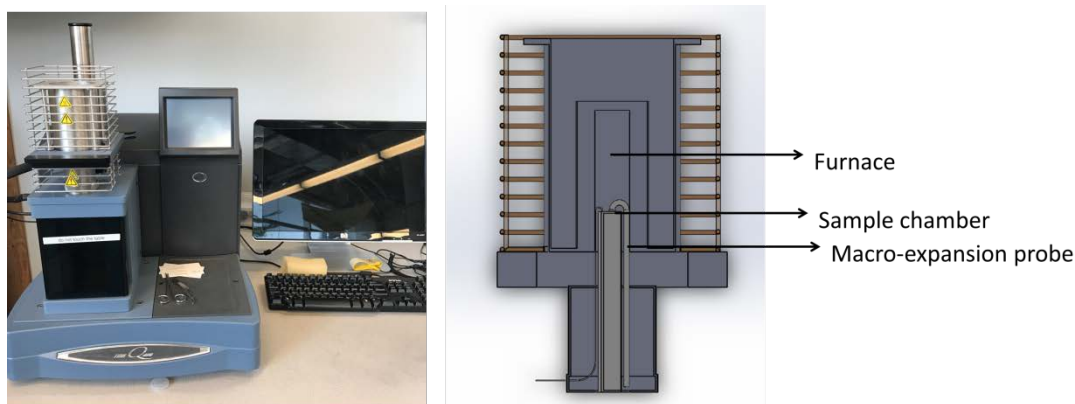
Figure 19. TMA schematic

4.3. Result and discussion

4.3.1. Pore-size distribution

The differential pore volume distribution of the silica and composite samples were obtained through analysis of the adsorption branch of the N_2 isotherms and is shown in Figure 20 (Appendix A and B). As summarised in Table 13, the 28 wt% in S6-CaCl$_2$; 25.5 wt% (total) in S6-

CaCl$_2$-PVP10 and PVP40 (30 wt% considering only CaCl$_2$ to S6) was distributed within the silica gel pores, decreasing the S_{BET} and V, and increasing the average pore diameter from 4.8 to 7 nm. Comparing samples S6-CaCl$_2$-PVP10 and S6-CaCl$_2$-PVP40, the surface area and pore volume decreased significantly for the sample containing PVP10, the lower molecular weight binder. The SEM images of loose grain silica gel, S6, and S6-CaCl$_2$-PVP40 composite shown in Figure 21, indicate that the binder does not fill the voids between silica gel particles.

Table 13. Surface characteristics of silica gel and silica-supported CaCl$_2$ composites

Sample	S_{BET} (m^2·g^{-1})	V (cm^3·g^{-1})	D (nm)	Product Specifications S_{BET}, V, particle size
S6	494	0.77	4.8	514 m^2/g, 0.75 cm^3/g, 0.2-0.5mm
S6-CaCl$_2$	134	0.31	7.0	—
S6-CaCl$_2$-PVP10	91	0.15	4.8	—
S6-CaCl$_2$-PVP40	102	0.21	6.1	—
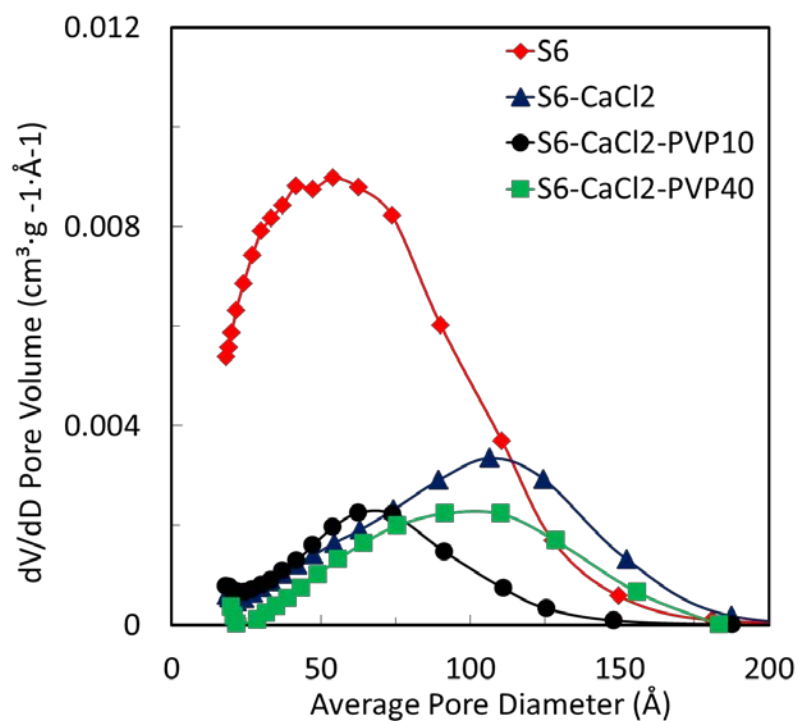
Figure 20. Pore size distribution plots for silica gel and composites from N_2 adsorption isotherms fit with BJH model.
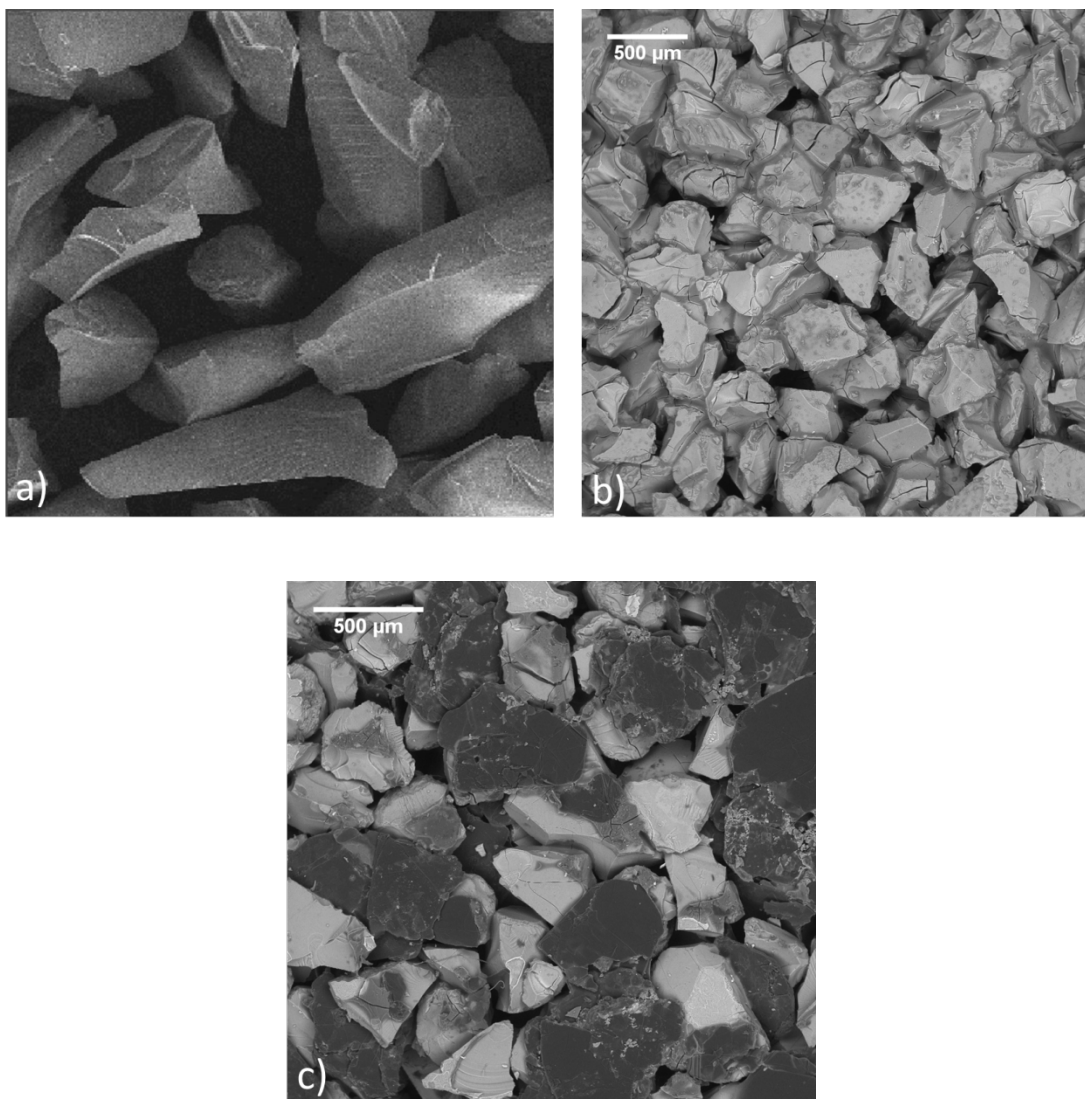
Figure 21. SEM images of (a) loose grain S6 (b) S6-CaCl$_2$-PVP40 (c) S6-CaCl$_2$-PVP40-20%G

4.3.2. Water vapor sorption

The water sorption properties of sorbents with PVP10 and PVP40 binders were measured at 25, 35 and 78°C, as shown in Figure 22 (Appendix C). Water uptake capacity, *w,* is calculated as $m_{water}/m_{dry\ sorbent}$, where the mass of the dry sorbent includes all ingredients (salt, porous matrix, binder, and thermally conductive additives). For S6-CaCl$_2$-PVP40, the water uptake at 34.7°C and 2 kPa was 0.34 g/g while for S6-CaCl$_2$-PVP10 it was only 0.29 g/g. The greater infiltration of the

pore structure by the lower molecular weight PVP10 (Table 14) has a negative impact on absorption.

Hysteresis is commonly observed in water isotherms on silica gel-CaCl- composites. At high partial pressures the hysteresis is due to capillary condensation effects on the salt solution inside the mesoporous silica gel. However, the hysteresis at low partial pressure, as shown in the 78.5°C curve in Figure 22 b, occurs in the transition from $CaCl_2$ to solid $CaCl_2 \cdot 2H_2O$. There is a lack of literature on this phenomena, however Molenda et al. conducted dynamic differential scanning calorimeter experiments on $CaCl_2$ under controlled vapor pressure and observed differences between the hydration and dehydration curves, specifically an additional step in the dehydration associated with the monohydrate [146]. They suggested the thermal hysteresis was due to an activation barrier in the dehydration process. The hysteresis in not observed in the Figure 22 a, however this is more likely due to the resolution of the isotherm data than any effect of the PVP10 binder.

The difference in equilibrium water content of the samples under operational cycle conditions for adsorption (1.2 kPa, 35°C) and desorption (2.3 kPa, 80°C) are summarized in Table 14. There was no loss in the water uptake capacity of the active materials in the sorbents containing 20 wt% binder. PVP is a hygroscopic binder with water uptake of up to 6.6 wt% at 1.2 kPa, 35°C for the bulk material. In Figure 23, water sorption isotherms (35°C) for the composite samples are plotted in mol_{H2O} per mol_{CaCl2} the water uptake per mole of active material, the salt, indicates minimal variation in performance. However, the overall performance of sorbent material is reduced in proportion to the dead weight of additives.

Table 14. Sorption cycle equilibrium uptake.

Sample	H_2O uptake capacity (mass%)		Δw (dry weight of $CaCl_2$ and silica gel only)
	35°C, 1.1kPa	80°C, 2.3 kPa	
S6	0.54	0.20	0.34
S6-$CaCl_2$	0.33	0.10	0.22
S6-$CaCl_2$-PVP10	0.20	0.43	0.19
S6-$CaCl_2$-PVP40	0.23	0.33	0.23
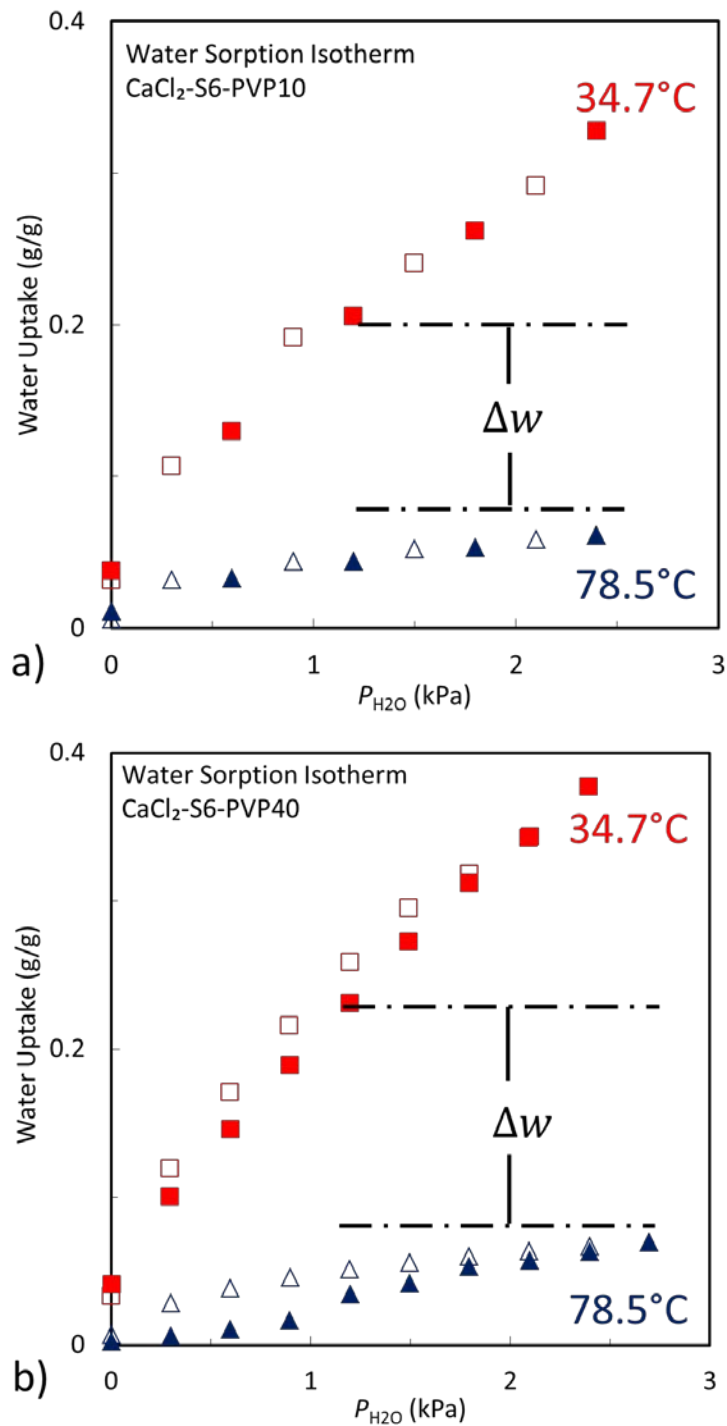
Figure 22. Water uptakes with respect to pressure are shown for (a) S6-CaCl₂-PVP10 and (b) S6-CaCl₂-PVP40 at different temperatures 34.7 and 78.5°C sorption (closed symbols) and desorption (open symbols).
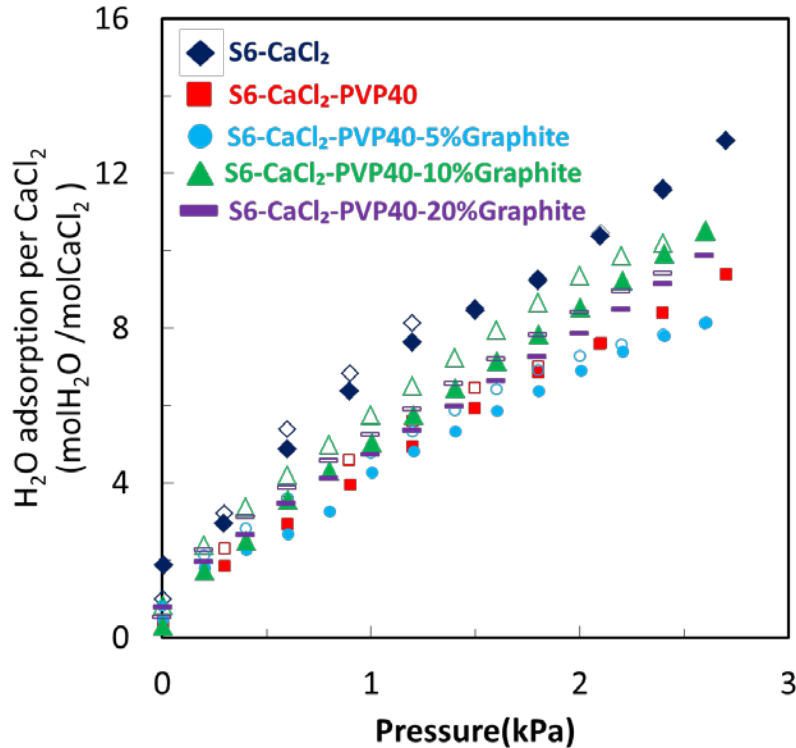
Figure 23. Effect of binder and graphite flakes on water sorption capacity at 34.7°C sorption (closed symbols) and desorption (open symbols)

The isosteric heat of water sorption is determined as a function of the slope of the linear isosters, where $Ln(P) = B(w)/T + C(w)$ and $\Delta H_{is}(w) = B(w)R$ and R is the universal gas constant. As w approaches 0.1 g/g (shown in Figure 24), the $\Delta H_{is}(w)$ reaches to -62.8 kJ/mol (Appendix D). The initial deep slope is the formation of solid $CaCl_2$ dihydrate and tetrahydrate. The slope after 0.25 g/g is the heat of dilution of aqueous $CaCl_2$ solution. The unusual section of lower $\Delta H_{is}(w)$ from 0.14 to 0.25 g/g occurs during the phase change from solid hydrate to molten hydrate. Further investigation would be required to determine whether the low ΔH_{is} values are due to confinement of molten salt within the mesoporous silica gel or effect relate to measurement technique, example equilibrium wait time.
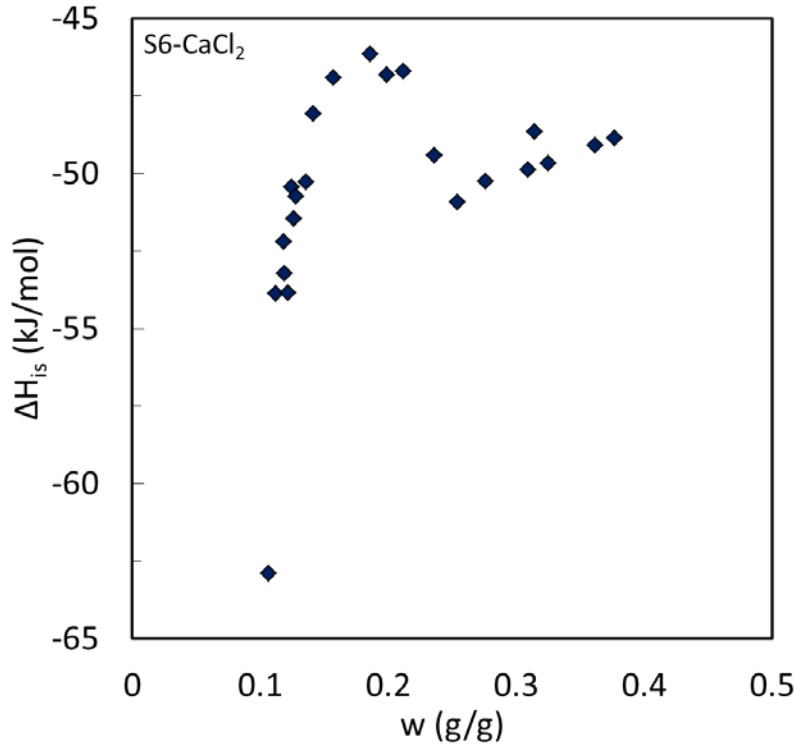
Figure 24. Isosteric water sorption heat for S6-CaCl$_2$

The kinetic curves were fitted with the linear driving force (LDF) model,

$$u(t) = \Delta u \left(1 - e^{-\frac{t}{k}}\right)$$
Eq. 8

where $u(t)$ is uptake at time t, k is time constant and Δu is the total change in uptake [49]. The kinetic curves for 0.2 kPa steps 1.5 to 1.7 kPa at 35°C are shown in Figure 25 for samples with and without binder. The sorption relaxation coefficient of the samples at different low pressures (0.9, 1.2 and1.8 kPa) are summarised in Table 15. The water sorption constant rate of loose grain S6-CaCl$_2$ is greater than S6-CaCl$_2$-PVP40 as a result of its surface area and total volume. Addition of binder reduces the gap between particles and vapor diffusion inside pores.

Table 15. Sorption rate coefficient of silica-supported CaCl₂ composites at 34.7°C

Sample name	Water sorption relaxation constant at 0.9-1.8 kPa vapor pressure [s] (0.3 kPa pressure step)		
	0.9 kPa	1.2 kPa	1.8 kPa
S6-CaCl₂	539±0.01	683±0.02	788±0.02
S6-CaCl₂-PVP40	869±0.03	969±0.02	1090±0.01
Sample name	Water sorption relaxation constant at 0.8-1.8 kPa vapor pressure [s] (0.2 kPa pressure step)		
	0.8 kPa	1.2 kPa	1.8 kPa
S6-CaCl₂-PVP40-10%G	-	507±0.02	644±0.02
S6-CaCl₂-PVP40-20%G	-	601±0.02	768±0.01
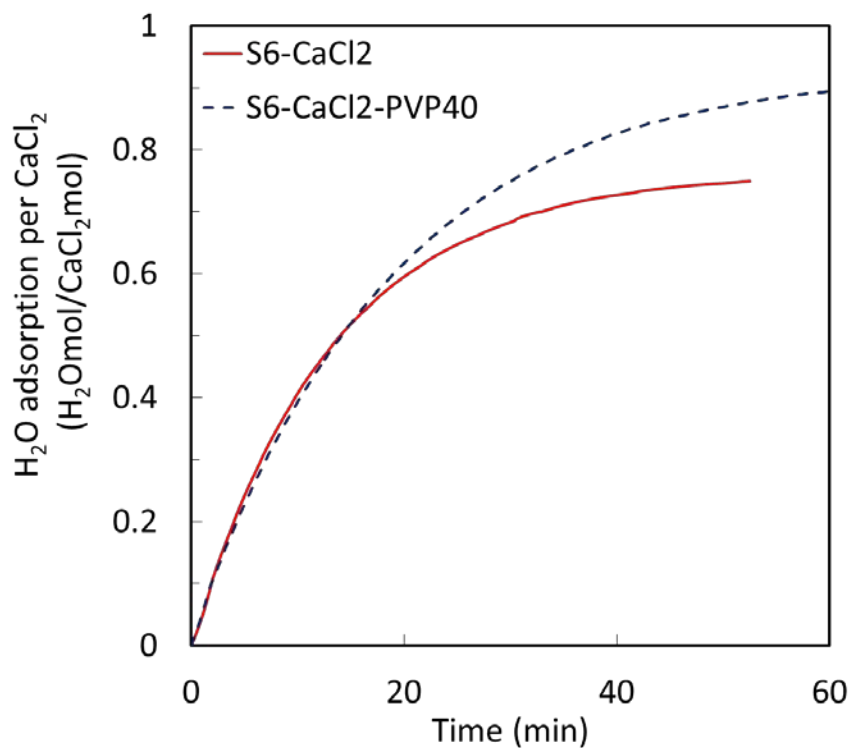
Figure 25. Water vapor sorption rate of loose grain and consolidated composites containing graphite flake at 34.7°C, 1.5 to 1.7 kPa pressure

Specific cooling performance (SCP) of both loose grains composite (S6-CaCl$_2$) and consolidated composite (S6-CaCl$_2$-PVP40) is calculated from:

$$SCP = \frac{0.8 \cdot \Delta\omega \cdot h_{fg}}{\tau_{0.8}}$$

<div align="right">Eq. 9</div>

where $\Delta\omega$ is total weight change, h_{fg} is water enthalpy of evaporation considered 2478 kJ·kg^{-1} and τ is characteristic time, when time and weight changes are collected from thermogravimetric analyser with 0.2 kPa pressure step at 35°C. The SCP$_{0.8}$ of S6-CaCl$_2$ is 55 W·kg^{-1}, achieving 80% of its equilibrium uptake in 20 minutes. However, the SCP$_{0.8}$ of S6-CaCl$_2$-PVP40 is 45 W·kg^{-1} reaching 80% of its equilibrium uptake after 27 minutes. The difference in the 0.2 kPa pressure step SCP$_{0.8}$ for the samples is due to the dead weight (binder) in the S6-CaCl$_2$-PVP40 sample. For a more dramatic pressure swing, 0 to 1.2 kPa at 35°C, the SCP$_{0.8}$ of S6-CaCl$_2$-PVP40 is 671 W·kg^{-1}.

Multi-cycle performance

The large batch adsorbent composite S6-CaCl$_2$-PVP40 with 21 wt% binder was selected for cyclic testing. Figure 26 shows pressure swing sorption cycles for S6-CaCl$_2$-PVP40. Pressure swings were done between 0 and 1.2 kPa at 25 and 35C° to study the consistency of sorption performance of sorbent. In Table 16, the sorption capacity of samples at both temperatures is shown to be consistent for 150 cycles.
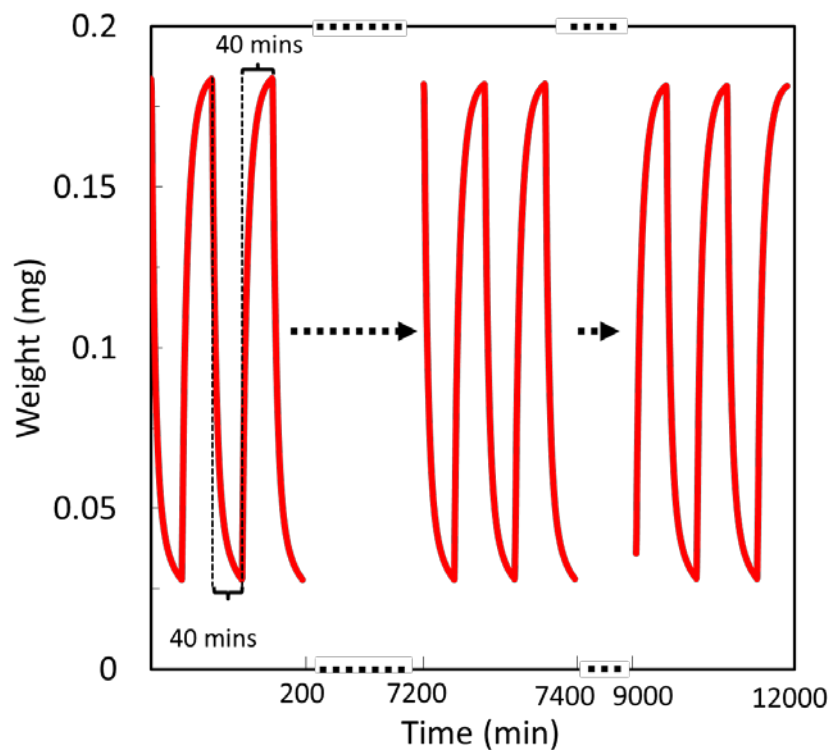
Figure 26. Pressure swing (0-1.2 kPa) sorption-desorption cycles of S6-CaCl2-PVP40 at 35°C, water uptake vs time

Table 16. Multi-cycle performance of S6-CaCl$_2$-PVP40

T	Cycle number	Δw (g/g)
	1	0.28
25°C	10	0.28
	20	0.29
	150	0.29
35°C	160	0.18
	300	0.18

58

4.3.3. Thermal conductivity

The thermal conductivities of composite absorbents containing silica gel, PVP40 and 0-20 wt% of graphite flakes or copper powder are shown in Figure 27 (Appendix E). The copper powder was inhomogeneously distributed, with a greater concentration at the bottom surface of samples, while the graphite flakes were evenly dispersed in the composite absorbent. The bottom surfaces of the sample pairs tested, smooth from contact with the mold, were placed in contact with the TPS sensor. The thermal conductivity tests probed the material to a depth of 3.5 mm.

As the copper and graphite thermally conductive additives had different distributions in the composite samples, as well as different particle sizes and aspect ratios, the comparison of the thermal conductivities of the different composites is limited. However, the graphite flakes had substantially more effect on thermal conductivity than the copper powder. The thermal conductivity of the composite absorbents increased from 0.13 to 0.14 $W \cdot m^{-1} \cdot K^{-1}$ as the copper powder content was increased from 0 and 20 wt%. The addition of 20 wt% graphite flakes to the composite absorbent increased the thermal conductivity from 0.13 $W \cdot m^{-1} \cdot K^{-1}$ to 0.27 $W \cdot m^{-1} \cdot K^{-1}$, a ~107% enhancement.
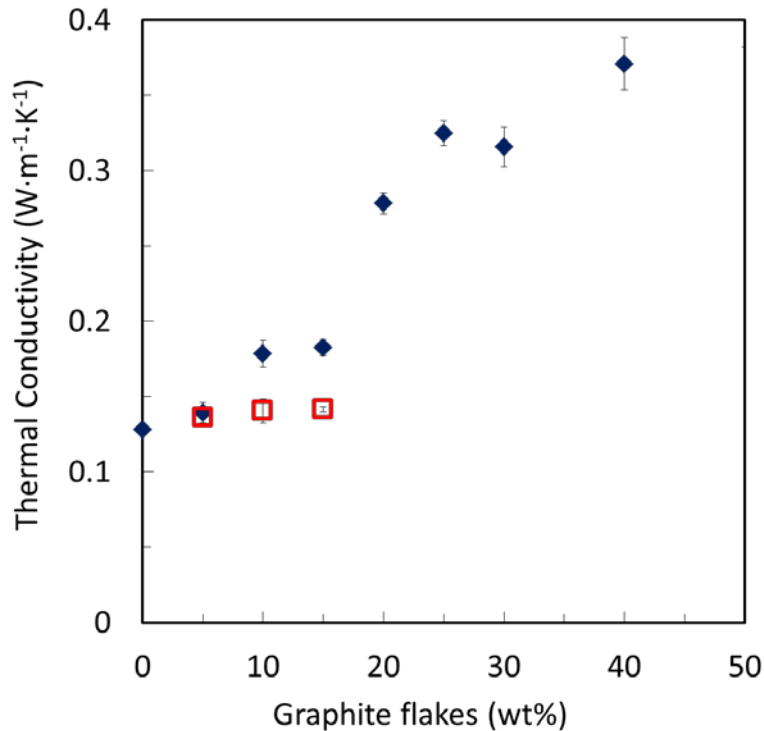
Figure 27. Thermal conductivity of silica gel consolidated with 15 wt% PVP40 binder and 0-50 wt% of either graphite flakes (◆) and copper powder(□)

When the hygroscopic salt absorbs water vapor, it dissolves creates a liquid film inside the pores of the host silica gel. This increases the thermal conductivity and specific heat of the composite absorbent [42]. At high relative humidity, there is a sharp increase in thermal conductivity associated with leakage of salt solution out of pores.

The S6-CaCl$_2$-PVP40-G sample set was tested at low RH%, 2 and 20% to evaluate the effect of water content on the thermal conductivity of the absorbent composites. As shown in Figure 28, the increase in thermal conductivity associated with the increase in water content was moderate. For instance, the thermal conductivity of composite absorbent containing 10 wt% graphite flakes increased from 0.29 to 0.31 W·m^{-1}·K^{-1} as its equilibrium water content increased from 0.06 g/g and 0.19 g/g, for 2 and 20 %RH test conditions, respectively.
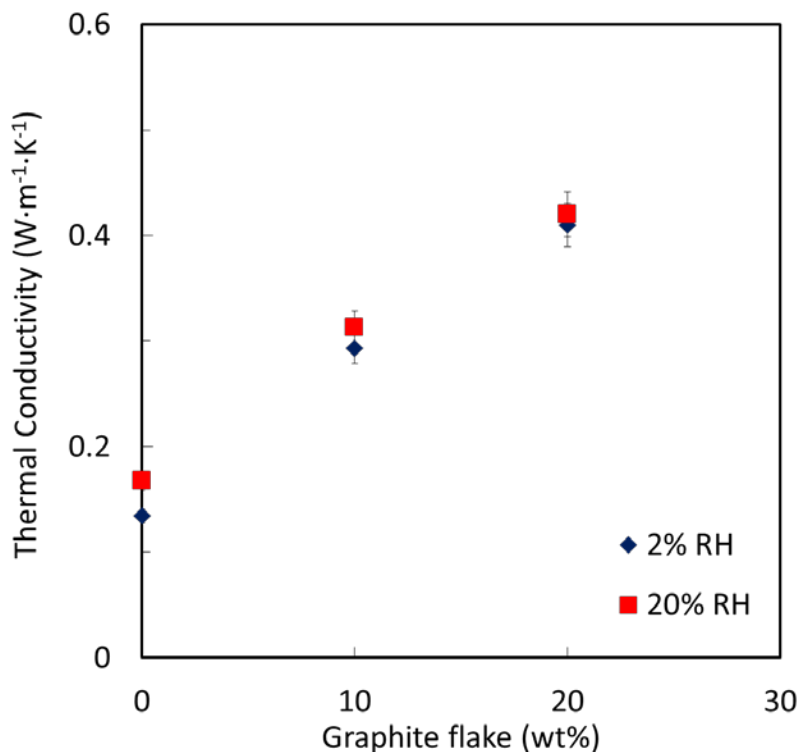
Figure 28. Thermal conductivity of consolidated composite sorbents (S6- CaCl$_2$-PVP40-0%, 5%, 10% and 20% G) with 0-20 wt% graphite flakes at 2 and 20 RH%

4.3.4. Effect of graphite flakes on elastic modulus

The stress-strain graph of composite absorbents containing silica gel, PVP40 and 0, 10 and 20 wt% of graphite flakes are shown in Figure 29. Loading and unloading lines are shown in the graph for three cycles at 40°C. The behavior shows a linear trend which means material properties does not change with pressure. The addition of graphite flakes decreases the compressibility of adsorbent material and increase the rigidity and elastic modulus of consolidated composite adsorbent. Moreover, it can be seen that there is a hysteresis effect in compression for this material. However, after the first cycle, the material behaviour remains constant and there is less hysteresis effect for the second and third cycle.
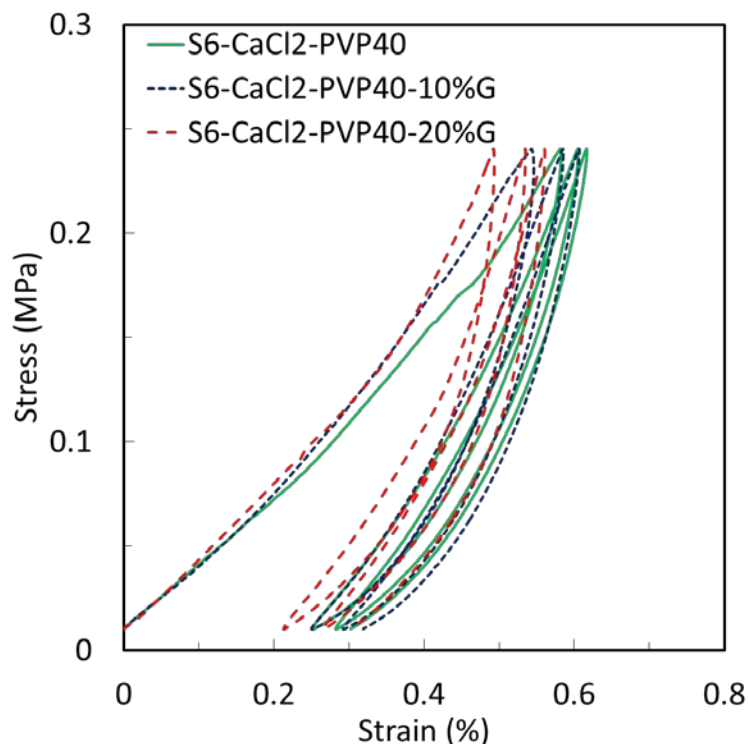
Figure 29. Stress-strain behaviour of consolidated composite sorbents (S6- CaCl$_2$-PVP40-0% and 20% G) with 0-20 wt% graphite flakes

The elastic moduli of the consolidated composites are listed in Table 17. The elastic modulus of the adsorbent material increases 18% by adding 20 wt% of graphite flakes to the adsorbent material S6-CaCl$_2$-PVP40.

Table 17. Elastic modulus of S6- CaCl$_2$-PVP40 containing different amount of graphite flakes

Sample	E (MPa)
S6- CaCl$_2$ PVP40	65
S6- CaCl$_2$-PVP40-10%G	72
S6- CaCl$_2$-PVP40-20%G	77

The compression test is also performed in different temperatures to investigate the effect of temperature on rigidity of the material. Since the adsorbent material is working under 100°C, the tests are done in three different temperatures 40, 70 and 90°C. Figure 30a shows the effect of temperature on compression of the S6-CaCl$_2$-PVP40 without any graphite. It can be seen that the material behaviour is not changing with temperature over the studied temperature range. Also,

the hysteresis effect is the same in different temperatures. Figure 30b shows the compression behavior on S6-CaCl2-PVP40 with 0-20 wt% graphite flakes at different temperatures. It is obvious that temperature does not affect the compression behaviour of the material and the material elastic modulus remains constant in this range of temperature. Also the hysteresis effect can be seen in the first cycle and the material does not show hysteresis effect after two cycles.
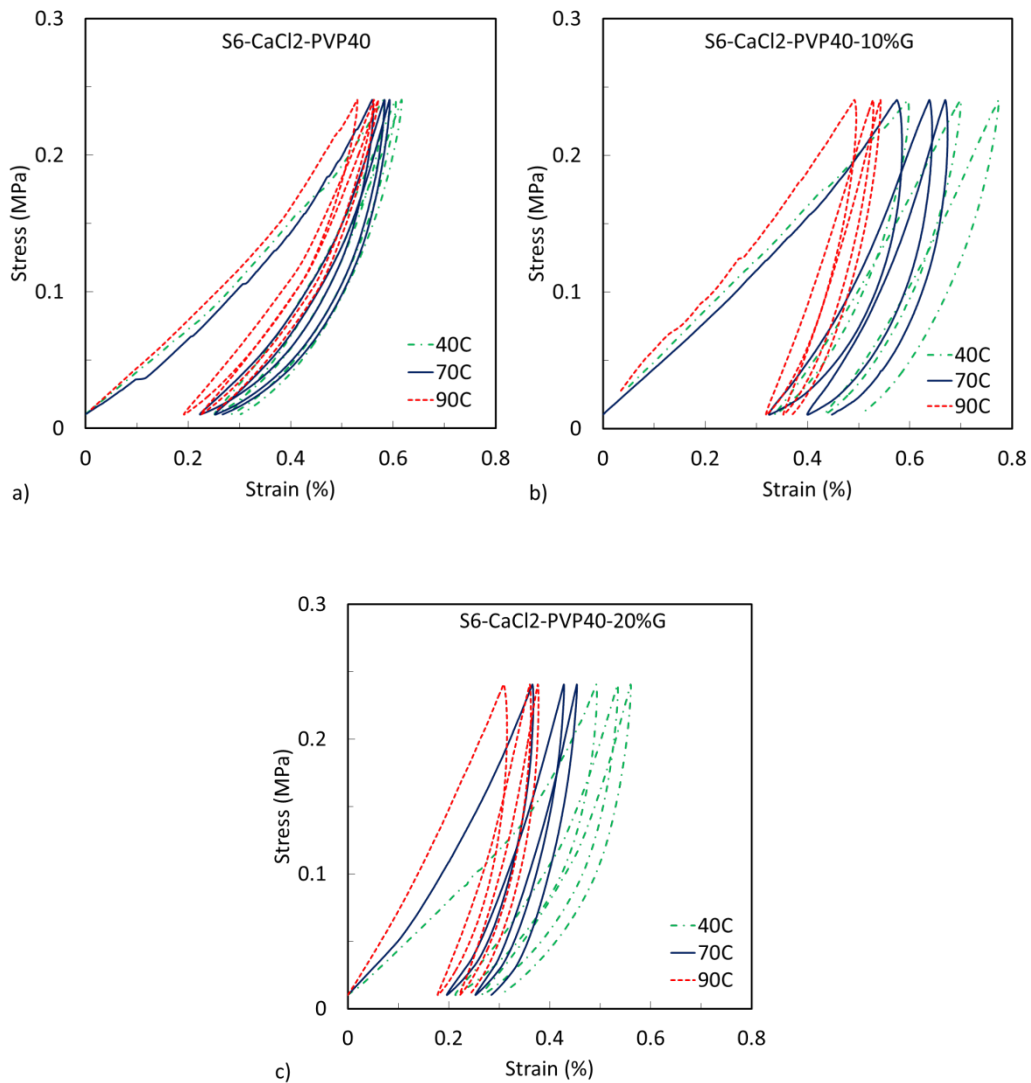
Figure 30. Effect of temperature on compression of consolidated composite S6-CaCl$_2$-PVP40 a) 0, b) 10 and c) 20 wt% G

4.3.5. Effect of graphite flakes on the coefficient of thermal expansion (CTE)

Effect of addition of thermally conductive additive, graphite flake, on the coefficient of expansion (CTE) of consolidated composite have been studied. Average thermal expansion of

adsorbent material S6-CaCl$_2$-PVP40 with different amount of graphite flakes is shown in Figure 31. Since the thickness of the samples is different, the dimension change or change in thickness is reported in the figure non-dimensionally in order to be able to compare the results for different concentration. The length of samples with different amount of graphite flake is decreased gradually by increasing temperature. This is actually the result of the addition of graphite flakes. Graphite flakes have low thermal expansion compared to metals. Thermal expansion of ordinary steel is 6 times the thermal expansion of longitudinal sections of graphite and about four times the value for transverse sections [147].
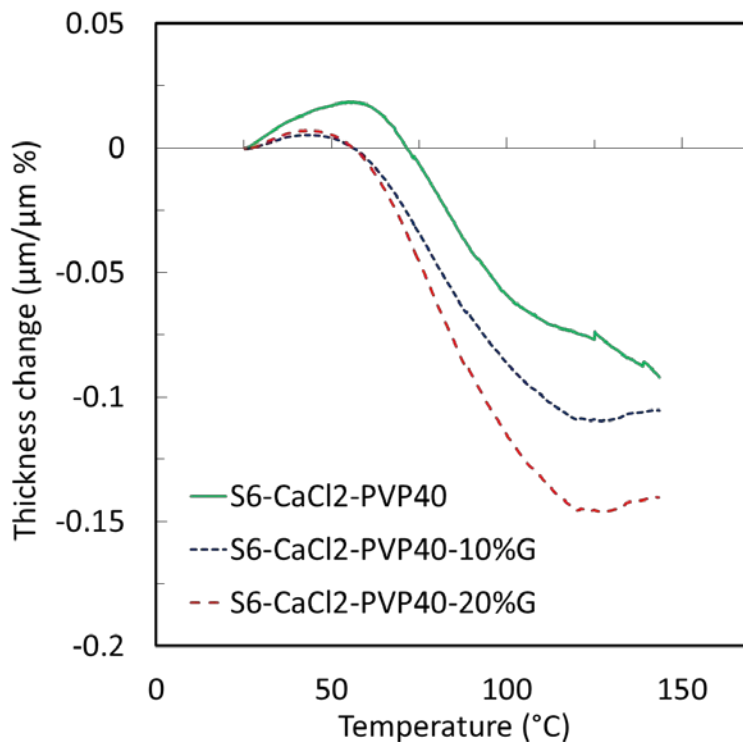
Figure 31. Non-dimensional thickness change of consolidated composite S6-CaCl$_2$-PVP40 a) 0, b) 10 and c) 20 wt% G

4.4. Summary

New composite adsorbents were prepared by consolidating graphite flakes with silica gel using binders with different molecular weights, and their water uptake capacities measured at different partial pressures. The effect of thermally conductive additives on water uptake and thermal conductivity was studied. The following highlights the findings of this chapter:

- The 40,000 MW PVP binder had substantially less effect on the pore volume, pore size distribution and water uptake of silica gel-$CaCl_2$ composites than the 10,000 MW PVP binder.

- The water uptake of the silica gel-$CaCl_2$-PVP40 composite was consistent through the first 300 pressure swing cycles.

- The thermal conductivity of a set of S6-$CaCl_2$–PVP40 sorbent with 0-20 wt% graphite flakes were tested at 2 and 20 RH%. The absorbed water at 20 RH% increased the thermal conductivity of the sample by 0.13-0.16 $W \cdot m^{-1} \cdot K^{-1}$.

- Addition of 20 wt% graphite flakes to the adsorbent material S6-$CaCl_2$-PVP40 increased the elastic modulus by 18%.

- Coefficient of expansion of consolidated composite highly depends on addition of graphite flakes.

Chapter 5. Effective thermal conductivity modeling of consolidated sorption composites containing graphite flakes

The objective of this work is to provide an accurate model to predict the effective thermal conductivity of consolidated composite adsorbent material containing randomly oriented graphite flakes. This chapter includes: 1) a review of the theoretical models on the topic, 2) development of a preliminary model for the upper and lower bounds for steady-state conduction heat transfer, and 3) development of a model to predict the effective thermal conductivity of consolidated adsorbent material containing graphite as a function of the wt%, average size, and orientation of the graphite flakes.

5.1. Sample preparation

Silica gel (SiliaFlash® B60, Lot 011112, Silicycle, Inc., Quebec, Canada) with irregular shaped grains (0.2-0.5 mm), average pore diameters of 6 nm and surface area (S_{BET}) 514 $m^2 \cdot g^{-1}$ was combined with different amount of graphite flakes (Sigma Aldrich, +100 mesh) and 40,000 MW polyvinylpyrrolidone (PVP40, Amresco) binder solution. The slurries were baked for one hour at 50°C, and then heated to 180°C for one hour to cross-link the binder. Table 18 shows silica gel composites based adsorbent prepared with different amount of graphite flakes 0 to 20 wt%.

Table 18. Composites prepared with SiliaFlash B60 silica gel matrix

Sample name	Adsorbent	PVP	Graphite flakes
S6-CaCl$_2$-PVP40-0%G	4 g, 1.71 g	1 g	-
S6-CaCl$_2$-PVP40-5%G	4 g, 1.71 g	1 g	0.35 g
S6-CaCl$_2$-PVP40-10%G	4 g, 1.71 g	1 g	0.74 g
S6-CaCl$_2$-PVP40-20%G	4 g, 1.71 g	1 g	1.67 g

5.2. Thermal conductivity measurement

A thermal constants analyzer (TPS 2500S, ThermTest Inc., Frederiction, Canada) capable of precise measurement of thermal conductivity, diffusivity and specific heat was used for this study. The instrument has different sensor types and software modules to perform measurements on bulk materials (isotropic and anisotropic), thin films, powders and liquids. This apparatus uses the transient plane source method in accordance with ISO Standard 22007-2.2. In this study, a bulk sensor (7577) with a 2 mm diameter nickel double spiral insulated in a thin layer of Kapton was used for both transient heating of the sample and temperature measurements. A humidifier (P-10C-1C-2-0-031300-v7, Cellkraft AB, Sweden) was connected to thermal constant analyzer to control the humidity inside the TPS chamber.

For bulk material (isotropic) measurements, the sensor was placed on either side of a pair of dried identical samples. After 20 minutes for temperature and 2 %RH equilibration, measurements were performed on each sample three times at different locations and a standard deviation of 10% was measured.

5.3. Geometrical parameters of the consolidated graphite-doped composite

Geometrical parameters, i.e. the particle size distribution and graphite flakes size should be measured to be used as input to the model. An optical microscope (Nikon Eclipse LV100) was used to measure the shape and size distribution of 100 graphite flakes, shown in Figure 32.

Figure 32 shows that the graphite flakes have irregular shapes which make it difficult to be represented with one geometry and one size for geometric modeling. In this study, graphite flakes are assumed to have a disc shape with an averaged diameter estimated through statistical measurements. The statistical distribution of graphite flakes effective diameter is shown in Figure 33. The average thickness and diameter for 100 measured graphite flakes was calculated to be 4.3 and 700 μm, with an standard deviation of 7%, see Appendix E and F for sample measurements and statistical analysis.
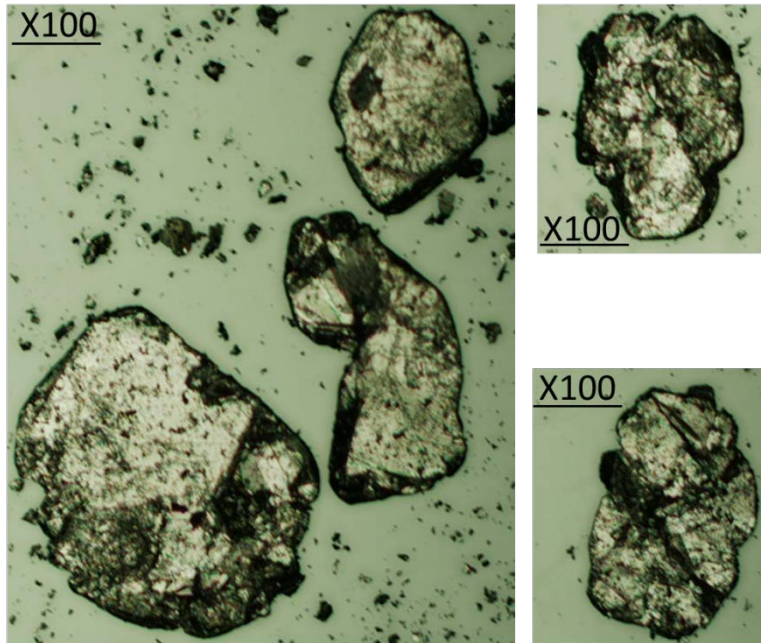
Figure 32. Sample optical microscope images of graphite flakes.
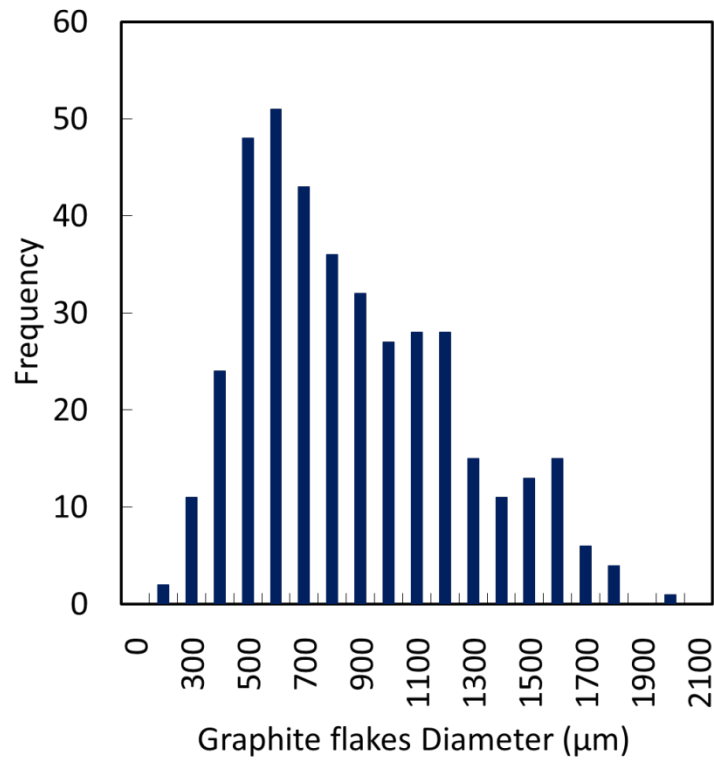
Figure 33. Graphite flakes diameter measurement distribution of 100 particles.

5.4. Existing models

A wide range of models, known as effective medium approximation or effective medium theory, have been developed to calculate the effective thermal conductivity of a medium made of inclusions of one substance (e.g. spheres, cylinders, irregular particles), embedded in a matrix of a different material [148]. In this section, some of the existing methods for calculating the effective thermal conductivity of porous media with different dispersed particles geometries are presented.

Maxwell's [149][150] effective thermal conductivity expression for a non-contacting packed spherical bed is as follow;

$$k_e^* = \frac{k_P^*(1+2\phi)+2(1-\phi)}{k_P^*(1-\phi)+(2+\phi)}$$

Eq. 10

Where k_e^* is the effective thermal conductivity of the medium, $k_P^* = k_P / k_m$, $k_e^* = k_e / k_m$ and ϕ is volume fraction. The effective thermal conductivity of medium, k_m, and particle, k_P, can be measured. Maxwell's model has three limitations: 1) the thermal resistance between the dispersed particles in the medium is not considered, 2) the model assumes a small volume fraction of dispersed particles in medium, and 3) the model is developed for spherical fillers [151][150][149], [152].

Hamilton and Crosser [149][150] included the effect of non-spherical particles on effective thermal conductivity by extending Maxwell's model as follow;

$$k_e^* = \frac{k_P^*[1+(n-1)\phi]+(n-1)(1-\phi)}{k_P^*(1-\phi)+(n-1)+\phi}$$

Eq. 11

where n is a shape factor, and n=3 for spherical particle [150]. For cylindrical particles, Hamilton and Crosser suggested the following correlation;

$$n = \frac{3}{\psi}$$

Eq. 12

where ψ is the sphericity ($0.58 < \psi < 1$) and $n{=}6$ for cylindrical particles. This model is limited to two geometries, spherical and cylindrical and low volume fractions.

The upper and lower bounds of the thermal conductivity for the conduction model developed by Bahrami et al. for a uniform spherical particle in a simple cubic unit cell for steady state heat conduction are [150]

$$k_L^* = 1 - \frac{\pi}{4}\phi^{*2} - \frac{\pi}{2}\phi^* - \frac{\pi}{2}\ln(1-\phi^*)$$

Eq. 13

$$k_U^* = \frac{1}{1-\phi^*}$$

Eq. 14

Where k_L and k_U are the lower and upper bound thermal conductivity, respectively. The non-dimensional upper and lower bound thermal conductivity can be calculated from $k_L^* = k_L / k_m$ and $k_U^* = k_U / k_m$. In this model, the volume fraction depends on the particle radius and unit cell dimensions, and can be defined as;

$$\phi^* = \frac{r_p}{2b} = (\frac{6}{\pi}\phi)^{1/3}$$

Eq. 15

where r_p is the spherical particle radius and b is a basic cell half-side. This method is only applicable for spherical particles in porous medium with small volume faction.

All the above methods are helpful to study the effective thermal conductivity of particles in porous medium; however, each model has its own limitations, and is specifically developed for certain purposes or conditions. Salient geometrical parameters in effective thermal conductivity modeling are particles geometry, volume fraction and the orientation. All the above-mentioned models can affect the effective thermal conductivity of the medium.

Figure 34 shows a comparison between the existing models and the present data for thermal conductivity. As shown in Figure 34, Maxwell and Hamilton-Crosser models can only

predict the thermal conductivity for the sample with 5 wt% and fail to predict higher graphite flake concentrations.
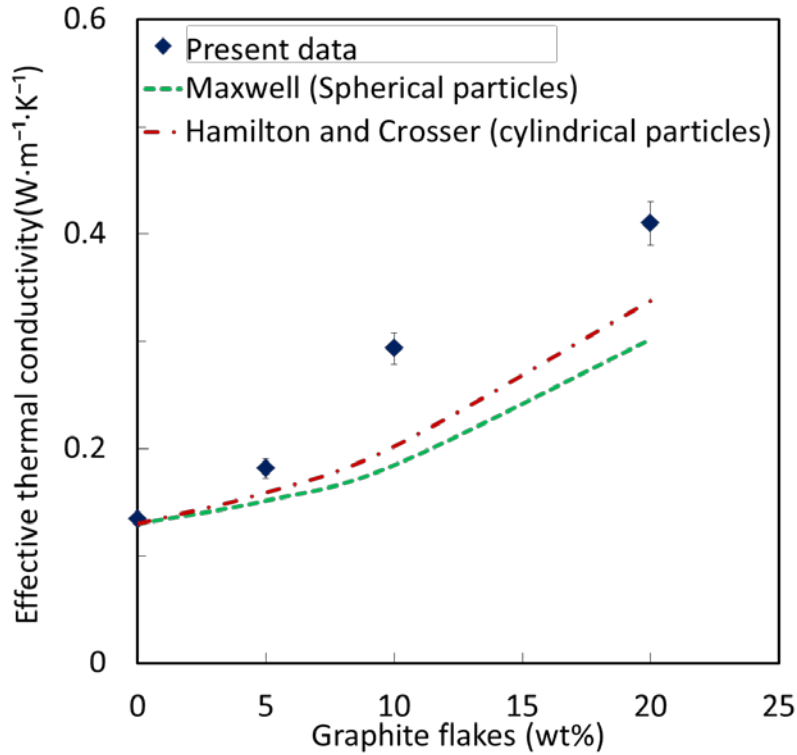
Figure 34. Comparison of various models with measured thermal conductivity of consolidated composite adsorbents (CaCl2-S6-G) with different amount of graphite flakes (0-20 wt %) at 2 %RH.

5.5. Bounds of conduction for disk shape particle in a basic unit cell

In this section, following the methodology introduced in [150], upper and lower bounds for steady-state through-plane heat conduction in consolidated composite containing graphite flakes samples are established for horizontally and vertically oriented disk-shaped flakes, as schematically shown in (Figure 35). A "unit cell" is considered to represent the entire geometry of the consolidated composite with the dispersed graphite flakes. The size of the unit cell depends on the volume fraction of flakes in each sample, and is calculated using the density of particles and porous medium. The model is compared to the experimental data collected from consolidated

composite adsorbent samples. The data should lay between the upper and lower bound, if the bounds are established properly. It can be then expanded for particles with a range of orientation angles in a porous media.
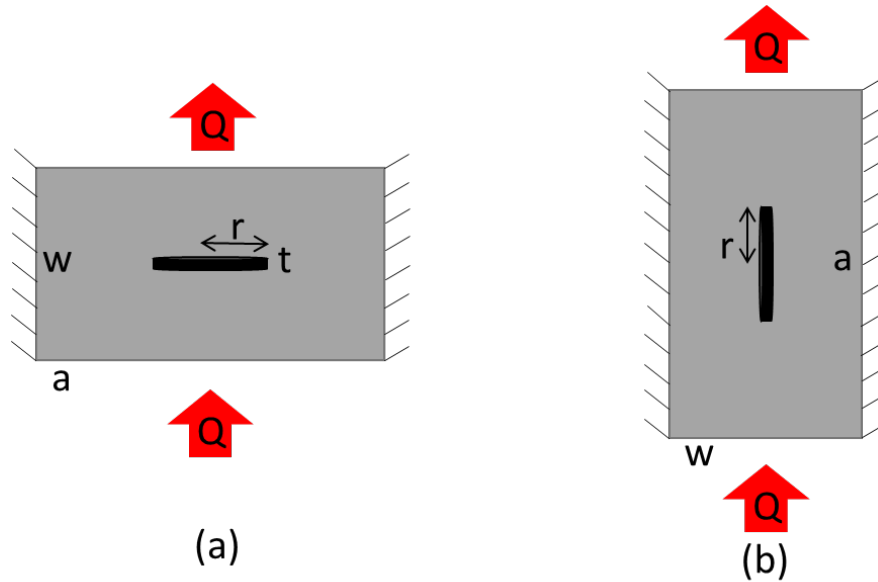
Figure 35. Disk-shape graphite flakes dispersed in consolidated composite, two extreme cases establishing (a) a lower bound for thermal conductivity (same direction with heat flow) and (b) an upper bound for thermal conductivity (perpendicular to the heat flow direction).

The assumptions used in the development of the present model are:

- Steady-state, one-dimensional heat conduction,

- Identical disk-shape graphite flakes are evenly dispersed throughout the composite,

- The contact between the graphite flakes and the sorption material is perfect, i.e., no thermal contact resistance is considered between the particles and the substrate,

- Constant sorption material and graphite flake properties, which are listed in Table 19.

The sorption material in the composite used in this study is $CaCl_2$-silica gel-PVP40.

Table 19. Material properties measured at RH = 2%

$\rho_{silica\ gel}$ (g·cm⁻³)	$\rho_{graphite\ flakes}$ (g·cm⁻³)	$r_{graphite\ flake}$ (μm)	$t_{thicknes}$ (μm)	k_s [measured] (W·m⁻¹·K⁻¹)	$k_{g\text{-}in\ plane}$[153] (W·m⁻¹·K⁻¹)	$k_{g\text{-}through\ plane}$[153] (W·m⁻¹·K⁻¹)
0.5	0.64	544	4.3	0.135	750	8

5.6. Unit cell with horizontal particles

5.6.1.   Lower bound: flakes perpendicular to the heat flow

A lower bound for effective thermal conductivity, and its associated thermal resistance network, can be established by assuming isotherms perpendicular to the direction of heat flow, as shown in Figure 36.
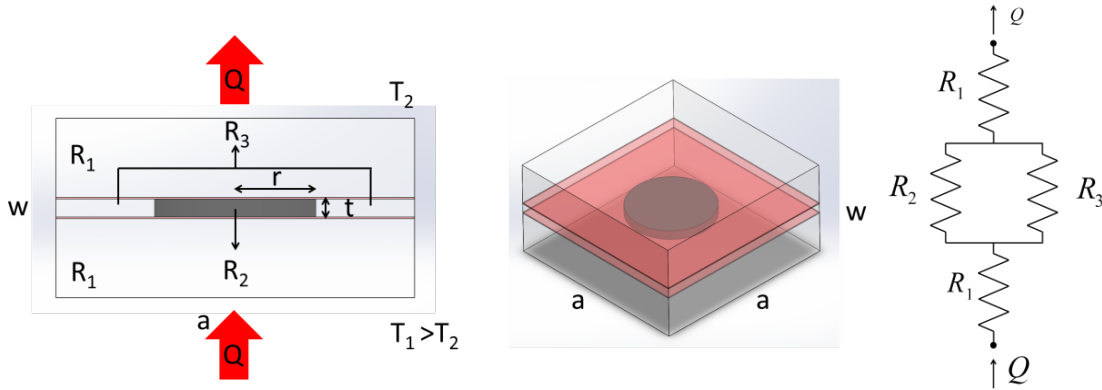
Figure 36. Lower bound for horizontal disk in unit cell with perpendicular isotherms

Based on the thermal resistance network shown in Figure 36, the lower bound of effective thermal conductivity of the consolidated composite can be found from Eq. 15

$$k_{eff-L} = \frac{k_s w a^2 [k_s(a^2 - \pi r^2) + k_g \pi r^2]}{[k_s a^2 t + [k_s(a^2 - \pi r^2) + k_g \pi r^2] \cdot (w-t)] \cdot a^2}$$

Eq. 16

where w and a are unit cell dimensions, as shown in Figure 36.

5.6.2.   Upper bound: flakes parallel to heat flow

To calculate the upper bound effective thermal conductivity of a vertical disk particle in a cubic unit cell, parallel adiabats to the direction of heat is assumed, as shown in Figure 37. The similar approach for the lower bound calculation is used to determine the upper bound.
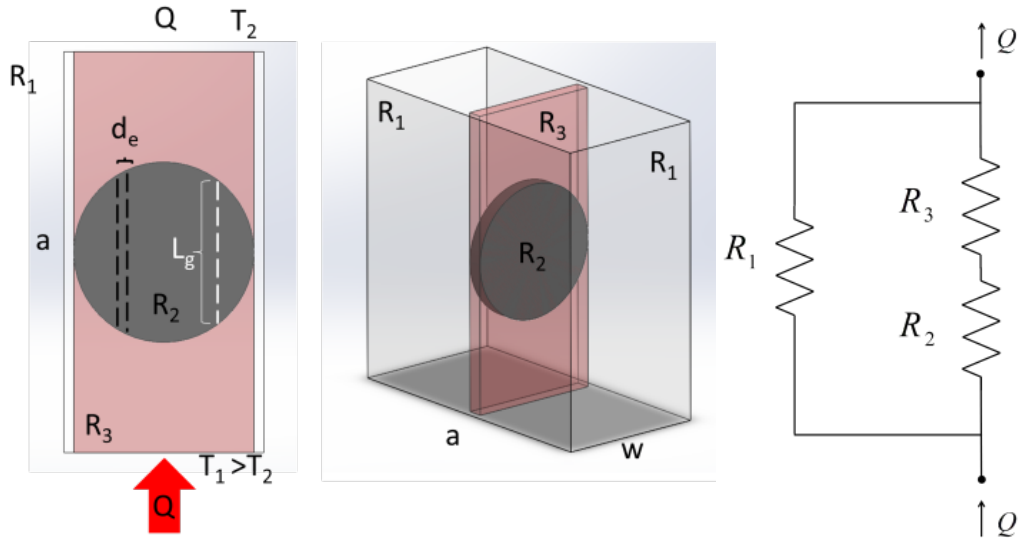
Figure 37. Upper bound for vertical disks in a unit cell with parallel adiabats

To calculate R_2, a new parameter is introduced named as L_g,

Eq. 17

$$L_g = 2\sqrt{r^2 - d_e^2}$$

Then, the total R_2 can be calculated from

Eq. 18

$$R_2 = \frac{1}{2t} \int_0^r \left[\frac{a - L_g}{K_s} + \frac{L_g}{K_g} \right] d(d_e)$$

The upper bound effective thermal conductivity can be calculated:

$$k_{eff-U} = \frac{a \int_0^r [\frac{a-L_g}{k_s} + \frac{L_g}{k_g}] \mathrm{d}(\mathrm{d}_e)}{w \cdot [k_s(wa - 2rt) \int_0^r [\frac{a-L_g}{k_s} + \frac{L_g}{k_g}] \mathrm{d}(\mathrm{d}_e) + 2ta]}$$

Eq. 19

5.7. Results and discussion

The established upper and lower bounds for effective thermal conductivity of consolidate adsorbent graphite flakes are shown in Figure 38. As expected, the experimental data fall between the two bounds.
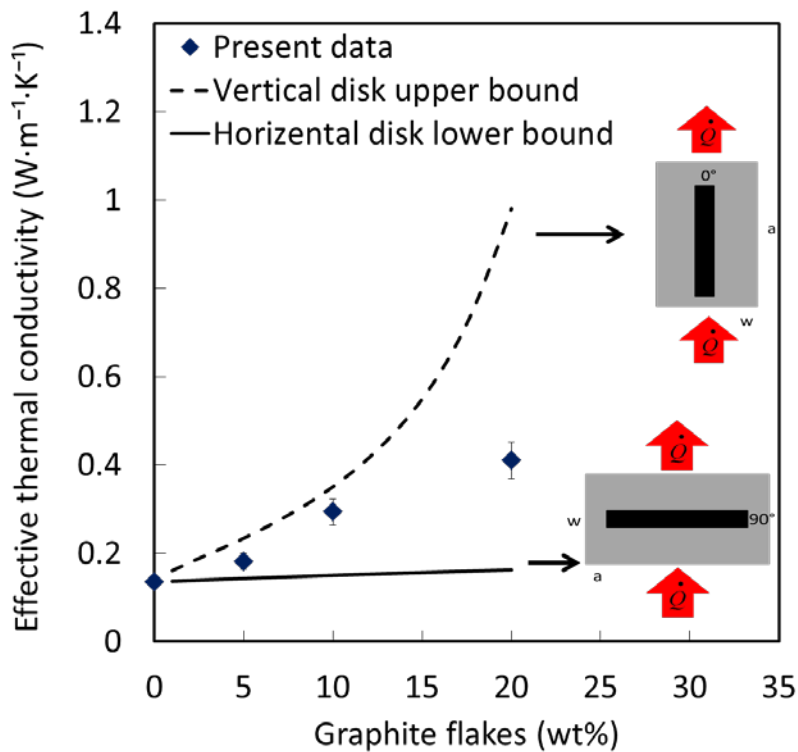
Figure 38. Highest and lowest possibility of graphite flake orientation in a unit cell is shown. Thermal conductivity of consolidated composite adsorbents (CaCl₂-S6-G) with different amount of graphite flakes (0-20 wt %) at 2 %RH.

In reality, the graphite flakes in the composite adsorbent are expected to be randomly oriented. The introduced upper and lower bounds are used, as two extreme cases, to predict the

effective thermal conductivity of the consolidated composites. Using a similar approach, a thermal resistance network and its effective thermal conductivity can be calculated for consolidated composites containing graphite discs with different angles, as shown in Eq. 20:

$$[\mathrm{k}_{eff-\theta}] = \cos^2(\theta) \cdot \frac{a \int_0^r [\frac{a-L_g}{k_s} + \frac{L_g}{k_g}] \mathrm{d}(\mathrm{d}_e)}{w \cdot [k_s(wa-2rt) \int_0^r [\frac{a-L_g}{k_s} + \frac{L_g}{k_g}] \mathrm{d}(\mathrm{d}_e) + 2ta]} + \sin^2(\theta) \cdot \frac{k_s wa^2 [K_s(a^2 - \pi r^2) + k_g \pi r^2]}{[k_s a^2 t + [k_s(a^2 - \pi r^2) + k_g \pi r^2] \cdot (w-t)] \cdot a^2}$$

Eq. 20

The effective thermal conductivity model of disk particles in different angles compared to the measured thermal conductivity of S6-CaCl$_2$-G is shown in Figure 39 .
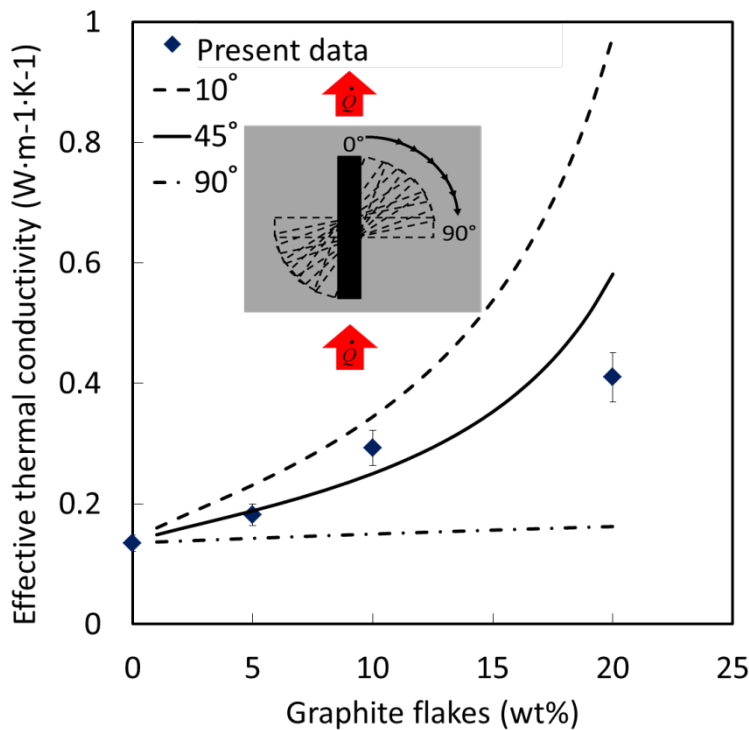
Figure 39. Thermal conductivity comparison of angled disk particles with uniform distribution in porous medium with measured thermal conductivity of consolidated composite adsorbents (CaCl2-S6-G) with different amount of graphite flakes (0-20 wt %) at 2 %RH.

Bound conduction model for disk shaped particles in consolidated sorbent composite shows relative good agreement with experimental data when the angle of the disk particles is

assumed 45° in Eq. 18. The relative difference between the experimental data and the modeling result for low volume fraction disk shape thermally conductive additive (0-10 wt%) in porous medium is 10%. As shown in Figure 32, graphite flakes have a diameter range of 200-1300 μm, which small particles help to make a path through consolidated sorbent composite.

5.8. Summary

Effective thermal conductivity of composite adsorbent containing graphite flakes was measured at 35°C (2 %RH). The results showed thermal conductivity of consolidated composite increased significantly by adding thermally conductive particles. New upper and lower bounds were established for effective thermal conductivity for two extreme cases of flake orientations, i.e., horizontal and vertical.

In addition to the experimental measurements, a new analytical model was developed that can predict the effect of thermally conductive additive on thermal conductivity of consolidated adsorbent. The model captured the trend while different disk shape particles angle and size considered. This model was limited by the geometry of additive, volume fraction, the dispersion of particles in composite.

Chapter 6.   Thermal diffusivity of consolidated composite adsorbent containing graphite flakes: Applications for sorption chillers

To the best knowledge of the author, the open literature lacks the information on thermal properties of consolidated composite adsorbent containing graphite flakes. In this section, based on existing effective medium theory, new models are developed for the specific heat and thermal diffusivity of consolidated composite samples as a function of the graphite flake volume fraction at different relative humidity (RH). Several samples are fabricated and tested by transient plane source (TPS) to validate the proposed models.

6.1. Sample preparation

Dry irregular shaped silica gel (SiliaFlash® B60, Lot 011112, Silicycle, Inc., Quebec, Canada) with grains (0.2-0.5 mm) and average pore diameter of 6 nm was combined with 40,000 MW polyvinylpyrrolidone (PVP40, Amresco) binder solution and thermally conductive graphite flakes (150 μm, Sigma-Aldrich) and $CaCl_2$ solution. The slurries were shaped to samples with thickness of 4.5 mm, baked for one hour at 80°C, and then heated to 150°C for one hour. More details on the prepared samples including the composition and density are provided in Table 20. Density of each dried sample was calculated by measuring volume and weight.

Table 20. Composites prepared with SiliaFlash B60 silica gel matrix

Sample name	Silica gel	CaCl$_2$	PVP	Graphite flakes	Density
S6-CaCl$_2$-PVP40-0%G	4 g	1.71 g	1 g	-	678.23 kg·m^{-3}
S6-CaCl$_2$-PVP40-10%G	4 g	1.71 g	1 g	0.74 g	700.05 kg·m^{-3}
S6-CaCl$_2$-PVP40-20%G	4 g	1.71 g	1 g	1.67 g	705.81 kg·m^{-3}

6.2. Sample Characterization

Thermogravimetric vapor sorption analyzer (IGA-002, Hiden Isochema) were used to measure the water sorption isotherms (0-0.6 P/P$_0$) of S6-CaCl$_2$-PVP40-G samples at 35°C. Samples were dried under vacuum for 6 hours at 90°C and the dry masses were recorded. The composite microstructure was imaged with a scanning electron microscope (FEI/Aspex-Explorer) at room temperature (Figure 40).

The SEM images of S6-CaCl$_2$-PVP40, and S6-CaCl$_2$-PVP40-20%G composite shown in Figure 40, indicate that the binder does not fill the voids between silica gel particles. Graphite flake particles have darker color where white particles are CaCl$_2$ confined silica gel.
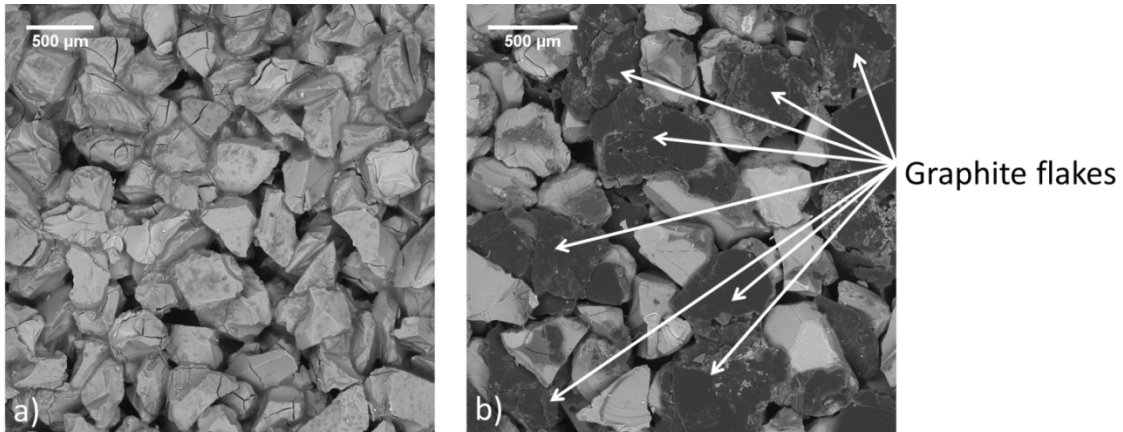
Figure 40. SEM images of (a) S6-CaCl$_2$-PVP40 and(b) S6-CaCl$_2$-PVP40-20%G

A transient plane source 'hot disk' thermal constants analyzer (TPS 2500S, ThermTest Inc., Fredericton, Canada) was used to measure the thermal conductivity, diffusivity and specific heat of the samples. For the specific heat measurements, sample diameter should be between 10 to 19 mm, besides, they should be thick enough (not more than 5 mm) to properly fill the specific heat cell. A thermally insulated sample holder made of a high thermal conductivity material was sandwiched between insulated backing material when the cell constantly was exposed to power output from the TPS permanently attached [141]–[143]. Dry samples were exposed to 2% and 20% RH for 3 hours before each measurement to ensure they reached equilibrium (see Figure 41). A standard deviation of 7% has been measured for each sample; Appendix F and G show the data and the detailed analysis.
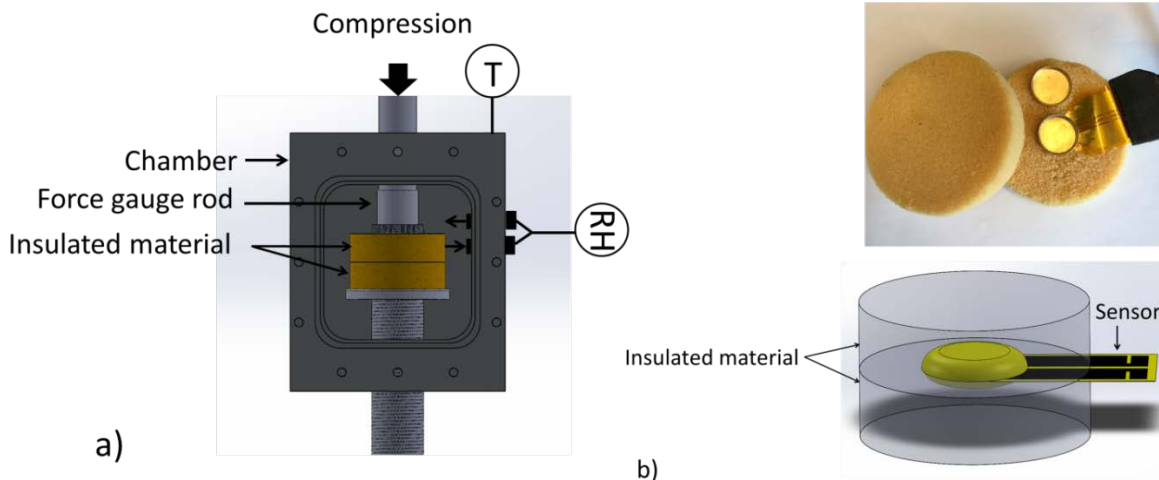
Figure 41. a) TPS 2500S used for the specific heat measurements and b) Specific heat sensor.

For thermal conductivity measurements, two identical samples with thickness of 4.5 mm were placed on either side of a bulk sensor (7577) with a 2 mm diameter nickel double spiral insulated in a thin layer of Kapton (see Figure 17).

Tests were performed in a temperature and relative humidity controlled chamber. Humidity of the chamber was monitored and controlled by a humidifier (P-10C-1C-2-0-031300-v7, Cellkraft AB, Sweden) with 5 nominal liters per minute humid air flow. Samples with 17 mm diameter and 4.5 mm thickness were exposed to 5%, 20% and 60% RH at 35°C for 2 hours. Measurements are performed on each sample three times at different locations; a standard deviation of 5% has been measured.

6.3. Results and discussion

6.3.1. Water vapor sorption

The 35°C water sorption isotherms for the samples are plotted in Figure 42 (Appendix C), showing grams per gram of composite material including the non-adsorbing thermally conductive graphite flake additive. The water uptake per gram of active material indicates minimal loss of performance from 0.21 g/g for consolidated composite to 0.18 and 0.15 g/g for consolidated composite containing 10 and 20 wt% graphite flakes at 0.2 P/P_0. This trend is expected as the graphite flakes do not adsorb water.
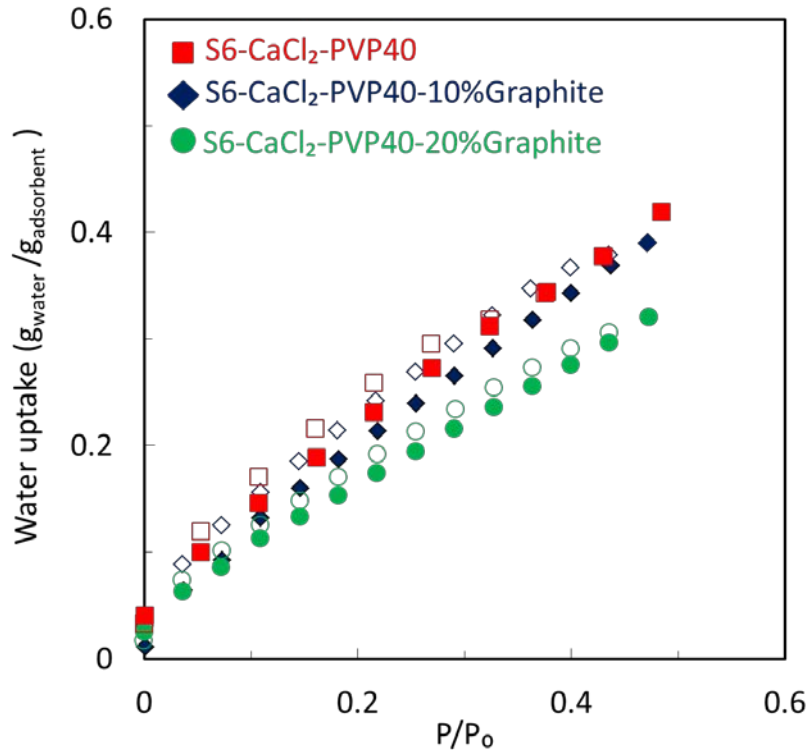
Figure 42. Effect of binder and graphite flakes on water sorption capacity at 34.7°C sorption (closed symbols) and desorption (open symbols).

6.3.2. Thermal property modeling

In section 5.6, two extreme cases are introduced to predict thermal conductivity of consolidated composite containing graphite flakes. To predict thermal properties of consolidated composite at different relative humidity, different mixing models used to predict thermal conductivity with minimum relative difference from experimental data at 2% RH. In Figure 43, Geometric average shows the 12% relative difference from experimental data when harmanic average, arithmetic average and, Churchill blending technique [154] show more than 20% relative difference from experimental data.
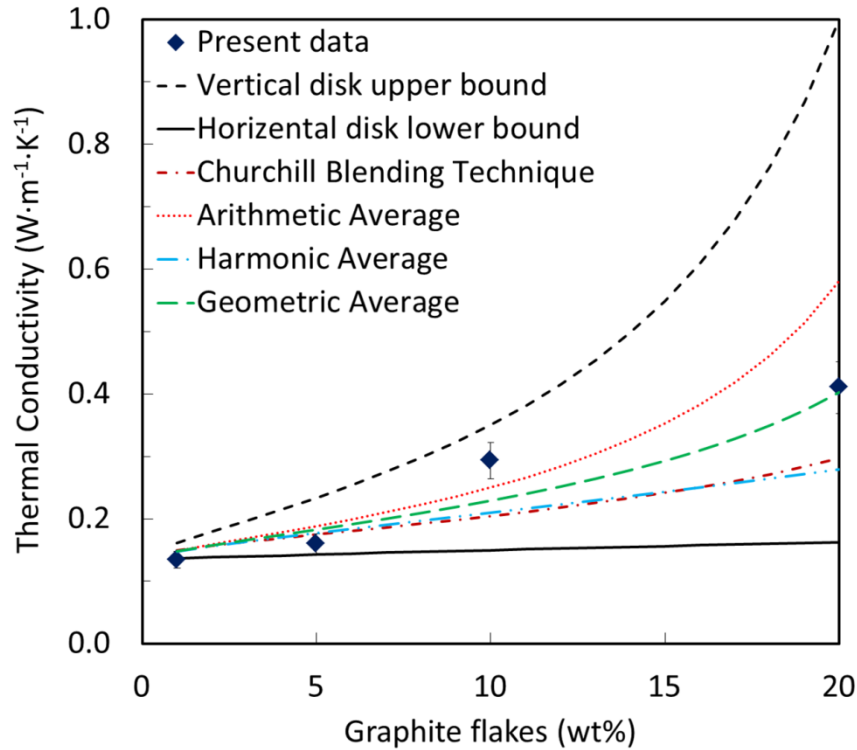
Figure 43. Comparison of different mixing methods with experimental data

There are few researches in the literature focusing on thermophysical properties modeling of consolidated adsorbents as a function of water uptake and thermal properties of each component, namely Thermal conductivity k, specific heat c_p and thermal diffusivity α. In this section, analytical model for effective medium properties, listed in Table 21, are used to calculate specific heat and thermal diffusivity of the synthesized consolidated composite at 2% and 20% RH.

Table 21. Existing thermal properties model

Name	Assumptions	Equation	Ref.
Maxwell's Model	•Dilute dispersion •Spherical particles	$\dfrac{k_{P_e}}{k_{P_1}} = \dfrac{\lambda + 2 - 2\phi(1-\lambda)}{\lambda + 2 + \phi(1-\lambda)}$ $\lambda = k_{P_2} / k_{P_1}$	[149][150]

The following assumptions are used to develop the proposed modeling:

- Graphite flakes are evenly dispersed throughout the composite,

- The sorbent material and graphite flakes have constant and anisotropic properties,

- Geometric Average of two extreme cases defined in section 5.6 is used to model effective thermal conductivity of consolidated composite containing graphite at different relative humidity.

- Specific heat of samples at 2% RH are used as the baseline for the all measurements and input to the models. Furthermore, Thermal conductivity and specific heat of water is considered 0.6 $W \cdot m^{-1} \cdot K^{-1}$ and 4,200 $J \cdot kg^{-1} \cdot K^{-1}$.

- Considering thermal properties of the solid adsorbent and adsorbate (water), the adsorbed water volume fraction is obtained from Eq. 21, where ω is the water uptake and ρ_{ads} is the density of the adsorbent:

$$\phi = \frac{\omega \cdot \rho_{water}}{\rho_{ads} + \omega \cdot \rho_{water}}$$

Eq. 21

The thermal conductivity of S6-CaCl$_2$-PVP40-G samples were measured at low RH, 2%, 20%,40% and 60%, to evaluate the effect of water uptake on the thermal conductivity (Appendix E and F). As shown in Figure 44, the increase in thermal conductivity at 60% RH associated with the increase in water content. When the hygroscopic salt absorbs water vapor a liquid film is created inside the pores of porous matrix and silica gel. Therefore, the thermal conductivity and specific heat of the composite adsorbent increases [42]. Salt solution leakage out of pores at higher up take is associated with these phenomena. For instance, the thermal conductivity of composite absorbent containing 10 wt% graphite flakes increased from 0.29 to 0.31 $W \cdot m^{-1} \cdot K^{-1}$ as its equilibrium water content increased from 0.17 g/g and 0.21 g/g, for 2 and 20% RH test conditions, respectively.
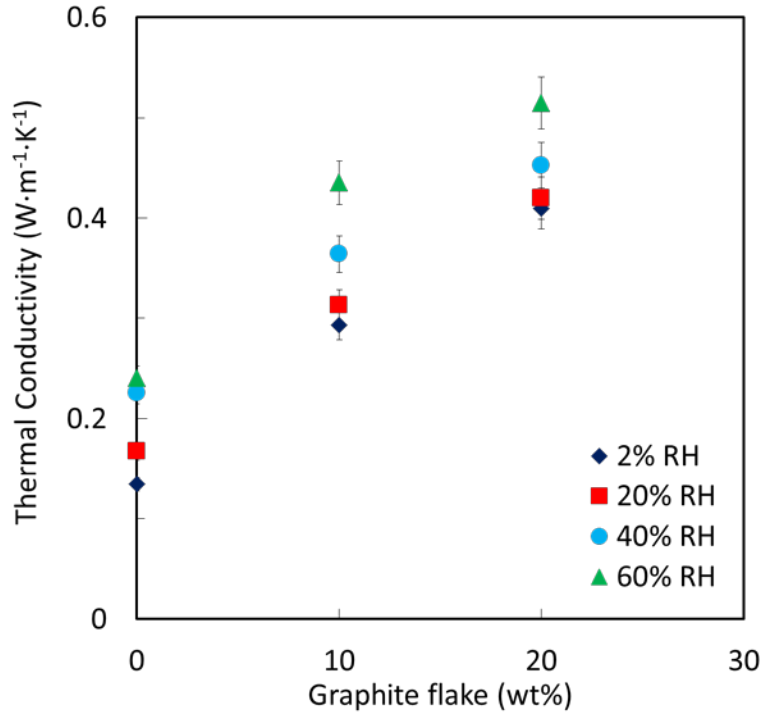
Figure 44. Thermal conductivity of consolidated composite sorbents (S6- CaCl$_2$-PVP40-0%, 10%, 20% G) with 0-20 wt% graphite flakes at 2, 20, 40 and 60 RH%

Maxwell model is in good agreement with experimental data as shown in Figure 45 when the average relative difference between model and present data is about 10%.
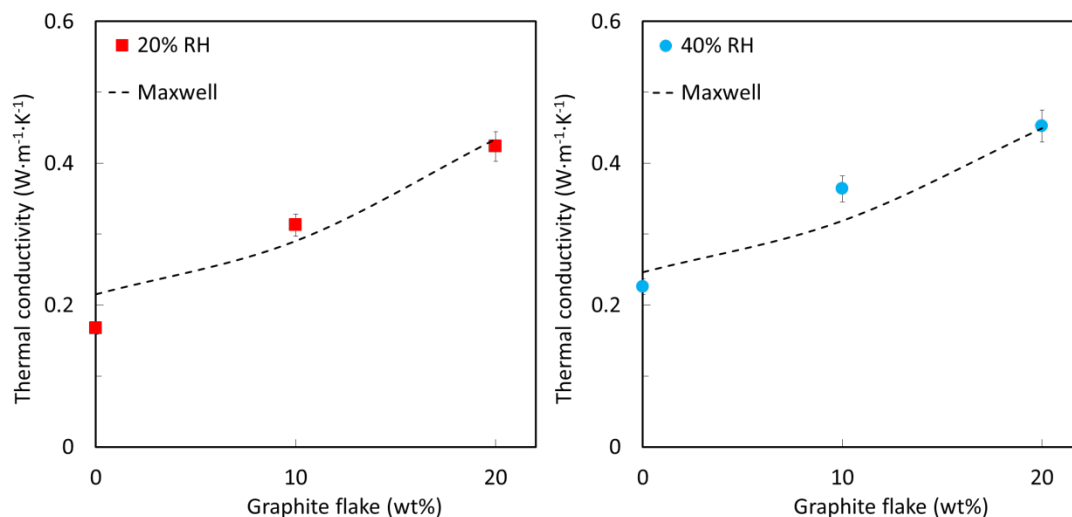
Figure 45. Comparison of various models with measured thermal conductivity of consolidated composite adsorbents (S6-CaCl₂-PVP40-G) with different amount of graphite flakes (0-20 wt %) at 20% and 40%RH.

Specific heat of consolidated composites containing different amount of graphite flakes were measured at 20% and 40% RH (Appendix E). As shown in Figure 46, specific heat of consolidated adsorbent increased from 792.3 to 956.9 $J \cdot kg^{-1} \cdot K^{-1}$ as its thermally conductive additive content (graphite flakes) increased from 0 to 20 wt% at 2% RH, a ~20% enhancement. Consolidated adsorbent exposed to 20% RH and specific heat of samples increased from 1226.1.3 to 1237.1 $J \cdot kg^{-1} \cdot K^{-1}$ as its thermally conductive additive content (graphite flakes) increased from 0 to 20 wt%. The same trend can be seen for measurements at 40%RH.
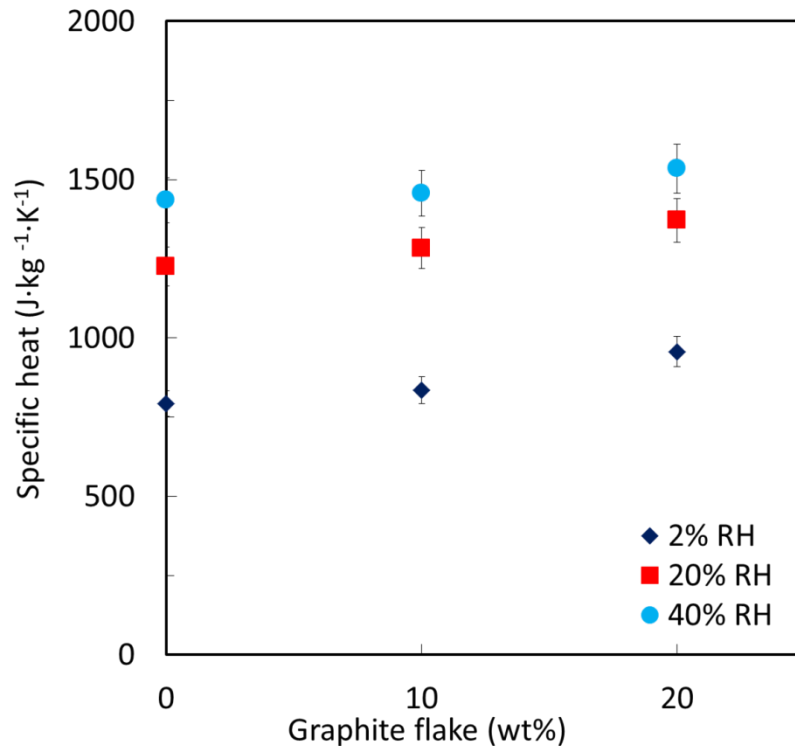
Figure 46. Specific heat of consolidated composite adsorbents (S6-CaCl$_2$-PVP40-G) with different amount of graphite flakes (0-20 wt %) at 2%, 20% and 40% RH.

Specific heat of samples at 2% RH are used as the baseline (dried material specific heat) for all the measurements and input to the models. Furthermore, specific heat of water is considered to be 4,200 J·kg^{-1}·K^{-1}. In Figure 47, Maxwell model is in good agreement with the experimental data with less than 10% relative difference.

The increase in specific heat, associated with the increase in water content, was moderate when samples were exposed to 20% RH. As the equilibrium water content of consolidated composite was increased from 0.06 g/g to 0.15 g/g, for 2 and 20% RH test conditions, the specific heat of the sample was increased from 956.9 to 1371.1 J·kg^{-1}·K^{-1}.
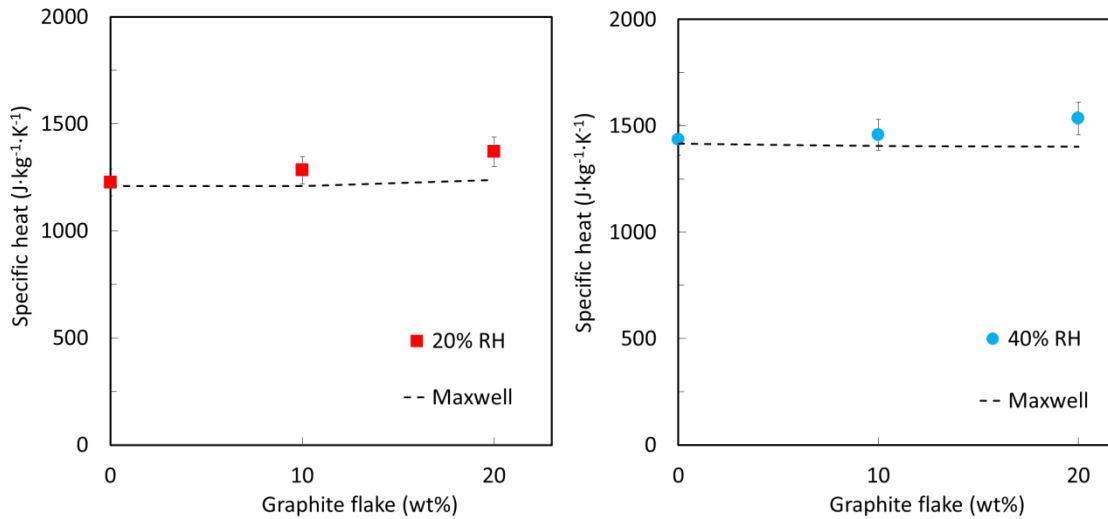
Figure 47. Comparison of various models with measured specific heat of consolidated composite adsorbents (S6-CaCl$_2$-PVP40-G) with different amount of graphite flakes (0-20 wt %) at 20% and 40%RH.

6.3.3. Thermal diffusivity

Figure 48 shows thermal diffusivity of S6-CaCl$_2$-PVP40-G samples at 20% RH when compared with available analytical models in the literature listed in Table 21. Addition of graphite flakes enhanced thermal diffusivity significantly, by 136%. Present model can predict thermal diffusivity of sorption material with a relative difference of 10%.

88
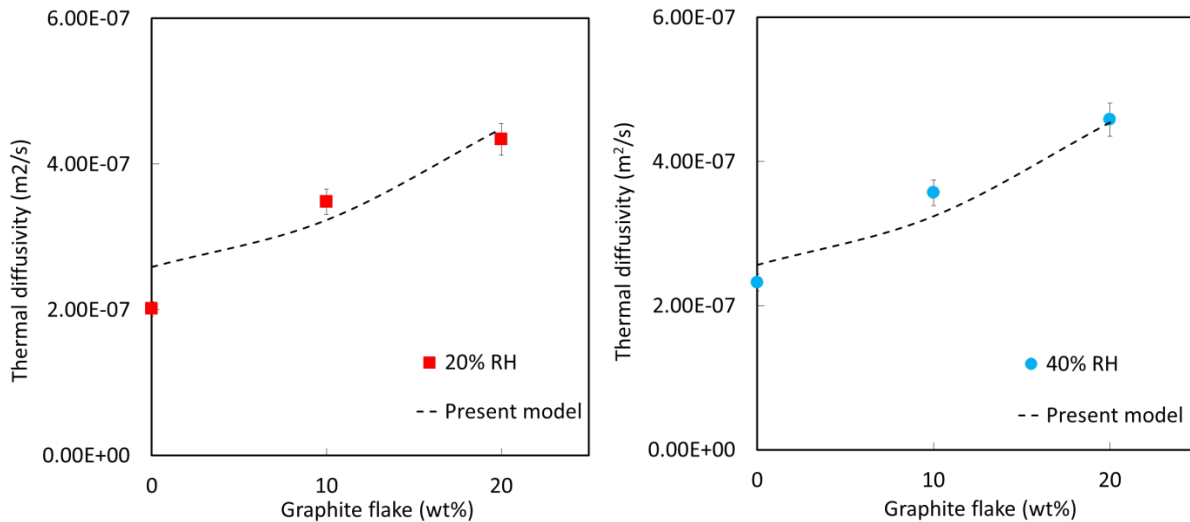
Figure 48. Comparison of the analytical models with measured thermal diffusivity of consolidated composite adsorbents (S6-CaCl$_2$-PVP40-G) with different amount of graphite flakes (0-20 wt %) at 20% and 40%RH.

6.4.　Summary

New composite adsorbents were fabricated by consolidating graphite flakes with silica gel and hygroscopic salt (CaCl$_2$) using binder, and their water uptake capacities were measured at different relative humidity. The effect of thermally conductive additive, graphite flakes, on water uptake and thermal properties of adsorbent materials were studied. The following highlights the findings of this study:

- Slight decrease was observed on water uptake as a result of addition of graphite flakes and binder.

- Thermal diffusivity of S6-CaCl$_2$-PVP40-G samples showed a significant increase of 136% as a result of adding graphite flakes. This increase is particularly important for sorption chiller applications where specific cooling power (SCP) is a major concern.

- The thermal conductivity of a set of S6-CaCl$_2$-PVP40-G sorbent with 0-20 wt% graphite flakes were tested at 2%, 20% and 60% RH. The absorbed water at 20 RH% and addition of graphite flakes increased the thermal conductivity of the sample by 12%.

- Specific heat of consolidated composite adsorbent containing graphite flakes was measured at 35°C (2 and 20 %RH). Specific heat of composite samples increased 45% by relative humidity implementation and 20 wt% graphite flake addition.

- Thermal diffusivity of sorbent material was measured at 20%RH. Addition of graphite flakes and increasing relative humidity has great impact on thermal diffusivity of consolidated adsorbent samples.

In addition to the experimental measurements, new analytical models were developed from existing model to include water content for prediction of the specific heat and thermal diffusivity of consolidated composite adsorbent. Analytical models captured the trend when water content and presence of thermally conductive additive are considered.

Chapter 7.   Conclusions and Future work

In this Ph.D. program, the research began with selection of a porous medium, silica gel. Three types of silica gel with different pore and particle size were selected. A method to confine hygroscopic salt, $CaCl_2$, into silica gel was prepared. Water sorption performances of the prepared composite adsorbents were studied with a lab scale gravimetric vapor sorption apparatus. Consolidated composites with different binders reported in literature were made to find optimum binder concentration with minimum effect on water sorption capacity of adsorbent.

In sorption process, a heat transport property, i.e. thermal diffusivity, thermal conductivity, and specific heat of the adsorbent material plays an important role in their performance. Increasing thermal diffusivity can enhance the heat transfer rate that leads to faster sorption/desorption cycles and thus more efficient (more compact) heat-driven sorption chillers. Thermally conductive additives, copper powder and graphite flake, added to consolidated composite to improve heat transfer in adsorbent. The effect of this addition on sorption performance, mechanical and thermal properties of consolidated adsorbent were studied and described thoroughly in this dissertation.

7.1. Conclusions

The followings are the conclusions of this research:

- Textural properties and water sorption capacity of $CaCl_2$-silica gel composites prepared from three silica gels were studied. Addition of hygroscopic salt, $CaCl_2$, decreases the surface area and increase average pore diameter of composites compare to pure silica gel. Sorption performance of adsorber bed layers were evaluated using a constructed gravimetric vapor sorption apparatus. Water sorption rate of thicker samples slowed down considerably by the heat of reaction.

- New consolidated composites, containing thermally conductive additive and graphite flake, were prepared with different molecular weights binder. The effect of additives, binder and graphite flakes on water uptake performance, durability, mechanical properties and thermal properties were studied.

- A new analytical model was developed to predict the effective thermal conductivity of consolidated composites containing graphite flakes when flakes assumed to have random orientation and a mean size.

- Thermal properties, namely, thermal conductivity, specific heat and thermal diffusivity of consolidated composites containing graphite flakes were studied at different relative humidity. Existing analytical models were modified to predict specific heat and thermal diffusivity of the consolidated adsorbent at different relative humidity.

7.2. Future work

The following future work is suggested to further improve the model present in this thesis:

- Small scale gravimetric large pressure jump setup built to study sorbent performance and durability of coated sorbent on graphite and metal sheets. To reduce fluctuation in weight measurement in small scale system, different methods applied such as placing a heavy marble slab under the scale to remove vibration, change its location in lab and placing it on concrete table. Still some fluctuation can be detected in data.

- Preparing large batches of consolidated composite with and without thermally conductive additive to study their performances in available lab-scale sorption cooling system. An existing heat exchanger is coated with composited sobent and thermally conductive additive to compare with loose grain composite sobent in available lab scale system.

- Small scale coated graphite based heat exchanger with be made to compare the performance of coated sorber bed with loose grain system. The effect of coating thickness and surface feature on both graphite based heat exchanger and sorbent will be studied.

- Improve thermal properties of consolidated composite sorbent by addition of different thermally conductive additives such as carbon nano tubes (CNT) and metal shave. Considering metal organic frames (MOF) as host matrix for thermal properties enhancement.

References

[1]   A. Sharafian and M. Bahrami, "Assessment of adsorber bed designs in waste-heat driven adsorption cooling systems for vehicle air conditioning and refrigeration," *Renew. Sustain. Energy Rev.*, vol. 30, pp. 440–451, 2014.

[2]   J. M. Cullen and J. M. Allwood, "The efficient use of energy: Tracing the global flow of energy from fuel to service," *Energy Policy*, vol. 38, no. 1, pp. 75–81, 2010.

[3]   M. Isaac and D. P. van Vuuren, "Modeling global residential sector energy demand for heating and air conditioning in the context of climate change," *Energy Policy*, vol. 37, pp. 507–521, 2009.

[4]   L. Pérez-Lombard, J. Ortiz, and C. Pout, "A review on buildings energy consumption information," *Energy Build.*, vol. 40, pp. 394–398, 2008.

[5]   R. Wang and R. Oliveira, "Adsorption refrigeration—An efficient way to make good use of waste heat and solar energy," *Prog. Energy Combust. Sci.*, vol. 32, no. 4, pp. 424–458, 2006.

[6]   Y. I. Aristov, "Adsorptive transformation of heat: Principles of construction of adsorbents database," *Appl. Therm. Eng.*, vol. 42, pp. 18–24, 2012.

[7]   a. O. Dieng and R. Z. Wang, "Literature review on solar adsorption technologies for ice-making and air-conditioning purposes and recent developments in solar technology," *Renew. Sustain. Energy Rev.*, vol. 5, pp. 313–342, 2000.

[8]   G. E. Hulse, "Freight car refrigeration by an adsorption system employing silica gel," *Refrig. Eng.*, vol. 17, pp. 41–54, 1929.

[9]   W. Bauer, J., Herrmann, R., Mittelbach, W., Schwieger, "Zeolite/aluminum composite adsorbents for application in adsorption refrigeration," *Int. J. Energ. Res*, vol. 33, pp. 1233–1249, 2009.

[10]   Y. I. Aristov, "Challenging offers of material science for adsorption heat transformation: A review," *Appl. Therm. Eng.*, vol. 50, no. 2, pp. 1610–1618, 2013.

[11]   J. W. Ruzhu Wang, Liwei Wang, *Adsorption Refrigeration Technology: Theory and Application*. Wiley, 2014.

[12]   L. Z. Zhang and L. Wang, "Performance estimation of an adsorption cooling system for automobile waste heat recovery," *Appl. Therm. Eng.*, vol. 17, no. 12, pp. 1127–1139, 1997.

[13]   Z. S. Lu and R. Z. Wang, "Experimental performance investigation of small solar air-conditioning systems with different kinds of collectors and chillers," *Sol. Energy*, vol. 110, pp. 7–14, 2014.

[14] X. Zheng, T. S. Ge, and R. Z. Wang, "Recent progress on desiccant materials for solid desiccant cooling systems," *Energy*, vol. 74, pp. 280–294, 2014.

[15] A. A. Askalany, M. Salem, I. M. Ismail, A. H. H. Ali, and M. G. Morsy, "A review on adsorption cooling systems with adsorbent carbon," *Renew. Sustain. Energy Rev.*, vol. 16, no. 1, pp. 493–500, 2012.

[16] I. Glaznev, D. Ovoshchnikov, and Y. I. Aristov, "Effect of residual gas on water adsorption dynamics under typical conditions of an adsorption chiller," *Heat Transf. Eng.*, vol. 31, no. April, pp. 924–930, 2010.

[17] A. Sharafian, S. M. Nemati Mehr, W. Huttema, and M. Bahrami, "Effects of different adsorber bed designs on in-situ water uptake rate measurements of AQSOA FAM-Z02 for vehicle air conditioning applications," *Appl. Therm. Eng.*, vol. 98, p. under review, 2015.

[18] Z. Tamainot-Telto and R. E. Critoph, "Monolithic carbon for sorption refrigeration and heat pump applications," *Appl. Therm. Eng.*, vol. 21, no. 1, pp. 37–52, Jan. 2001.

[19] M. Louajari, A. Mimet, and A. Ouammi, "Study of the effect of finned tube adsorber on the performance of solar driven adsorption cooling machine using activated carbon-ammonia pair," *Appl. Energy*, vol. 88, no. 3, pp. 690–698, 2011.

[20] R. E. Critoph, "Multiple bed regenerative adsorption cycle using the monolithic carbon-ammonia pair," *Appl. Therm. Eng.*, vol. 22, no. 6, pp. 667–677, 2002.

[21] G. Cacciola, G. Restuccia, and L. Mercadante, "Composites of activated carbon for refrigeration adsorption machines," *Carbon N. Y.*, vol. 33, no. 9, pp. 1205–1210, Jan. 1995.

[22] L. W. Wang, J. Y. Wu, R. . Wang, Y. X. Xu, S. G. Wang, and X. . Li, "Study of the performance of activated carbon–methanol adsorption systems concerning heat and mass transfer," *Appl. Therm. Eng.*, vol. 23, no. 13, pp. 1605–1617, Sep. 2003.

[23] Z. S. Lu and R. Z. Wang, "Study of the new composite adsorbent of salt LiCl/silica gel-methanol used in an innovative adsorption cooling machine driven by low temperature heat source," *Renew. Energy*, vol. 63, pp. 445–451, 2014.

[24] I. I. El-Sharkawy, K. Kuwahara, B. B. Saha, S. Koyama, and K. C. Ng, "Experimental investigation of activated carbon fibers/ethanol pairs for adsorption cooling system application," *Appl. Therm. Eng.*, vol. 26, no. 8–9, pp. 859–865, Jun. 2006.

[25] Y. L. Liu, R. Z. Wang, and Z. Z. Xia, "Experimental performance of a silica gel-water adsorption chiller," *Appl. Therm. Eng.*, vol. 25, pp. 359–375, 2005.

[26] R. J. H. Grisel, S. F. Smeding, and R. De Boer, "Waste heat driven silica gel/water adsorption cooling in trigeneration," *Appl. Therm. Eng.*, vol. 30, no. 8–9, pp. 1039–1046, 2010.

[27] D. Wang, J. Zhang, X. Tian, D. Liu, and K. Sumathy, "Progress in silica gel–water

adsorption refrigeration technology," *Renew. Sustain. Energy Rev.*, vol. 30, pp. 85–104, Feb. 2014.

[28]   D. C. Wang, Z. Z. Xia, and J. Y. Wu, "Design and performance prediction of a novel zeolite-water adsorption air conditioner," *Energy Convers. Manag.*, vol. 47, pp. 590–610, 2006.

[29]   I. Amber, R. O. Odekhe, and Y. S. Sanusi, "Experimental determination of the adsorption capacity of synthetic Zeolite A/water pair for solar cooling applications," *J. Mech. Eng. Res.*, vol. 4, no. 4, pp. 142–147, Apr. 2012.

[30]   İ. Solmuş, B. Kaftanoğlu, C. Yamalı, and D. Baker, "Experimental investigation of a natural zeolite–water adsorption cooling unit," *Appl. Energy*, vol. 88, no. 11, pp. 4206–4213, Nov. 2011.

[31]   G. Cacciola and G. Restuccia, "Reversible adsorption heat pump: a thermodynamic model," *Int. J. Refrig.*, vol. 18, no. 2, pp. 100–106, 1995.

[32]   S. Jiangzhou, R. Z. Wang, Y. Z. Lu, Y. X. Xu, and J. Y. Wu, "Experimental investigations on adsorption air-conditioner used in internal-combustion locomotive driver-cabin," *Appl. Therm. Eng.*, vol. 22, pp. 1153–1162, 2002.

[33]   J. Jänchen, D. Ackermann, E. Weiler, H. Stach, and W. Brösicke, "Calorimetric investigation on zeolites, AlPO4's and CaCl2 impregnated attapulgite for thermochemical storage of heat," *Thermochim. Acta*, vol. 434, pp. 37–41, 2005.

[34]   S. Vasta, A. Freni, A. Sapienza, F. Costa, and G. Restuccia, "Development and lab-test of a mobile adsorption air-conditioner," *Int. J. Refrig.*, vol. 35, no. 3, pp. 701–708, 2012.

[35]   B. N. Okunev and Y. I. Aristov, "Making adsorptive chillers faster by a proper choice of adsorption isobar shape: Comparison of optimal and real adsorbents," *Energy*, vol. 76, pp. 400–405, 2014.

[36]   A. A. Askalany, B. B. Saha, K. Kariya, I. M. Ismail, M. Salem, A. H. H. Ali, and M. G. Morsy, "Hybrid adsorption cooling systems-An overview," *Renew. Sustain. Energy Rev.*, vol. 16, no. 8, pp. 5787–5801, 2012.

[37]   N. C. Srivastava and I. W. Eames, "A review of adsorbents and adsorbates in solid–vapour adsorption heat pump systems," *Appl. Therm. Eng.*, vol. 18, no. 9–10, pp. 707–714, Sep. 1998.

[38]   Y. I. Aristov and L. L. Vasiliev, "Review new composite sorbents of water and ammonia for chemical and adsorption heat pumps," vol. 79, no. 6, pp. 160–175, 2006.

[39]   D. C. Wang, Y. H. Li, D. Li, Y. Z. Xia, and J. P. Zhang, "A review on adsorption refrigeration technology and adsorption deterioration in physical adsorption systems," vol. 14, pp. 344–353, 2010.

[40]   R. E. Critoph and Y. Zhong, "Review of trends in solid sorption refrigeration and heat

pumping technology," *Proc. Inst. Mech. Eng. Part E J. Process Mech. Eng.*, vol. 219, no. 3, pp. 285–300, 2005.

[41]   L. W. Wang, R. Z. Wang, and R. G. Oliveira, "A review on adsorption working pairs for refrigeration," *Renew. Sustain. Energy Rev.*, vol. 13, no. 3, pp. 518–534, Apr. 2009.

[42]   Y. Y. Tanashev, A. V. Krainov, and Y. I. Aristov, "Thermal conductivity of composite sorbents 'salt in porous matrix' for heat storage and transformation," *Appl. Therm. Eng.*, vol. 61, no. 2, pp. 401–407, 2013.

[43]   F. B. Cortés, F. Chejne, F. Carrasco-Marín, A. F. Pérez-Cadenas, and C. Moreno-Castilla, "Water sorption on silica- and zeolite-supported hygroscopic salts for cooling system applications," *Energy Convers. Manag.*, vol. 53, pp. 219–223, 2012.

[44]   D. S. Ovoshchnikov, I. S. Glaznev, and Y. I. Aristov, "Water sorption by the calcium chloride/silica gel composite: The accelerating effect of the salt solution present in the pores," *Kinet. Catal.*, vol. 52, no. 4, pp. 620–628, 2011.

[45]   D. S. Ovoshchnikov, I. S. Glaznev, and Y. I. Aristov, "Water sorption by the calcium chloride/silica gel composite: The accelerating effect of the salt solution present in the pores," *Kinet. Catal.*, vol. 52, no. 4, pp. 620–628, Aug. 2011.

[46]   L. G. Gordeeva, A. Freni, T. a. Krieger, G. Restuccia, and Y. I. Aristov, "Composites 'lithium halides in silica gel pores': Methanol sorption equilibrium," *Microporous Mesoporous Mater.*, vol. 112, no. 1–3, pp. 254–261, Jul. 2008.

[47]   H. Li, X. Bu, L. Wang, Z. Lu, and W. Ma, "Composite adsorbents of CaCl2 and sawdust prepared by carbonization for ammonia adsorption refrigeration," *Front. Energy*, vol. 6, no. 4, pp. 356–360, Nov. 2012.

[48]   Y. I. Aristov, "New Family of Solid Sorbents for Adsorptive Cooling : Material Scientist Approach 1," vol. 16, no. 2, pp. 63–72, 2007.

[49]   S. Santamaria, A. Sapienza, A. Frazzica, A. Freni, I. S. Girnik, and Y. I. Aristov, "Water adsorption dynamics on representative pieces of real adsorbers for adsorptive chillers," *Appl. Energy*, vol. 134, pp. 11–19, 2014.

[50]   Y. I. Aristov, I. V. Koptyug, L. G. Gordeeva, L. Y. Il'ina, and I. S. Glaznev, "Dynamics of water vapor sorption in a CaCl2/Silica Gel/Binder bed: The effect of the bed pore structure," *Kinet. Catal.*, vol. 47, no. 5, pp. 776–781, Oct. 2006.

[51]   L. G. Gordeeva and Y. I. Aristov, "Composite sorbent of methanol 'LiCl in mesoporous silica gel' for adsorption cooling: Dynamic optimization," *Energy*, vol. 36, no. 2, pp. 1273–1279, Feb. 2011.

[52]   Y. I. Aristov, L. G. Gordeeva, Y. D. Pankratiev, L. M. Plyasova, I. V. Bikova, A. Freni, and G. Restuccia, "Sorption equilibrium of methanol on new composite sorbents 'CaCl2/silica gel,'" *Adsorption*, vol. 13, no. 2, pp. 121–127, Sep. 2007.

[53] P. Hu, J.-J. Yao, and Z.-S. Chen, "Analysis for composite zeolite/foam aluminum–water mass recovery adsorption refrigeration system driven by engine exhaust heat," *Energy Convers. Manag.*, vol. 50, no. 2, pp. 255–261, Feb. 2009.

[54] D. T. A.E. Rodrigues, M. Douglas LeVan, *Adsorption: Science and Technology*. 1988.

[55] A. A. Askalany, M. Salem, I. M. Ismail, A. H. H. Ali, and M. G. Morsy, "A review on adsorption cooling systems with adsorbent carbon," *Renew. Sustain. Energy Rev.*, vol. 16, no. 1, pp. 493–500, 2012.

[56] Y. I. Aristov, I. S. Glaznev, A. Freni, and G. Restuccia, "Kinetics of Water Sorption on a CaCl2-in-Silica-Gel-Pores Sorbent: The Effects of the Pellet Size and Temperature," *Chem. Eng. Sci.*, vol. 61, pp. 1453–1458, 2006.

[57] A. Ristić, N. Z. Logar, S. K. Henninger, and V. Kaučič, "The performance of small-pore microporous aluminophosphates in low-temperature solar energy storage: The structure-property relationship," *Adv. Funct. Mater.*, vol. 22, no. 9, pp. 1952–1957, 2012.

[58] Y. Aristov, "Concept of adsorbent optimal for adsorptive cooling/heating," *Appl. Therm. Eng.*, vol. 72, no. 2, pp. 166–175, 2014.

[59] L. Gordeeva, A. Grekova, T. Krieger, and Y. Aristov, "Composites 'binary salts in porous matrix' for adsorption heat transformation," *Appl. Therm. Eng.*, vol. 50, no. 2, pp. 1633–1638, Feb. 2013.

[60] Y. Zhong, R. E. Critoph, R. N. Thorpe, Z. Tamainot-Telto, and Y. I. Aristov, "Isothermal sorption characteristics of the BaCl2-NH3 pair in a vermiculite host matrix," *Appl. Therm. Eng.*, vol. 27, no. 14–15, pp. 2455–2462, 2007.

[61] A. Solé, L. Miró, C. Barreneche, I. Martorell, and L. F. Cabeza, "Corrosion of metals and salt hydrates used for thermochemical energy storage," *Renew. Energy*, vol. 75, pp. 519–523, 2015.

[62] A. Sapienza, A. Frazzica, A. Freni, and Y. Aristov, "Dramatic effect of residual gas on dynamics of isobaric adsorption stage of an adsorptive chiller," *Appl. Therm. Eng.*, vol. 96, pp. 385–390, 2016.

[63] R. E. Critoph and S. J. Metcalf, "Specific cooling power intensification limits in ammonia–carbon adsorption refrigeration systems," *Appl. Therm. Eng.*, vol. 24, no. 5–6, pp. 661–678, Apr. 2004.

[64] J. W. Ruzhu Wang, Liwei Wang, *Adsorption Refrigeration Technology: Theory and Application*. 2014.

[65] A. Dabrowski, "Adsorption - From theory to practice," *Adv. Colloid Interface Sci.*, vol. 93, pp. 135–224, 2001.

[66] H. H. Guyer, *Industrial Processes and Waste Stream Management*. John Wiley & Sons,

INC., 1998.

[67]   Sivasankar. B., *Engineering Chemistry*. Tata McGraw-Hill Publishing Company Limited, 2008.

[68]   R. S. Jürgen U. Keller, *Gas Adsorption Equilibria: Experimental Methods and Adsorptive Isotherms*. Springer Sience +Business Media, INC., 2005.

[69]   T. Horikawa, D. D. Do, and D. Nicholson, "Capillary condensation of adsorbates in porous materials," *Adv. Colloid Interface Sci.*, vol. 169, no. 1, pp. 40–58, 2011.

[70]   R. I. Masel, *Principles of Adsorption and Reaction on Solid Surfaces*. John Wiley & Sons, INC., 1996.

[71]   J. E. S. Seymour Lowell, *Powder Surface Area and Porosity*. Springer Sience +Business Media, INC., 1991.

[72]   J. Bauer, R. Herrmann, W. Mittelbach, and W. Schwieger, "Zeolite / aluminum composite adsorbents for application in adsorption refrigeration," no. May, pp. 1233–1249, 2009.

[73]   A. Rezk, R. K. Al-Dadah, S. Mahmoud, and A. Elsayed, "Effects of contact resistance and metal additives in finned-tube adsorbent beds on the performance of silica gel/water adsorption chiller," *Appl. Therm. Eng.*, vol. 53, no. 2, pp. 278–284, 2013.

[74]   A. Freni, A. Frazzica, B. Dawoud, S. Chmielewski, L. Calabrese, and L. Bonaccorsi, "Adsorbent coatings for heat pumping applications: Verification of hydrothermal and mechanical stabilities," *Appl. Therm. Eng.*, vol. 50, no. 2, pp. 1658–1663, Feb. 2013.

[75]   A. Freni, L. Bonaccorsi, L. Calabrese, A. Caprì, A. Frazzica, and A. Sapienza, "SAPO-34 coated adsorbent heat exchanger for adsorption chillers," *Appl. Therm. Eng.*, vol. 82, pp. 1–7, 2015.

[76]   H. Negishi, A. Miyamoto, and A. Endo, "Preparation of thick mesoporous silica coating by electrophoretic deposition with binder addition and its water vapor adsorption-desorption properties," *Microporous Mesoporous Mater.*, vol. 180, pp. 250–256, 2013.

[77]   H. van Heyden, G. Munz, L. Schnabel, F. Schmidt, S. Mintova, and T. Bein, "Kinetics of water adsorption in microporous aluminophosphate layers for regenerative heat exchangers," *Appl. Therm. Eng.*, vol. 29, no. 8–9, pp. 1514–1522, Jun. 2009.

[78]   A. Sharafian, K. Fayazmanesh, C. McCague, and M. Bahrami, "Thermal conductivity and contact resistance of mesoporous silica gel adsorbents bound with polyvinylpyrrolidone in contact with a metallic substrate for adsorption cooling system applications," *Int. J. Heat Mass Transf.*, vol. 79, pp. 64–71, 2014.

[79]   S. G. Wang, R. Z. Wang, and X. R. Li, "Research and development of consolidated adsorbent for adsorption systems," *Renew. Energy*, vol. 30, no. 9, pp. 1425–1441, Jul. 2005.

[80] a. Rezk, R. K. Al-Dadah, S. Mahmoud, and a. Elsayed, "Effects of contact resistance and metal additives in finned-tube adsorbent beds on the performance of silica gel/water adsorption chiller," *Appl. Therm. Eng.*, vol. 53, no. 2, pp. 278–284, 2012.

[81] I. Glaznev, I. Ponomarenko, S. Kirik, and Y. Aristov, "Composites CaCl2/SBA-15 for adsorptive transformation of low temperature heat: Pore size effect," *Int. J. Refrig.*, vol. 34, no. 5, pp. 1244–1250, Aug. 2011.

[82] A. Freni, A. Sapienza, I. S. Glaznev, Y. I. Aristov, and G. Restuccia, "Experimental testing of a lab-scale adsorption chiller using a novel selective water sorbent 'silica modified by calcium nitrate,'" *Int. J. Refrig.*, vol. 35, no. 3, pp. 518–524, May 2012.

[83] Y. I. Aristov, G. Restuccia, G. Cacciola, and V. N. Parmon, "A family of new working materials for solid sorption air conditioning systems," *Appl. Therm. Eng.*, vol. 22, pp. 191–204, 2002.

[84] I. V. Ponomarenko, I. S. Glaznev, a. V. Gubar, Y. I. Aristov, and S. D. Kirik, "Synthesis and water sorption properties of a new composite 'CaCl2 confined into SBA-15 pores,'" *Microporous Mesoporous Mater.*, vol. 129, no. 1–2, pp. 243–250, 2010.

[85] I. Glaznev, I. Ponomarenko, S. Kirik, and Y. Aristov, "Composites CaCl2/SBA-15 for adsorptive transformation of low temperature heat: Pore size effect," *Int. J. Refrig.*, vol. 34, no. 5, pp. 1244–1250, 2011.

[86] A. Freni, G. Maggio, A. Sapienza, A. Frazzica, G. Restuccia, and S. Vasta, "Comparative analysis of promising adsorbent/adsorbate pairs for adsorptive heat pumping, air conditioning and refrigeration," *Appl. Therm. Eng.*, vol. 104, pp. 85–95, 2016.

[87] A. Sapienza, S. Santamaria, A. Frazzica, A. Freni, and Y. I. Aristov, "Dynamic study of adsorbers by a new gravimetric version of the Large Temperature Jump method," *Appl. Energy*, vol. 113, pp. 1244–1251, 2014.

[88] Y. I. Aristov, "Experimental and numerical study of adsorptive chiller dynamics: Loose grains configuration," *Appl. Therm. Eng.*, vol. 61, no. 2, pp. 841–847, 2013.

[89] K. E. N'Tsoukpoe, G. Restuccia, T. Schmidt, and X. Py, "The size of sorbents in low pressure sorption or thermochemical energy storage processes," *Energy*, vol. 77, pp. 983–998, 2014.

[90] G. G. Ilis, M. Mobedi, and S. Ülkü, "Comparison of Uniform and Non-uniform Pressure Approaches Used to Analyze an Adsorption Process in a Closed Type Adsorbent Bed," *Transp. Porous Media*, vol. 98, pp. 81–101, 2013.

[91] A. Sharafian and M. Bahrami, "Adsorbate uptake and mass diffusivity of working pairs in adsorption cooling systems," *Int. J. Heat Mass Transf.*, vol. 59, no. April 2013, pp. 262–271, 2013.

[92] K. Sen Chang, M. T. Chen, and T.-W. Chung, "Effects of the thickness and particle size of

silica gel on the heat and mass transfer performance of a silica gel-coated bed for air-conditioning adsorption systems," *Appl. Therm. Eng.*, vol. 25, no. 14–15, pp. 2330–2340, Oct. 2005.

[93]   L. Pino, Y. U. Aristov, G. Cacciola, and G. Restuccia, "Composite Materials Based on Zeolite 4A for Adsorption Heat Pumps," *Adsorption*, vol. 40, pp. 33–40, 1997.

[94]   S. Vasta, G. Giacoppo, O. Barbera, L. Calabrese, L. Bonaccorsi, and A. Freni, "Innovative zeolite coatings on graphite plates for advanced adsorbers," *Appl. Therm. Eng.*, vol. 72, pp. 153–159, 2014.

[95]   Y. I. Aristov, "Challenging offers of material science for adsorption heat transformation: A review," *Appl. Therm. Eng.*, vol. 50, no. 2, pp. 1610–1618, Feb. 2013.

[96]   Y. Y. Tanashev, A. V. Krainov, and Y. I. Aristov, "Thermal conductivity of composite sorbents 'salt in porous matrix' for heat storage and transformation," *Appl. Therm. Eng.*, vol. 61, no. 2, pp. 401–407, 2013.

[97]   T. Eun, H. Song, J. Hun, K. Lee, and J. Kim, "Enhancement of heat and mass transfer in silica-expanded graphite composite blocks for adsorption heat pumps : Part I . Characterization of the composite blocks," *Int. J. Refrig.*, vol. 23, pp. 64–73, 2000.

[98]   H. Demir, M. Mobedi, and S. Ülkü, "The use of metal piece additives to enhance heat transfer rate through an unconsolidated adsorbent bed," *Int. J. Refrig.*, vol. 33, no. 4, pp. 714–720, Jun. 2010.

[99]   C.-H. Wu, S.-H. Hsu, R. Q. Chu, M.-T. Chen, and T.-W. Chung, "Enhancing the Thermal Conductivity of the Heat Exchanger in a Noncompressive System as a Means of Energy Efficiency Improvement of the System," *Int. J. Green Energy*, vol. 6, no. June 2014, pp. 490–507, 2009.

[100]   H. Demir, M. Mobedi, and S. Ülkü, "The use of metal piece additives to enhance heat transfer rate through an unconsolidated adsorbent bed," *Int. J. Refrig.*, vol. 33, pp. 714–720, 2010.

[101]   Y. Y. Tanasheva, Yu. I. , Aristov, "Thermal conductivity of silica gel + calcium chloride system: the effect of adsorbed water," *J. Eng. Phys. Thermophys.*, vol. 73, no. 5, pp. 876–883, 2003.

[102]   A. Freni, M. M. Tokarev, G. Restuccia, a. G. Okunev, and Y. I. Aristov, "Thermal conductivity of selective water sorbents under the working conditions of a sorption chiller," *Appl. Therm. Eng.*, vol. 22, pp. 1631–1642, 2002.

[103]   L. W. Wang, S. J. Metcalf, R. E. Critoph, R. Thorpe, and Z. Tamainot-Telto, "Development of thermal conductive consolidated activated carbon for adsorption refrigeration," *Carbon N. Y.*, vol. 50, no. 3, pp. 977–986, 2012.

[104]   L. W. Wang, Z. Tamainot-Telto, R. Thorpe, R. E. Critoph, S. J. Metcalf, and R. Z. Wang,

"Study of thermal conductivity, permeability, and adsorption performance of consolidated composite activated carbon adsorbent for refrigeration," *Renew. Energy*, vol. 36, no. 8, pp. 2062–2066, Aug. 2011.

[105] K. Wang, J. Y. Wu, R. Z. Wang, and L. W. Wang, "Effective thermal conductivity of expanded graphite–CaCl2 composite adsorbent for chemical adsorption chillers," *Energy Convers. Manag.*, vol. 47, no. 13–14, pp. 1902–1912, 2006.

[106] B. Dawoud, M. I. Sohel, a. Freni, S. Vasta, and G. Restuccia, "On the effective thermal conductivity of wetted zeolite under the working conditions of an adsorption chiller," *Appl. Therm. Eng.*, vol. 31, no. 14–15, pp. 2241–2246, 2011.

[107] H. Bjurstrom, E. Karawacki, and B. Carlsson, "Thermal conductivity of a microporous particulate medium: moist silica gel," *Int. J. Heat Mass Transf.*, vol. 27, no. 11, pp. 2025–2036, 1984.

[108] K. C. Ng, H. T. Chua, C. Y. Chung, C. H. Loke, T. Kashiwagi, A. Akisawa, and B. B. Saha, "Experimental investigation of the silica gel-water adsorption isotherm characteristics," *Appl. Therm. Eng.*, vol. 21, no. 16, pp. 1631–1642, 2001.

[109] Y. I. Aristov, Y. A. Kovalevskaya, M. M. Tokarev, and I. E. Paukov, "Low temperature heat capacity of the system 'silica gel-calcium chloride-water,'" *J. Therm. Anal. Calorim.*, vol. 103, no. 2, pp. 773–778, 2011.

[110] H. Kakiuchi, M. Iwade, S. Shimooka, and K. Ooshima, "Novel zeolite adsorbents and their application for AHP and Desiccant system," *IEA-Annex*, 2005.

[111] A. Li, A. Bin Ismail, K. Thu, M. W. Shahzad, K. C. Ng, and B. B. Saha, "Formulation of Water Equilibrium Uptakes on Silica Gel and Ferroaluminophosphate Zeolite for Adsorption Cooling andDesalination Applications," *Nov. Carbon Resour. Sci. Green Asia Strateg.*, vol. 1, no. 2, pp. 37–45, 2014.

[112] M. Schicktanz, P. Hügenell, and S. K. Henninger, "Evaluation of methanol/activated carbons for thermally driven chillers, part II: The energy balance model," *Int. J. Refrig.*, vol. 35, no. 3, pp. 554–561, 2012.

[113] K. Thu, K. C. Ng, B. B. Saha, A. Chakraborty, and S. Koyama, "Operational strategy of adsorption desalination systems," *Int. J. Heat Mass Transf.*, vol. 52, no. 7–8, pp. 1811–1816, 2009.

[114] R. E. Critoph and S. J. Metcalf, "Specific cooling power intensification limits in ammonia–carbon adsorption refrigeration systems," *Appl. Therm. Eng.*, vol. 24, no. 5–6, pp. 661–678, Apr. 2004.

[115] L. W. Wang, R. Z. Wang, Z. S. Lu, C. J. Chen, K. Wang, and J. Y. Wu, "The performance of two adsorption ice making test units using activated carbon and a carbon composite as adsorbents," *Carbon N. Y.*, vol. 44, no. 13, pp. 2671–2680, Nov. 2006.

[116]   a. Freni, F. Russo, S. Vasta, M. Tokarev, Y. I. Aristov, and G. Restuccia, "An advanced solid sorption chiller using SWS-1L," *Appl. Therm. Eng.*, vol. 27, pp. 2200–2204, 2007.

[117] J. K. Kiplagat, R. Z. Wang, R. G. Oliveira, T. X. Li, and M. Liang, "Experimental study on the effects of the operation conditions on the performance of a chemisorption air conditioner powered by low grade heat," *Appl. Energy*, vol. 103, pp. 571–580, 2013.

[118] I. S. Girnik, A. D. Grekova, L. G. Gordeeva, and Y. I. Aristov, "Dynamic Optimization of Adsorptive Chillers: Compact Layer Vs. Bed of Loose Grains," *Appl. Therm. Eng.*, 2017.

[119] D. C. Wang, Z. Z. Xia, J. Y. Wu, R. Z. Wang, H. Zhai, and W. D. Dou, "Study of a novel silica gel-water adsorption chiller. Part I. Design and performance prediction," *Int. J. Refrig.*, vol. 28, no. 7, pp. 1073–1083, 2005.

[120] D. C. Wang, Z. Z. Xia, J. Y. Wu, R. Z. Wang, H. Zhai, and W. D. Dou, "Study of a novel silica gel-water adsorption chiller. Part II. Design and performance prediction," *Int. J. Refrig.*, vol. 28, no. 7, pp. 1073–1083, 2005.

[121] X. Yang and P. Knochel, "Research on a compact adsorption room air conditioner," *Synthesis (Stuttg).*, vol. 47, no. 13, pp. 2167–2172, 2006.

[122] A. Sapienza, S. Santamaria, A. Frazzica, and A. Freni, "Influence of the management strategy and operating conditions on the performance of an adsorption chiller," *Energy*, vol. 36, no. 9, pp. 5532–5538, 2011.

[123] Z. S. Lu, R. Z. Wang, Z. Z. Xia, Q. B. Wu, Y. M. Sun, and Z. Y. Chen, "An analysis of the performance of a novel solar silica gel-water adsorption air conditioning," *Appl. Therm. Eng.*, vol. 31, no. 17–18, pp. 3636–3642, 2011.

[124] Z. Lu, R. Wang, Z. Xia, and L. Gong, "Experimental investigation adsorption chillers using micro-porous silica gel-water and compound adsorbent-methanol," *Energy Convers. Manag.*, vol. 65, pp. 430–437, 2013.

[125] J. Y. San and F. K. Tsai, "Testing of a lab-scale four-bed adsorption heat pump," *Appl. Therm. Eng.*, vol. 70, no. 1, pp. 274–281, 2014.

[126] Q. W. Pan, R. Z. Wang, L. W. Wang, and D. Liu, "Design and experimental study of a silica gel-water adsorption chiller with modular adsorbers," *Int. J. Refrig.*, vol. 67, pp. 336–344, 2016.

[127] K. Oertel and M. Fischer, "Adsorption cooling system for cold storage using methanol/silicagel," *Appl. Therm. Eng.*, vol. 18, no. 9–10, pp. 773–786, 1998.

[128] G. Restuccia, A. Freni, S. Vasta, and Y. Aristov, "Selective water sorbent for solid sorption chiller: Experimental results and modelling," *Int. J. Refrig.*, vol. 27, no. 3, pp. 284–293, 2004.

[129] K. Daou, R. Z. Wang, G. Z. Yang, and Z. Z. Xia, "Theoretical comparison of the refrigerating

performances of a CaCl2 impregnated composite adsorbent to those of the host silica gel,” *Int. J. Therm. Sci.*, vol. 47, no. 1, pp. 68–75, 2008.

[130] L. X. Gong, R. Z. Wang, Z. Z. Xia, and C. J. Chen, “Design and performance prediction of a new generation adsorption chiller using composite adsorbent,” *Energy Convers. Manag.*, vol. 52, no. 6, pp. 2345–2350, 2011.

[131] R. E. Critoph, “Rapid cycling solar/biomass powered adsorption refrigeration system,” *Renew. Energy*, vol. 16, no. 1–4, pp. 673–678, 1999.

[132] F. P. Song, L. X. Gong, L. W. Wang, and R. Z. Wang, “Study on gradient thermal driven adsorption cycle with freezing and cooling output for food storage,” *Appl. Therm. Eng.*, vol. 70, no. 1, pp. 231–239, 2014.

[133] Q. W. Pan, R. Z. Wang, Z. S. Lu, and L. W. Wang, “Experimental investigation of an adsorption refrigeration prototype with the working pair of composite adsorbent-ammonia,” *Appl. Therm. Eng.*, vol. 72, no. 2, pp. 275–282, 2014.

[134] S. Santamaria, A. Sapienza, A. Frazzica, A. Freni, I. S. Girnik, and Y. I. Aristov, “Water adsorption dynamics on representative pieces of real adsorbers for adsorptive chillers,” *Appl. Energy*, vol. 134, pp. 11–19, 2014.

[135] S. Vasta, A. Freni, A. Sapienza, F. Costa, and G. Restuccia, “Development and lab-test of a mobile adsorption air-conditioner,” *Int. J. Refrig.*, vol. 35, no. 3, pp. 701–708, 2012.

[136] A. Sharafian, S. M. Nemati Mehr, P. C. Thimmaiah, W. Huttema, and M. Bahrami, “Effects of adsorbent mass and number of adsorber beds on the performance of a waste heat-driven adsorption cooling system for vehicle air conditioning applications,” *Energy*, vol. 112, pp. 481–493, 2016.

[137] P. P. Barrett, E.P., Joyner, L.G., Halenda, “The determination of pore volume and area distributions in porous substances, computations from nitrogen isotherms,” *J. Am. Chem. Soc.*, vol. 73, pp. 373–380, 1951.

[138] I. V. Ponomarenko, I. S. Glaznev, a. V. Gubar, Y. I. Aristov, and S. D. Kirik, “Synthesis and water sorption properties of a new composite ‘CaCl2 confined into SBA-15 pores,’” *Microporous Mesoporous Mater.*, vol. 129, no. 1–2, pp. 243–250, Apr. 2010.

[139] W.R.Busing, “An interpretation of the structures of alkaline earth chlorides in terms of interionic forces,” *T. Am. Crystallogr. Assoc.*, vol. 6, pp. 57–72, 1970.

[140] M. M. B. A.Leclaire, “Le dichlorure de calcium dehydrate,” *Acta Crystallogr. B*, vol. 33, pp. 1608–1610, 1977.

[141] S. A. Al-Ajlan, “Measurements of thermal properties of insulation materials by using transient plane source technique,” *Appl. Therm. Eng.*, vol. 26, no. 17–18, pp. 2184–2191, 2006.

[142] S. E. Gustafsson, "Transient plane source techniques for thermal conductivity and thermal diffusivity measurements of solid materials," *Rev. Sci. Instrum.*, vol. 62, no. 3, pp. 797–804, 1991.

[143] Y. He, "Rapid thermal conductivity measurement with a hot disk sensor: Part 1. Theoretical considerations," *Thermochim. Acta*, vol. 436, no. 1–2, pp. 122–129, 2005.

[144] W. Conshohocken, "Standard Test Method for Compressive Properties of Rigid Plastics 1," *Annu. B. ASTM Stand.*, vol. 8, no. April 2003, pp. 1–7, 2011.

[145] A. E831-14, "Standard Test Method for Linear Thermal Expansion of Solid Materials by Thermomechanical Analysis," *ASTM Int. West Conshohocken, PA*, 2014.

[146] M. Molenda, J. Stengler, M. Linder, and A. Wörner, "Reversible hydration behavior of CaCl2 at high H2O partial pressures for thermochemical energy storage," *Thermochim. Acta*, vol. 560, pp. 76–81, 2013.

[147] P. Hidnert and W. T. Sweeney, "Thermal expansion of graphite," *Bur. Stand.*, vol. 21, no. No 335, pp. 223–230, 1927.

[148] K. Pietrak and T. S. Wi, "A review of models for effective thermal conductivity of composite materials," *J. Power Technol.*, vol. 95, no. 1, pp. 14–24, 2015.

[149] M. Kandula, "Effective thermal conductivity of porous packed beds with uniform spherical particles," *J. Porous Media*, vol. 14, no. 10, pp. 919–926, 2011.

[150] M. Bahrami, M. M. Yovanovich, and J. R. Culham, "Assessment of relevant physical phenomena controlling thermal performance of nanofluids," *J. Thermophys. Heat Transf.*, vol. 21, no. 4, pp. 673–680, 2007.

[151] N. Silvestre, *Advanced computational nanomechanics*. Wiley, 2016.

[152] C. T. Hsu, P. Cheng, and K. W. Wong, "Modified Zehner-Schlünder models for stagnant thermal conductivity of porous media," *Int. J. Heat Mass Transf.*, vol. 37, no. 17, pp. 2751–2759, 1994.

[153] E. Pop, V. Varshney, and A. K. Roy, "Thermal properties of graphene: Fundamentals and applications," *MRS Bull.*, vol. 37, no. 12, pp. 1273–1281, 2012.

[154] S. W. Churchill and R. Usagi, "A standardized procedure for the production of correlations in the form of a common empirical equation," *Ind. Eng. Chem. Fundam.*, vol. 13, no. 1, pp. 39–44, 1974.

Appendix A.

N$_2$ physisorption porosimetry

S6- Adsorption		S6- Desorption	
Relative Pressure (P/Po)	Quantity Adsorbed (cm³/g STP)	Relative Pressure (P/Po)	Quantity Adsorbed (cm³/g STP)
0.010	73.416	0.994	486.209
0.029	88.880	0.971	485.613
0.060	101.848	0.932	484.612
0.076	106.662	0.906	483.902
0.099	112.969	0.900	483.633
0.120	117.863	0.874	482.973
0.139	122.376	0.850	482.283
0.159	126.774	0.825	481.403
0.179	131.070	0.801	479.735
0.200	135.335	0.751	467.927
0.245	144.929	0.697	409.716
0.301	157.286	0.646	342.335
0.352	169.358	0.603	293.834
0.399	181.928	0.548	251.843
0.449	196.559	0.494	222.316
0.499	213.276	0.444	197.78
0.549	233.238	0.400	181.852
0.599	257.433	0.353	169.087
0.648	286.758	0.304	157.081
0.698	325.567	0.251	145.110
0.745	371.332	0.202	134.556
0.802	434.394	0.142	121.528
0.823	455.109		
0.855	475.588		
0.869	479.746		
0.913	483.634		
0.943	484.510		
0.968	485.189		
0.974	485.443		
0.980	485.643		
0.990	485.957		
0.994	486.209		

S6-CaCl2 - Adsorption		S6-CaCl2 - Desorption	
Relative Pressure (P/Po)	Quantity Adsorbed (cm³/g STP)	Relative Pressure (P/Po)	Quantity Adsorbed (cm³/g STP)
0.009	21.842	0.994	203.655
0.031	26.837	0.971	203.426
0.060	30.140	0.931	203.153
0.078	31.641	0.906	202.960
0.100	33.164	0.899	202.881
0.120	34.411	0.874	202.720
0.139	35.513	0.851	202.509
0.160	36.643	0.825	202.083
0.180	37.671	0.802	200.337
0.200	38.673	0.746	147.420
0.248	40.973	0.682	90.912
0.302	43.588	0.639	76.844
0.353	46.174	0.600	68.870
0.400	48.768	0.556	62.358
0.450	51.835	0.502	56.364
0.500	55.397	0.452	51.699
0.550	59.703	0.399	48.141
0.600	65.155	0.352	45.471
0.649	72.299	0.301	42.820
0.699	82.262	0.252	40.395
0.747	97.248	0.200	37.885
0.793	122.383	0.145	35.016
0.817	143.126		
0.853	179.975		
0.878	197.947		
0.906	202.510		
0.942	203.062		
0.968	203.296		
0.993	203.568		
0.994	203.655		

S6-CaCl2-PVP10 - Adsorption		S6-CaCl2-PVP10- Desorption	
Relative Pressure (P/Po)	Quantity Adsorbed (cm³/g STP)	Relative Pressure (P/Po)	Quantity Adsorbed (cm³/g STP)
0.009	12.966	0.994	98.864
0.031	16.374	0.971	98.782
0.060	18.909	0.931	98.687
0.078	19.944	0.906	98.601
0.100	21.078	0.899	98.555
0.120	21.984	0.874	98.491
0.139	22.803	0.851	98.357
0.160	23.580	0.825	98.274
0.180	24.319	0.802	98.183
0.200	25.033	0.746	97.234
0.248	26.692	0.682	94.383
0.302	28.523	0.639	77.653
0.353	30.349	0.600	59.229
0.400	32.210	0.556	46.333
0.450	34.454	0.502	40.467
0.500	37.135	0.452	34.541
0.550	40.531	0.399	32.216
0.600	45.116	0.352	29.644
0.649	51.830	0.301	28.303
0.699	61.517	0.252	26.466
0.747	74.994	0.200	24.720
0.793	90.228	0.145	22.613
0.817	93.791		
0.853	96.955		
0.878	98.066		
0.906	98.462		
0.942	98.601		
0.968	98.694		
0.993	98.808		
0.994	98.864		

S6-CaCl2-PVP40 - Adsorption		S6-CaCl2-PVP40 - Desorption	
Relative Pressure (P/Po)	Quantity Adsorbed (cm³/g STP)	Relative Pressure (P/Po)	Quantity Adsorbed (cm³/g STP)
0.009	16.943	1.000	143.582
0.033	21.070	0.964	136.955
0.064	23.603	0.930	137.198
0.079	24.483	0.905	137.355
0.100	25.491	0.880	137.533
0.119	26.289	0.855	137.681
0.140	27.057	0.830	137.824
0.160	27.729	0.805	137.933
0.180	28.362	0.781	137.747
0.200	28.967	0.751	129.344
0.249	30.326	0.700	90.209
0.301	31.757	0.637	61.354
0.351	33.230	0.597	53.068
0.400	34.797	0.545	45.980
0.450	36.635	0.504	41.653
0.499	38.814	0.452	36.733
0.549	41.561	0.398	34.351
0.599	45.229	0.334	32.214
0.648	50.453	0.301	31.233
0.697	58.208	0.251	29.772
0.747	70.526	0.200	28.294
0.796	90.243	0.142	26.418
0.823	105.603		
0.853	123.983		
0.882	134.580		
0.915	136.839		
0.944	136.825		
0.969	136.683		
0.994	136.573		
1.000	143.582		

S15 - Adsorption		S15 - Desorption	
Relative Pressure (P/Po)	Quantity Adsorbed (cm³/g STP)	Relative Pressure (P/Po)	Quantity Adsorbed (cm³/g STP)
0.010	42.916	0.997	712.285
0.030	52.392	0.973	710.839
0.058	59.185	0.935	708.102
0.077	62.429	0.909	706.054
0.100	65.634	0.900	705.062
0.120	68.160	0.881	662.486
0.140	70.470	0.856	411.324
0.160	72.636	0.829	288.826
0.180	74.689	0.806	238.821
0.200	76.683	0.750	175.429
0.248	81.226	0.706	152.333
0.303	86.443	0.656	135.776
0.354	91.498	0.606	124.146
0.399	96.247	0.553	114.455
0.450	101.893	0.502	106.818
0.499	108.116	0.451	100.181
0.549	115.212	0.402	94.600
0.599	123.591	0.350	88.974
0.649	133.810	0.300	84.040
0.698	146.931	0.253	79.431
0.747	164.943	0.201	74.350
0.795	192.174	0.141	68.106
0.821	215.033		
0.846	248.684		
0.872	307.173		
0.897	415.815		
0.923	633.948		
0.997	712.285		
0.010	42.916		
0.030	52.392		

S15-CaCl$_2$ - Adsorption		S15-CaCl$_2$ - Desorption	
Relative Pressure (P/Po)	Quantity Adsorbed (cm³/g STP)	Relative Pressure (P/Po)	Quantity Adsorbed (cm³/g STP)
0.009	21.110	1.000	388.059
0.032	26.211	0.971	378.448
0.061	29.568	0.933	377.352
0.078	30.954	0.907	376.550
0.100	32.462	0.900	376.141
0.119	33.642	0.880	348.546
0.140	34.801	0.852	177.500
0.160	35.852	0.820	118.105
0.180	36.856	0.805	106.571
0.200	37.824	0.754	83.380
0.248	40.037	0.689	68.748
0.302	42.462	0.643	62.827
0.353	44.804	0.605	59.151
0.400	47.083	0.552	54.943
0.450	49.651	0.502	51.675
0.500	52.467	0.452	48.786
0.550	55.624	0.402	46.156
0.600	59.262	0.350	43.605
0.649	63.674	0.300	41.256
0.699	69.378	0.252	39.051
0.748	77.332	0.201	36.635
0.796	89.664	0.144	33.782
0.821	99.314		
0.848	115.178		
0.871	137.574		
0.895	179.933		
0.918	291.761		
1.000	388.059		

S9 - Adsorption		S9 - Desorption	
Relative Pressure (P/Po)	Quantity Adsorbed (cm³/g STP)	Relative Pressure (P/Po)	Quantity Adsorbed (cm³/g STP)
0.009	62.068	0.994	539.262
0.029	75.723	0.972	538.699
0.062	86.561	0.935	537.395
0.084	91.863	0.908	536.403
0.100	95.019	0.899	536.021
0.119	98.754	0.874	535.076
0.140	102.301	0.850	533.990
0.159	105.635	0.827	531.882
0.180	108.942	0.805	527.121
0.200	112.128	0.746	399.442
0.243	119.038	0.702	320.875
0.302	128.651	0.647	261.174
0.355	137.935	0.602	228.962
0.399	146.642	0.552	201.428
0.449	157.785	0.503	179.644
0.498	170.961	0.455	160.254
0.548	187.597	0.401	146.087
0.598	207.929	0.342	134.305
0.644	231.506	0.306	127.944
0.695	265.692	0.251	118.770
0.744	311.832	0.201	110.645
0.797	382.094	0.143	101.160
0.816	414.340		
0.847	479.026		
0.876	523.669		
0.908	535.154		
0.938	536.919		
0.965	537.969		
0.990	538.959		
0.994	539.262		

S9-CaCl$_2$ - Adsorption		S9-CaCl - Desorption	
Relative Pressure (P/Po)	Quantity Adsorbed (cm³/g STP)	Relative Pressure (P/Po)	Quantity Adsorbed (cm³/g STP)
0.010	23.764	0.995	237.028
0.033	28.896	0.972	236.696
0.063	32.465	0.932	236.272
0.079	33.802	0.906	235.978
0.100	35.371	0.900	235.901
0.120	36.693	0.875	235.621
0.140	37.915	0.851	235.239
0.160	39.057	0.827	233.821
0.180	40.146	0.803	218.377
0.200	41.215	0.755	140.265
0.249	43.705	0.694	96.067
0.302	46.432	0.652	82.093
0.352	49.148	0.598	70.661
0.400	51.900	0.554	64.260
0.450	55.075	0.502	58.751
0.500	58.677	0.451	54.581
0.550	62.911	0.401	51.230
0.599	68.211	0.350	48.247
0.649	75.196	0.300	45.502
0.698	84.964	0.251	42.928
0.747	99.882	0.200	40.240
0.795	124.921	0.143	37.025
0.822	146.746		
0.849	178.557		
0.872	211.892		
0.915	235.476		
0.943	236.214		
0.969	236.547		
0.994	236.922		
0.995	237.028		

Appendix B.

BJH adsorption data

S6	
BJH Adsorption dV/dD Pore Volume	
Pore Diameter (Å)	Pore Volume (cm³/g·Å)
2348.471	2.27373E-07
1192.522	5.35214E-07
865.542	1.55969E-06
688.811	2.76999E-06
418.186	4.34792E-06
270.141	1.34258E-05
180.935	9.99109E-05
149.801	0.000580971
127.590	0.001695203
110.614	0.003693614
90.071	0.006021208
73.844	0.008214546
62.578	0.008786552
54.025	0.008974089
47.254	0.008750707
41.743	0.008810991
37.192	0.008423517
33.304	0.008166425
29.995	0.007903787
27.002	0.007419731
24.062	0.006860452
21.590	0.006317839
20.136	0.005870684
19.192	0.005569799
18.253	0.005378197

S6-CaCl2	
BJH Adsorption dV/dD Pore Volume	
Pore Diameter (Å)	Pore Volume (cm³/g·Å)
731.855	1.95533E-07
417.945	1.44575E-06
255.075	7.65653E-06
187.473	0.000181646
152.370	0.001317957
124.527	0.002929666
106.594	0.003353203
89.474	0.002908913
74.296	0.002316417
63.020	0.001908466
54.400	0.00164694
47.580	0.001406289
42.061	0.00121186
37.475	0.001015918
33.572	0.000867645
30.299	0.000752471
27.324	0.000635342
24.448	0.000537915
21.923	0.000469553
20.415	0.000519911
19.471	0.000549632
18.505	0.00059937

S6-CaCl2-PVP10	
BJH Adsorption dV/dD Pore Volume	
Pore Diameter (Å)	Pore Volume (cm³/g·Å)
729.751	8.43192E-08
422.474	5.87942E-07
283.182	2.3179E-06
187.703	9.02542E-06
148.077	9.06472E-05
125.613	0.000330076
111.220	0.000729518
91.381	0.001471571
74.186	0.002217929
62.625	0.002252673
53.987	0.001962506
47.260	0.001596288
41.815	0.001290466
37.271	0.001080471
33.380	0.000903554
30.099	0.000797066
27.130	0.000707838
24.277	0.000650403
21.757	0.000670898
20.248	0.000691853
19.307	0.000758767
18.365	0.000773559

S6-CaCl2-PVP40	
BJH Adsorption dV/dD Pore Volume	
Pore Diameter (Å)	Pore Volume (cm³/g·Å)
183.378	1.16083E-06
156.001	0.000655367
128.676	0.001688278
110.337	0.002229813
91.536	0.00224173
75.676	0.001998593
64.317	0.00164769
55.740	0.001318167
49.004	0.001010886
43.525	0.000741124
38.958	0.000536943
35.057	0.000367754
31.724	0.000240418
28.738	0.0001004
21.921	2.3055E-05
20.974	0.000165645
20.037	0.000358157

Appendix C.

Experimental data for sorption/desorption of consolidated adsorbent

S6-CaCl$_2$-**PVP10**	34.7°C		
Sorption		**Desorption**	
Pressure (kPa)	Water Uptake (g/g)	Pressure (kPa)	Water Uptake (g/g)
0.002	0.037	2.399	0.327
0.598	0.129	2.099	0.291
1.198	0.205	1.499	0.240
1.798	0.261	0.899	0.191
2.399	0.327	0.299	0.106
		0.0025	0.031

S6-CaCl$_2$-**PVP10**	78.5°C		
Sorption		**Desorption**	
Pressure (kPa)	Water Uptake (g/g)	Pressure (kPa)	Water Uptake (g/g)
0.003	0.010	2.398	0.060
0.596	0.032	2.099	0.058
1.197	0.043	1.499	0.051
1.799	0.052	0.899	0.043
2.398	0.060	0.300	0.031
		0.002	0.005

S6-CaCl$_2$-**PVP40**		34.7°C	
Sorption		**Desorption**	
Pressure (kPa)	Water Uptake (g/g)	Pressure (kPa)	Water Uptake (g/g)
0.005	0.040	2.699	0.418
0.298	0.099	2.394	0.376
0.600	0.145	2.095	0.342
0.899	0.188	1.799	0.317
1.199	0.230	1.494	0.294
1.495	0.271	1.197	0.258
1.798	0.311	0.894	0.215
2.100	0.343	0.599	0.170
2.397	0.376	0.297	0.118
2.699	0.418	0.004	0.032

S6-CaCl$_2$-**PVP40** 78.5°C			
Sorption		**Desorption**	
Pressure (kPa)	Water Uptake (g/g)	Pressure (kPa)	Water Uptake (g/g)
0.003	0.002	2.697	0.069
0.299	0.005	2.398	0.066
0.599	0.010	2.093	0.063
0.895	0.016	1.793	0.059
1.197	0.033	1.498	0.055
1.495	0.041	1.196	0.050
1.795	0.052	0.898	0.045
2.098	0.056	0.599	0.037
2.397	0.062	0.299	0.028
2.697	0.069	0.004	0.006

S6-CaCl$_2$			
Sorption		Desorption	
Pressure (kPa)	H$_2$O adsorption per CaCl$_2$ (mol H$_2$O/molCaCl$_2$)	Pressure (kPa)	H$_2$O adsorption per CaCl$_2$ (mol H$_2$O/molCaCl$_2$)
0.006	1.873	2.699	12.848
0.295	2.958	2.399	11.616
0.590	4.868	2.099	10.455
0.897	6.365	1.799	9.284
1.198	7.637	1.499	8.506
1.500	8.458	1.199	8.118
1.799	9.228	0.899	6.833
2.098	10.374	0.599	5.377
2.398	11.567	0.299	3.200
2.699	12.848	0.003	0.987

S6-CaCl$_2$-PVP40			
Sorption		Desorption	
Pressure (kPa)	H$_2$O adsorption per CaCl$_2$ (mol H$_2$O/molCaCl$_2$)	Pressure (kPa)	H$_2$O adsorption per CaCl$_2$ (mol H$_2$O/molCaCl$_2$)
0.005	0.442	2.699	9.391
0.298	1.847	2.394	8.403
0.600	2.932	2.095	7.589
0.899	3.951	1.799	7.012
1.199	4.945	1.494	6.466
1.495	5.924	1.197	5.598
1.798	6.863	0.894	4.588
2.100	7.613	0.599	3.516
2.397	8.402	0.297	2.302
2.699	9.391	0.004	0.266

S6-CaCl$_2$-PVP40-5%G			
Sorption		Desorption	
Pressure (kPa)	H$_2$O adsorption per CaCl$_2$ (mol H$_2$O/molCaCl$_2$)	Pressure (kPa)	H$_2$O adsorption per CaCl$_2$ (mol H$_2$O/molCaCl$_2$)
0.005	0.469	2.604	8.134
0.204	1.800	2.598	8.115
0.404	2.270	2.399	7.826
0.603	2.683	2.199	7.573
0.803	3.266	1.999	7.290
1.003	4.266	1.799	6.909
1.204	4.805	1.599	6.416
1.404	5.321	1.399	5.881
1.604	5.850	1.199	5.332
1.804	6.367	1.000	4.775
2.005	6.896	0.799	4.202
2.204	7.396	0.599	3.600
2.405	7.789	0.399	2.823
2.604	8.134	0.199	2.132

S6-CaCl$_2$-PVP40-10%G			
Sorption		Desorption	
Pressure (kPa)	H$_2$O adsorption per CaCl$_2$ (mol H$_2$O/molCaCl$_2$)	Pressure (kPa)	H$_2$O adsorption per CaCl$_2$ (mol H$_2$O/molCaCl$_2$)
0.005	0.304	2.605	10.500
0.203	1.724	2.599	10.473
0.403	2.485	2.399	10.191
0.602	3.558	2.199	9.863
0.803	4.295	1.999	9.344
1.004	5.025	1.799	8.655
1.204	5.746	1.599	7.948
1.404	6.446	1.399	7.232
1.604559	7.141	1.199	6.499
1.804	7.835	0.999	5.752
2.004	8.533	0.799	4.985
2.205	9.223	0.599	4.197
2.404	9.908	0.399	3.375
2.605	10.500	0.199	2.385

S6-CaCl$_2$-PVP40-20%G			
Sorption		Desorption	
Pressure (kPa)	H$_2$O adsorption per CaCl$_2$ (mol H$_2$O/molCaCl$_2$)	Pressure (kPa)	H$_2$O adsorption per CaCl$_2$ (mol H$_2$O/molCaCl$_2$)
0.003	0.765	2.599	9.852
0.199	1.942	2.399	9.412
0.399	2.641	2.199	8.947
0.597	3.465	1.999	8.405
0.799	4.094	1.799	7.809
0.999	4.715	1.599	7.189
1.198	5.343	1.398	6.552
1.400	5.972	1.199	5.902
1.599	6.627	0.999	5.239
1.798	7.252	0.799	4.554
1.998	7.854	0.599	3.856
2.198	8.474	0.400	3.122
2.399	9.126	0.198	2.257
2.599	9.852	0.001	0.511

Appendix D.

Experimental data for Heat of adsorption for S6-CaCl$_2$

w (g/g)	ΔH_{is}(kJ/mol)
0.106	-62.89
0.111	-53.86
0.118	-52.21
0.119	-53.22
0.124	-50.45
0.126	-51.45
0.121	-53.85
0.128	-50.75
0.136	-50.29
0.141	-48.07
0.157	-46.92
0.186	-46.15
0.199	-46.84
0.212	-46.71
0.236	-49.41
0.254	-50.92
0.276	-50.27
0.309	-49.89
0.314	-48.65
0.325	-49.68
0.361	-49.10
0.376	-48.87
0.533	-46.00
0.806	-44.03
0.85	-44.44
10.99	-54.05

Appendix E.

Experimental data for thermal properties of consolidated composite adsorbent containing graphite flakes

Sample	2% RH		
	Thermal Conductivity $(W \cdot m^{-1} \cdot K^{-1})$	Specific heat $(J \cdot kg^{-1} \cdot K^{-1})$	Thermal diffusivity $(m^2/2)$
S6-CaCl2-PVP40-0%G	0.13	792.4	2.50E-7
S6-CaCl2-PVP40-10%G	0.29	834.8	5.02E-7
S6-CaCl2-PVP40-20%G	0.41	956.9	6.07E-7

Sample	20% RH		
	Thermal Conductivity $(W \cdot m^{-1} \cdot K^{-1})$	Specific heat $(J \cdot kg^{-1} \cdot K^{-1})$	Thermal diffusivity $(m^2/2)$
S6-CaCl2-PVP40-0%G	0.16	1226.1	2.01E-07
S6-CaCl2-PVP40-10%G	0.31	1283.6	3.48E-07
S6-CaCl2-PVP40-20%G	0.42	1371.1	4.34E-07

Sample	40% RH		
	Thermal Conductivity $(W \cdot m^{-1} \cdot K^{-1})$	Specific heat $(J \cdot kg^{-1} \cdot K^{-1})$	Thermal diffusivity $(m^2/2)$
S6-CaCl2-PVP40-0%G	0.22	1434.6	2.32E-07
S6-CaCl2-PVP40-10%G	0.36	1456.8	3.56E-07
S6-CaCl2-PVP40-20%G	0.45	1534.2	4.58E-07

Sample	60% RH		
	Thermal Conductivity $(W \cdot m^{-1} \cdot K^{-1})$	Specific heat $(J \cdot kg^{-1} \cdot K^{-1})$	Thermal diffusivity $(m^2/2)$
S6-CaCl2-PVP40-0%G	0.24	-	-
S6-CaCl2-PVP40-10%G	0.43	-	-
S6-CaCl2-PVP40-20%G	0.51	-	-

Appendix F.

Error Analysis

Thermal properties of prepared samples are measured three times and the average of the measurements is reported as the final value, the standard deviation of the reported average is obtained from

$$q = \sqrt{\frac{\sum_{l=1}^{r}(q_l - q_{ave})^2}{r - 1}}$$

Where r is the total number of measurements, q is the value of measurements and $q_{ave} = \frac{1}{r}\sum_{l=1}^{r} q_l$.